

Diss. ETH No 16399

**Quantification of Evolved Species in  
Hyphenated Thermal Analysis –  
MS – FTIR Spectroscopy Systems**

A dissertation submitted to the  
Swiss Federal Institute of Technology Zurich (ETH)  
for the degree of Doctor of Technical Sciences

presented by

Florian Eigenmann  
Dipl. Chem.-Ing. ETH  
born 5 July 1973  
citizen of Waldkirch (SG)

accepted on the recommendation of  
Prof. Dr. A. Baiker, examiner  
Prof. Dr. M. Morbidelli, co-examiner

2005

Seite Leer /  
Blank leaf

*dedicated to the reference samples  
allowing to measure the difference...*

Seite Leer /  
Blank leaf

# Acknowledgment

Firstly, I would like to express my sincere gratitude to Prof. Dr. Alfons Baiker for his support, both personally and scientifically, and the opportunity to complete my doctoral thesis in his group. I very much appreciate his efforts to support me and this work whenever it was necessary, no matter how difficult the circumstances.

Moreover, I would like to thank Prof. Dr. Massimo Morbidelli for accepting the duty of the co-examiner in this thesis.

I furthermore thank Dr. Marek Maciejewski for constructive discussions, his valuable suggestions and the big help during the last years. He was to me like a teacher and mentor as well generating lots of fabulous ideas, which resulted in several successful experimental investigations.

I would like to acknowledge the continuous interest, numerous discussion and very valuable suggestions given by Dr. Albrecht Rager (Bruker), and the help in solving experimental solutions offered by Netzsch GmbH (Germany). Special thanks are also due to Jürgen Gast (Bruker) and Dr. Wolf-Dieter Emmerich (Netzsch) for their support in settling the TA-FTIR system.

Many thanks go to Dr. Andy Gisler, Dr. Niklaus Künzle, Dr. Leo Schmid, Dr. Marco Burgener and Stefan Hannemann for sharing not only an office during the last years, but also the "ups and downs" of a doctoral thesis and for being friends I could turn to in order to discuss both scientific and general

topics. Additionally I thank the whole Baiker-group for the pleasant atmosphere. Especially I would like to mention besides my office mates the following members for spending a good time in and outside the ETH: Dr. Simon Frauchiger, Dr. Markus Rohr, Dr. Reto Hess, Dr. Csilla Keresszegi, Erika Wolf, Nils van Vegten, Ronny Wirz, Micha Ramin and Simon Diezi. In addition I wish, that my efforts to make Zsuzsanna Opre stop smoking will show success also in the future. I acknowledge also Dr. Jan-Dierk Grunwaldt and Micha Ramin for the careful rereading of the *Zusammenfassung*.

Besides the daily business, sport was an important part of my time at the ETH and was often an essential contrast to scientific research, Therefore a special thank is due to the rowing members of the *GC-Achter 00-05* and the *Poly-Achter* (Students and Professors) for sharing a lot of good times and unforgettable moments. I wish to thank also all the crew members who were joining my *RowingClasses* in ASVZ and especially Kaspar Egger and Heiner Iten for their support in many of my crazy rowing ideas, such as a *Guinness World Record*<sup>TM</sup> with the largest RowingClass, hold in 2004 at the ETH by 121 rowers.

Finally, I would like to thank my family and my friends for their support throughout all these years of my education.

Seite Leer /  
Blank leaf

Seite Leer /  
Blank leaf



# Table of Contents

<b>Acknowledgment</b> .....	v
<b>Table of Contents</b> .....	ix
<b>Summary</b> .....	xiii
<b>Zusammenfassung</b> .....	xvii
<b>1 Introduction</b> .....	1
1.1 General Aspects of Thermal Analysis .....	1
1.1.1 Thermogravimetry (TG) .....	2
1.1.2 Differential Thermal Analysis (DTA) and Differential Scanning Calorimetry (DSC) .....	2
1.2 Hyphenated Techniques in Thermal Analysis .....	3
1.2.1 Mass Spectrometry (MS) .....	4
1.2.2 Fourier Transform Infrared (FTIR) Spectroscopy .....	6
1.3 Pulse Thermal Analysis .....	7
1.4 Scope of this Thesis .....	7
1.5 References .....	8
<b>2 Experimental</b> .....	15
2.1 Simultaneous Thermal Analysis .....	15
2.2 Hyphenated Evolved Gas Analysis .....	17
2.3 Pulse Thermal Analysis .....	19
<b>3 Quantitative Calibration of FTIR Spectroscopic Signals</b> .....	25
3.1 Introduction .....	25
3.2 Experimental .....	28
3.2.1 Pulse Calibration .....	29

3.2.2	Pinhole Calibration .....	30
3.2.3	Differential Calibration .....	30
3.3	Results and Discussion .....	31
3.3.1	Quantification of FTIR Signals Using Gases .....	31
3.3.2	Quantification of FTIR Signals by Liquids .....	37
3.3.3	Quantification of FTIR Signals Using Solids .....	51
3.3.4	Comparison of the Calibration Methods .....	54
3.4	Conclusions .....	56
3.5	References .....	57
<b>4</b>	<b>Influence of Measuring Conditions on the Quantification of FTIR Signals .....</b>	<b>61</b>
4.1	Introduction .....	61
4.2	Experimental .....	64
4.3	Results and Discussion .....	65
4.3.1	Influence of Sample Mass and Concentration of the Gas .....	66
4.3.2	Influence of Parameters of Data-Acquisition and Carrier Gas .....	69
4.4	Conclusions .....	81
4.5	References .....	82
<b>5</b>	<b>Gas Adsorption Studied on Zeolites .....</b>	<b>85</b>
5.1	Introduction .....	85
5.2	Experimental .....	88
5.3	Results .....	89
5.3.1	Influence of Thickness of Adsorbent Bed .....	90
5.3.2	Influence of Temperature .....	92
5.3.3	Influence of Carrier Gas Flow .....	95
5.3.4	Determination of the Adsorption Heat .....	97
5.4	Discussion .....	100
5.5	Conclusions .....	104
5.6	References .....	105
<b>6</b>	<b>Selective Catalytic Reduction of NO by NH<sub>3</sub> over Manganese-Cerium Mixed Oxides .....</b>	<b>109</b>
6.1	Introduction .....	109

6.2	Experimental .....	111
6.3	Results and Discussion .....	113
6.3.1	Adsorption Behavior .....	114
6.3.2	Redox Behavior .....	119
6.3.3	Catalytic Activity in SCR .....	123
6.4	Conclusions .....	131
6.5	References .....	132
	<b>Final Remarks .....</b>	<b>135</b>
	<b>List of Publications .....</b>	<b>139</b>
	<b>Curriculum Vitae .....</b>	<b>143</b>

Seite Leer /  
Blank leaf

## Summary

In thermoanalytical investigations the determination of the composition of the evolved gases is very important, especially when investigating decomposition processes or gas-solid reactions occurring in multi-component systems. The potential of simultaneous techniques, enabling the qualitative analysis of evolved species, such as thermogravimetry-mass spectrometry or thermogravimetry-FTIR spectroscopy has been further improved by the introduction of the pulse thermal analysis (PulseTA<sup>®</sup>). This method provides a quantitative calibration by relating the mass spectrometric or FTIR signals to the injected quantity of probe gas.

So far, PulseTA<sup>®</sup> was only applied to combined TA-MS and its extension to TA-FTIR for quantitative and qualitative analysis was the main target of this thesis. Furthermore the influence of several experimental parameters such as concentration of the analyzed species, temperature and flow rate of the carrier gas on FTIR signals has been investigated. The reliability of quantifying FTIR signals was checked by relating them to the amount of evolved gases measured by thermogravimetry.

Comparisons with a mass spectrometer in tandem allowed precise optimization of several important parameters for FTIR spectroscopy. MS analysis, which was not significantly affected by the experimental conditions, was used as a reference for assessing the accuracy of quantification by FTIR. The quanti-

fication of the spectroscopic signals was verified by the decomposition ( $\text{NaHCO}_3$ ) or dehydration ( $\text{CuSO}_4 \cdot 5 \text{H}_2\text{O}$ ) of compounds with well known stoichiometry.

The linear dependence between the injected amount of liquids and the integral intensity of spectroscopic signals (peak area) enabled easy quantification of FTIR data. Systematic studies on a new method based on isothermal vaporization of liquids further widen the application range of *in situ* calibrations. For gases the quantification of FTIR signals is possible either by conventional calibration (varying concentrations of target gases) or, as mentioned above, by the injection of a known amount of the calibrating gas into the carrier gas stream. For the quantification of FTIR signals of liquids, we applied several methods, pulse calibration and two methods based on the evaporation of liquids: pinhole and differential calibrations. These methods were studied applying different organic liquids and water.

Based on these methods of quantification, pulse thermal analysis was applied in different catalytic studies, such as gas adsorption and selective reduction of nitrogen oxides by ammonia. In order to determine the acidity of a catalyst, adsorption of ammonia as a probe molecule is widely applied. PulseTA<sup>®</sup> allows studying adsorption and desorption at atmospheric pressure. Continuous monitoring of the concentration of the pulsed probe molecules in the carrier gas provided the opportunity to investigate the dynamics of physisorption processes. The desorption rate of physisorbed species is shown to depend on carrier gas flow and thickness of the sample bed. An important advantage of PulseTA<sup>®</sup>, compared to classical volumetric methods, is that pretreatment of the adsorbent, determination of the kind and amount of preadsorbed gases, as well as temperature programmed desorption can all be carried out using the same experimental set-up. Integral heats of adsorption and the amount of

chemisorbed ammonia were found to agree well with values reported in literature.

Finally TA-FTIR-MS was applied in selective catalytic reduction of nitrogen oxides by ammonia over manganese-cerium mixed oxides. Mixed oxide catalysts with different molar ratio  $Mn/(Mn+Ce)$  were prepared from the corresponding metal nitrates using the *citric acid method* and investigated concerning their adsorption behavior, redox properties and behavior in the selective catalytic reduction of  $NO_x$  by  $NH_3$ . These studies based on PulseTA<sup>®</sup> uncovered a clear correlation between the dependence of these properties and the mixed oxide composition. Highest activity to nitrogen formation was found for catalyst with a molar ratio  $Mn/(Mn+Ce)$  of 0.25, whereas the activity was much lower for the pure constituent oxides. The adsorption studies indicated that  $NO_x$  and  $NH_3$  are adsorbed on separate sites. Consecutive adsorption measurements of the reactants showed similar uptakes as separate measurements indicating that there was no interference between adsorbed reactants. Mechanistic investigations by changing the sequence of admittance of reactants ( $NO_x$ ,  $NH_3$ ) indicated that at 100–150 °C nitrogen formation follows an Eley-Rideal type mechanism where adsorbed ammonia reacts with  $NO_x$  in the gas phase, whereas adsorbed  $NO_x$  showed no significant reactivity under conditions used.

Seite Leer /  
Blank leaf



## Zusammenfassung

In thermoanalytischen Untersuchungen ist die Analyse der Gasphase (evolved gas analysis, EGA) sehr wichtig, insbesondere bei Untersuchungen von Zersetzungsvorgängen oder Gas-Feststoff-Reaktionen, die in Mehrstoffsystemen auftreten. Das Potential von kombinierten Techniken, insbesondere die qualitative Analyse der sich entwickelnden gasförmigen Produkte mit Hilfe der kombinierten Thermogravimetrie-Massenspektrometrie oder Thermogravimetrie-FTIR Spektroskopie wurde durch die Einführung der Pulsthermoanalyse (PulseTA<sup>®</sup>) erweitert. Diese Methode ermöglicht eine quantitative Kalibrierung, indem MS oder FTIR Signale mit der eingespritzten Menge des Prüf-gases in Beziehung gebracht werden.

Bisher wurde die PulseTA<sup>®</sup> nur in kombinierten TA-MS Systemen angewendet. Das Hauptziel dieser Arbeit war die Erweiterung zu TA-FTIR für die quantitative und qualitative Analyse. Der Einfluss einiger wichtiger experimenteller Parameter, wie der Konzentration der zu analysierenden Komponenten, der Temperatur und der Strömungsgeschwindigkeit des Trägergases auf die FTIR Signale wurde systematisch untersucht. Die Zuverlässigkeit der Quantifizierung der FTIR Signale wurde überprüft, indem man die Signale auf die Menge der entwickelten Gase bezog, die durch Thermogravimetrie gemessen wurden.

Vergleiche mit massenspektrometrischer Analyse erlaubten die Optimierung einiger wichtiger experimenteller Parameter für die FTIR Spektroskopie. Die MS Analyse, welche nicht signifikant durch experimentelle Bedingungen beeinflusst wurde, diente als Referenz für die Bestimmung der Genauigkeit der Quantifizierung von FTIR Signalen. Die Quantifizierung der spektroskopischen Signale wurde durch die Zersetzung ( $\text{NaHCO}_3$ ) oder Dehydratisierung ( $\text{CuSO}_4 \cdot 5 \text{H}_2\text{O}$ ) von Substanzen mit bekannter Stöchiometrie überprüft.

Die lineare Abhängigkeit zwischen der eingespritzten Menge der Flüssigkeiten und der integralen Intensität der spektroskopischen Signale ermöglichte eine einfache Quantifizierung von FTIR Daten. Für Gase ist die Quantifizierung der FTIR Signale entweder durch herkömmliche Kalibrierung (unterschiedliche Konzentrationen der Prüfgase) möglich, oder, durch die Einspritzung einer bekannten Menge des Kalibriergases in den Trägergasstrom. Für die Quantifizierung der FTIR Signale von Flüssigkeiten, wurden verschiedene Methoden untersucht, nämlich die Pulskalibrierung und zwei Methoden, die auf der Verdampfung von Flüssigkeiten basieren: Splintloch- (Pinhole-) und Differentialkalibrierung. Diese Methoden wurden am Beispiel der Quantifizierung verschiedener organischen Flüssigkeiten und Wasser getestet.

Basierend auf den getesteten Quantifizierungsmethoden, wurde die Puls-thermoanalyse für die Untersuchung verschiedener Prozesse angewandt, wie zum Beispiel die Bestimmung von sauren Zentren an Katalysatoroberflächen und die Verfolgung der katalytischen selektiven Reduktion von Stickoxiden durch Ammoniak. Die PulseTA<sup>®</sup> ermöglichte die Untersuchung der Adsorption als auch der Desorption unter Normaldruck. Die kontinuierliche Aufzeichnung der Konzentration der injizierten Moleküle im Trägergas liefert die Möglichkeit, die Dynamik der Physisorptionsprozesse zu bestimmen. Es wurde gezeigt, dass die Desorptionrate von physisorbierten Species vom Trägergas-

strom und von der Schichtdicke der Probe abhängt. Ein wichtiger Vorteil der PulseTA<sup>®</sup>, verglichen mit klassischen volumetrischen Methoden, ist, dass die Vorbehandlung des Adsorbens, die Bestimmung der Art und Menge des adsorbierten Gases, sowie die Desorption in der gleichen experimentellen Einrichtung untersucht werden können. Integrale Adsorptionswärmen und die Mengen von chemisorbiertem Ammoniak stimmten gut mit den Literaturwerten überein, welche mit anderen Methoden ermittelt wurden.

Schliesslich wurde mit Hilfe von TA-FTIR-MS die selektive katalytische Reduktion von Stickoxiden durch Ammoniak an Mangan-Cer-Mischoxiden untersucht. Mischoxidkatalysatoren mit unterschiedlichem molarem Verhältnis  $Mn/(Mn+Ce)$  wurden an den entsprechenden Metallnitraten mittels der *Zitronensäuremethode* hergestellt und hinsichtlich des Adsorptionsvermögens, der Redox-Eigenschaften und des katalytischen Verhaltens untersucht. Diese Studien, die auf der PulseTA<sup>®</sup> basierten, zeigten eine deutliche Korrelation zwischen der Abhängigkeit dieser Eigenschaften und der Mischoxidzusammensetzung auf. Höchste Aktivität bezüglich selektiver Stickstoff-Produktion wurde für den Katalysator mit einem molaren Verhältnis  $Mn/(Mn+Ce)$  von 0.25 gefunden, während die Aktivität für die reinen Oxidkomponenten viel niedriger war. Die Adsorptionsstudien zeigten, dass  $NO_x$  und  $NH_3$  an unterschiedlichen Zentren adsorbiert werden. Konsekutive Adsorptionsmessungen der Reaktanten zeigten ähnliche Adsorptionsmengen wie sie durch separate Messungen erhalten wurden, was eine Interferenz zwischen den Adsorbaten ausschloss. Untersuchungen zum Reaktionsmechanismus unter Variation der Zuführungsreihenfolge der Reaktanten ( $NO_x$ ,  $NH_3$ ) wiesen zwischen 100–150 °C bezüglich Stickstoff-Produktion auf einen Eley-Rideal-Mechanismus hin, wobei absorbiertes Ammoniak mit  $NO_x$  in der Gasphase reagiert, während

absorbiertes  $\text{NO}_x$  keine bedeutende Reaktivität unter den verwendeten Bedingungen zeigte.

## Introduction

### 1.1 General Aspects of Thermal Analysis

Thermal analysis (TA) is a well-known set of techniques enabling qualitative and quantitative information about the effects of various heat treatments on mainly solid materials, such as catalysts, polymers, pharmaceuticals, clays and minerals, metals and alloys. The change of the temperature in the system is performed under strictly controlled conditions and can reveal changes in mass and enthalpy due to physical and chemical phenomena occurring in the material studied. A widely accepted definition of thermal analysis (TA) is: *a group of techniques that study the relationship between a sample property and its temperature.*

There are different thermal methods allowing the measurement of several properties, including: heat (calorimetry), temperature (thermometry), temperature difference (differential thermal analysis), heat flow rate (differential scanning calorimetry), mass (thermogravimetry), mechanical properties (thermomechanical analysis), electrical properties (dielectric thermal analysis) pressure (thermomanometry or thermobarometry), optical properties (thermoptometry or thermoluminescence), acoustic (thermosonimetry or thermoacoustimetry) or structure (thermodiffractometry). Here we focus on the three most important techniques: thermogravimetry (TG), differential thermal analysis (DTA) and differential scanning calorimetry (DSC).

### 1.1.1 Thermogravimetry (TG)

The definition of TG as given by the International Confederation for Thermal Analysis and Calorimetry (ICTAC) is: *a technique in which the mass of a substance is measured as a function of temperature whilst the substance is subjected to a controlled temperature program*. A controlled temperature program can mean:

- Heating or cooling the sample at some defined constant rate, and monitoring the mass change as a function of temperature. This is the most common mode of operation.
- Holding the sample at some constant temperature and monitoring the mass change as a function of time, called isothermal TG.

Therefore, thermogravimetric data are usually presented as a plot of the mass against time or temperature (the TG curve), with the mass loss on the ordinate plotted downwards and mass gains plotted upwards.

Additionally the mass change can be presented as the derivative or differential thermogravimetric curve (DTG), which is a plot of the rate of mass change against time or temperature. The DTG curve is particularly useful in displaying subtle changes in mass which are not easily discernible on the TG curve. The DTG curve also allows the ready determination of the temperature at which the rate of mass loss has a maximum and provides an additional characteristic temperature depicting the point of inflection of the investigated TG curve.

### 1.1.2 Differential Thermal Analysis (DTA) and Differential Scanning Calorimetry (DSC)

Differential thermal analysis (DTA) and differential scanning calorimetry (DSC) have had a great impact on material science by enabling the measurement of a great number of physical and chemical properties. These techniques

have allowed elucidation of endothermic and exothermic processes in a wide temperature range. Some of the physical properties measured by these thermal analytical methods include melting, crystallizations temperatures, enthalpy of these processes, specific heat capacity, liquid crystal transitions, vaporization, sublimation, solid-solid transition, thermal conductivity and glass transition temperature. Chemical properties which could be monitored by DSC and DTA are dehydration, decomposition, oxidative and reductive reactions, solid state reactions, chemisorption, combustion, polymerization, curing and catalytic reactions.

According to ICTAC:

*In DTA, the temperature difference between the substance and a reference material is measured as a function of temperature, while the substance and reference material are subjected to a controlled temperature program.*

*In DSC, the difference in energy input into a substance and a reference material is measured as a function of temperature, while the substance and reference material are subjected to a controlled temperature program.*

It is often advantageous to combine two main thermal analysis techniques so that measurements of mass (TG) and changes in heat capacity of the sample (DTA or DSC), are measured simultaneously. Such a combination is called simultaneous thermal analysis (STA).

## 1.2 Hyphenated Techniques in Thermal Analysis

The success of simultaneous techniques has led to the coupling of other conventional analytical methods with an STA system. Analytical methods such as MS, FTIR spectroscopy, GC, condensation of volatiles and their chemical

analysis have proven to be suitable for analyzing the gaseous product evolved from a sample as it undergoes thermal treatment in an STA system. The main goals of coupling these techniques are to enhance the specificity of a single system and to eliminate the problems that are associated with trying to compare data sets that were collected under different experimental conditions. There are many detection methods available to analyze the gaseous samples but clear advantage have those which can monitor continuously the composition of the gas phase. Therefore, the most useful methods are MS and FTIR. The development of TA-MS and TA-FTIR hyphenated techniques from the first experimental attempts has been reviewed in detail by Materazzi et al. [1-3].

### 1.2.1 Mass Spectrometry (MS)

Due to the possibility of continuous monitoring of the gas composition, MS is probably the most universal technique for analyzing multicomponent systems and reactions resulting in gaseous products. Their identification is the main application of the TA-MS technique, which together with thermal analysis aids in interpreting the course of the investigated reaction. The qualitative MS analysis is generally done by comparing the recorded spectrum with references containing key fragment ions and their relative intensities for known elements and compounds. Much more difficult, but very important is the quantitative interpretation of mass spectrometric data, which needs the calibration of the system, i.e. the determination of the relationship between the observed intensities of the ion currents and the amount of the analyzed species.

One of the earliest reports of the coupling of MS with evolved gas analysis (EGA) was published by Gohlke and Langer [4]. Over the years several designs for linking a mass spectrometer to a TG/DTA system have been reported in lit-



erature. Raemaeker and Bart [5] gave a detailed review and summarized the main development of TG-MS settings (cf. Table 1-1). One of the pioneers of

**Table 1-1:** History of thermogravimetry–mass spectrometry up to 1996. Table taken from Raemaekers and Bart [5].

---

1965	Usefulness of MS to TG coupling suggested by Wendlandt et al. [28] and Gohlke et al. [29]; (Friedman [30] describes Py-TOFMS for plastics thermal decomposition studies)
1968	Zitomer [31] designs unique TG-TOFMS instrument; first application to polymers
1968	Wiedemann et al. [32] develop Mettler-Balzers TG-QMS instrument with direct vacuum coupling
1969	Stanton et al. [33] describe a TG-CT-MS arrangement
1975	Advanced coupling systems for TG-QMS [34]
1977	Critical review of simultaneous TG-QMS couplings [35]; introduction of TG-CIMS by Baumgartner et al. [36]; development of Linseis-Leybold-Heraeus TG-MS instrument [37]
1979	Introduction of commercial Netzsch high temperature TG/DTG/DTA-MS equipment [38] with two-stage pressure reduction system (quantitative interface); coupling of TG to magnetic sector instrument [39]
1980	First Du Pont-Du Pont TG-MS apparatus [40,41]
1982	Development of TG-APCI QMS [42]
>1982	Strong improvement in data collection; software development [43,44]
1983	Commercially available TG-MS interface [45–48]
1984	Shushan et al. [49] describe TG-APCI MS/MS; Holdiness [50] and Dollimore et al. [51] review TG-MS instrumental developments
1986/87	Introduction of Stanton Redcroft-VG commercial apparatus [52,53]
1997	Development of simultaneous TG-modulated molecular beam mass spectrometry apparatus (STMMBA) by Behrens et al. [54]
1987/88	Reviews of application of TG-MS for polymer characterization by Chiu [55] and Jones et al. [56]
1988/91	Optimization of capillary sampling system [57,58]
1991	TG-MS,-FFIR Conference in Würzburg [59]; application of TG-LVMS by Yun et al. [60]
1993	Hi-Res TG-MS coupling by Lever et al. [61]
1994	Development of high sensitivity commercial Netzsch-Balzers instrument with improved orifice-skimmer coupling [62]
1997	Special issue of <i>Thermochimica Acta</i> on TG-MS

---

the hyphenated TA-MS technique was Netzsch, later other manufacturers put this system on the market: Mettler, Perkin Elmer, TA Instruments (former Du Pont) and others. Mass spectrometers used for coupling mainly originate from Balzers, VG, Finnigan and Sciex.

### 1.2.2 Fourier Transform Infrared (FTIR) Spectroscopy

The coupling of FTIR spectroscopy with a thermal analysis unit to perform EGA is another well-established method for the analysis of gaseous species. Although the suggestion for using FTIR in EGA was first made by Low [6] in 1967, and while experimental results obtained from coupling of TA and FTIR spectroscopy were reported in 1981 [7], the commercial coupling TA-FTIR was not available until 1987 [8-10]. Up to that time most work on the identification of evolved gases from TG has been carried out on TA-MS systems and reports on studies using hyphenated TA-FTIR were rare. The TA-FTIR system introduced on the market by e.g. Netzsch in cooperation with Bruker offers a new powerful method with the following advantages:

- Functional group identification and specific compound analysis on the basis of vibrational spectra.
- Simultaneous spectral information on many species.
- Reference spectral libraries for over 250 000 species.

On the other hand it is rather difficult to use IR to analyze mixtures of compounds with similar functional groups, moreover FTIR cannot detect homonuclear gases not showing IR absorbance (e.g. O<sub>2</sub>, N<sub>2</sub>) or does not readily distinguish hydrocarbons above C<sub>3</sub>H<sub>6</sub>.

### 1.3 Pulse Thermal Analysis

Pulse Thermal Analysis (PulseTA<sup>®</sup>) was developed in 1996 [11] in order to increase the potential of conventional thermal analysis, and arrived on the market in 1997. The basis of the PulseTA<sup>®</sup> technique is the injection of a specific amount of the desired gas into the inert carrier gas stream and monitoring changes in the mass and enthalpy which result from the incremental reaction progress. In addition, with coupled TA-MS or TA-FTIR systems, PulseTA<sup>®</sup> makes it possible to analyze gas phase composition changes resulting from the reactions caused by the injected pulses. The PulseTA<sup>®</sup> box can be used with MS as well as the FTIR coupling systems. Depending on the type of gas injected, PulseTA<sup>®</sup> offers three primary options for the investigation of gas-solid reactions:

- Injection of gas which reacts chemically with solids.
- Injection of gas which adsorbs on the solid.
- Injection of inert gas in order to calibrate spectroscopic signals.

PulseTA<sup>®</sup> in combination with MS was applied for investigation of: catalytic combustion of methane [11,12], properties of gold catalyst [13,14], mechanism of decomposition of solids [15,16], redox properties of ceria [17-20], and NO<sub>x</sub> removal [16,21-27].

### 1.4 Scope of this Thesis

In recent years hyphenated techniques involving thermal analysis became more and more important. The aim of this thesis was to extend the application of *in situ* quantification from TA-MS to TA-FTIR. Special effort has been devoted to exploring PulseTA<sup>®</sup> and finding optimal measuring conditions, which allow

quantification of spectroscopic signals in TA-FTIR-MS systems. Since MS and FTIR complement each other, for studies of complex gas-solid reactions the linking of TA to both a MS and FTIR spectrometer (either in parallel or in series) enables more complete evaluations.

Another important aspect of this study was the application of PulseTA<sup>®</sup> in catalytic research such as the adsorption of ammonia for assessing the acidic sites on catalysts (Chapter 5) and the investigation of the mechanism of the selective reduction of nitric oxides over manganese-cerium mixed oxides by ammonia (Chapter 6). In both studies the quantification of the evolved gases during reaction/adsorption on the catalyst was a crucial issue and lead to interesting results which would have been difficult to gain by other experimental methods.

## 1.5 References

- [1] S. Materazzi, *Appl. Spectrosc. Rev.* 32 (1997) 385.
- [2] S. Materazzi, *Appl. Spectrosc. Rev.* 33 (1998) 189.
- [3] S. Materazzi, R. Curini, *Appl. Spectrosc. Rev.* 36 (2001) 1.
- [4] R.S. Gohlke, H.G. Langer, *Anal. Chim. Acta* 36 (1966) 530.
- [5] K.G.H. Raemakers, J.C.J. Bart, *Thermochim. Acta* 295 (1997) 1.
- [6] M.J.D. Low, In: W. Lodding, Editor, *Gas Effluent Analysis*, M. Dekker, New York (1967).
- [7] C.A. Cody, L. DiCarlo, B.K. Faulseit, *Am. Lab.* 13 (1981) 93.
- [8] D.A.C. Compton, *Intl. Labmate* 12 4 (1987) 37.
- [9] R.C. Wieboldt, G.E. Adams, S.R. Lowry, R.J. Rosenthal, *Am. Lab.* 20 1 (1988) 70.

- [10] P.R. Solomon, M.A. Serio, R.M. Carangelo, R. Bassilakis, Z.Z. Yu, S. Charpenay, J. Whelan, *J. Anal. Appl. Pyrolysis* 19 (1991) 1
- [11] M. Maciejewski, C.A. Muller, R. Tschan, W.D. Emmerich, A. Baiker, *Thermochim. Acta* 295 (1997) 167.
- [12] C.A. Müller, M. Maciejewski, R. Koeppel, A. Baiker, *Catal. Today* 47 (1999) 245.
- [13] J.-D. Grunwaldt, M. Maciejewski, O.S. Becker, P. Fabrizioli, A. Baiker, *J. Catal.* 186 (1999) 458.
- [14] M. Maciejewski, P. Fabrizioli, J.-D. Grunwaldt, O.S. Becker, A. Baiker, *Phys. Chem. Chem. Phys.* 3 (2001) 3846.
- [15] M. Maciejewski, E. Ingier-Stocka, W.-D. Emmerich, A. Baiker, *J. Therm. Anal. Cal.* 60 (2000) 735.
- [16] E. Ingier-Stocka E, M. Maciejewski, *Thermochim. Acta* 432 (2005) 56.
- [17] E. Rocchini, A. Trovarelli, J. Llorca, G.W. Graham, W.H. Weber, M. Maciejewski, A. Baiker, *J. Catal.* 194 (2000) 461.
- [18] W.J. Stark, L. Mädler, M. Maciejewski, S.E. Pratsinis and A. Baiker, *J. Catal.* 220 (2003) 35.
- [19] H. Schulz H, WJ. Stark, M. Maciejewski, S.E. Pratsinis, A. Baiker, *J. Mater. Chem.* 13 (2003) 2979.
- [20] WJ. Stark, J.D. Grunwaldt, M. Maciejewski, S.E. Pratsinis, A. Baiker, *Chem. Mater.* 17 (2005) 3352.
- [21] C. Wögerbauer, M. Maciejewski, A. Baiker, *Top. Catal.* 16/17 (2001) 181.
- [22] C. Wögerbauer, M. Maciejewski, M.M. Schubert, A. Baiker, *Cat. Lett.* 74 (2001) 1.

- [23] C. Wögerbauer, M. Maciejewski, A. Baiker, U. Göbel, *J. Catal.* 201 (2001) 113.
- [24] C. Wögerbauer, M. Maciejewski, A. Baiker, *Appl. Catal. B* 34 (2001) 11.
- [25] C. Wögerbauer, M. Maciejewski, A. Baiker, *J. Catal.* 205 (2002) 157.
- [26] M. Piacentini, M. Maciejewski, T. Burgi, A. Baiker, *Top. Catal.* 30 (2004) 71.
- [27] M. Piacentini, M. Maciejewski, A. Baiker, *Appl. Cat. B* 59 (2005) 187.
- [28] W.W. Wendlandt, T.M. Southern, *Anal. Chim. Acta* 32 (1965) 405.
- [29] R.S. Gohlke, H.G. Langer, *Anal. Chem.* 37 (1965) 25.
- [30] H.L. Friedman, *J. Appl. Polym. Sci.* 9 (1965) 651.
- [31] F. Zitomer, *Anal. Chem.* 40 (1968) 1091.
- [32] R. Giovanoli, H.G. Wiedemann, *Helv. Chim. Acta* 51 (1968) 1134.
- [33] H.L. Friedman, *Thermochim. Acta* 1 (1970) 199.
- [34] W. Dünner, H. Eppler, In: I. Buzas, Editor, *Therm. Anal., Proc. ICTA, 4th, Mtg. date 1974 Vol. 3*, Heyden and Son, London (1975) 1049.
- [35] H. Eppler, H. Selhofer, *Thermochim. Acta* 20 (1977) 45.
- [36] E. Baumgartner, E. Nachbaur, *Thermochim. Acta* 19 (1977) 3.
- [37] W. Lampert and G. Koopmann, *Keram. Ztschr.* 29 (1977), p. 457.
- [38] W.D. Emmerich, E. Kaisersberger, *J. Therm. Anal.* 17 (1979) 197.
- [39] K.W. Smalldon, R.E. Ardrey, L.R. Mullings, *Anal. Chim. Acta* 107 (1979) 327.
- [40] J. Chiu, A.J. Beattie, *Thermochim. Acta* 40 (1980) 251
- [41] R.L. Hassel (to Du Pont), *Appl. Brief TA* 45 (n.d.).
- [42] S.M. Dyszel, In: B. Miller, Editor, *Therm. Anal., Proc. ICTA, 7th Vol. 1*, Wiley Heyden, Chichester (1982) 272.

- [43] H.K. Yuen, G.W. Mappes, W.A. Grote, *Thermochim. Acta* 52 (1982) 143.
- [44] G. Várhegyi, F. Till, T. Székely, *Thermochim. Acta* 102 (1986) 115.
- [45] E. Kaisersberger, M. Gebhardt, *Thermochim. Acta* 148 (1989) 493.
- [46] E. Kaisersberger, *Intl. J. Mass Spectrosc. Ion Phys.* 46 (1983) 155.
- [47] E. Kaisersberger, W.-D. Emmerich, *Thermochim. Acta* 85 (1985) 275.
- [48] E. Kaisersberger, W.-D. Emmerich, H. Pfaffenberger, *Thermochim. Acta* 88 (1985) 319.
- [49] B. Shushan, B. Davidson, R.B. Prime, *Anal. Calorim.* 5 (1984) 105.
- [50] D. Dollimore, G.A. Gamlen, T.J. Taylor, *Thermochim. Acta* 75 (1984) 59.
- [51] W.R. Holdiness, *Thermochim. Acta* 75 (1984) 361.
- [52] E.L. Charsley, N.J. Manning, S.B. Warrington, *Thermochim. Acta* 114 (1987) 47.
- [53] E.L. Charsley, N.J. Manning, S.B. Warrington, *Journ. Calorim., Anal. Therm. Thermodyn. Chim.* 17 (1986) 164.
- [54] R. Behrens. *Rev. Sci. Instrum.* 58 (1987) 451.
- [55] J. Chiu, In: J. Mitchell, Editor, *Applied Polymer Analysis and Characterisation: Recent Developments in Techniques, Instrumentation, Problem Solving*, Hanser Publ., München (1987) 175.
- [56] E.G. Jones, D.L. Pedrick, I.J. Goldfarb, *Polym. Eng. Sci.* 28 (1988) 1046.
- [57] W. Schwanebeck, H.W. Wenz, *Fresenius Z. Anal. Chem.* 331 (1988) 61.
- [58] H. Wenz and H. Rohrbach, *Fachtagung, Kopplungen der Instrumentellen Analytik (TA, IR, MS) für die Kunststoff- und Kautschukindustrie.* (1988) Würzburg

- [59] Fachtagung, Kopplungen der Instrumentellen Analytik (TA, IR, MS) für die Kunststoff- und Kautschukindustrie (1972) Würzburg .
- [60] Y. Yun, H.L.C. Meuzelaar, N. Simmleit, H.-R. Schulten, *Energy Fuels* 5 (1991) 22.
- [61] T.J. Lever, A. Sutkowski, *J. Therm. Anal.* 40 (1993) 257.
- [62] E. Kaisersberger, E. Post, J. Janoschek, In: *ACS Symp. Ser.* 581 (1994) 74.



Seite Leer /  
Blank leaf

Seite Leer /  
Blank leaf

## Experimental

This chapter describes the experimental setup used and reports general features of the analytical methods. Specific descriptions of the experiments are given in the pertinent chapters.

### 2.1 Simultaneous Thermal Analysis

The heart of the experimental set up used for the simultaneous thermal analysis is a Netzsch STA 449 C Jupiter<sup>®</sup>, which is schematically presented in Figure 2-1. Thermogravimetry (TG) and differential thermal analysis/differential thermal calorimetry (DTA/DSC) are applied simultaneously to the same sample. The results of both techniques can be directly compared, as the target reaction is not affected by different experimental conditions which can occur with single measurements. In addition, the thermal effects measured simultaneously with mass changes are easier to interpret and enthalpy changes can be corrected for mass loss or gain. Moreover, simultaneous thermal analysis eliminates the uncertainties arising with separate TG and DTA/DSC measurements, caused by the inhomogeneity and geometry of samples and inaccuracy in the temperature control. This is especially significant when complex multistage reactions are investigated.

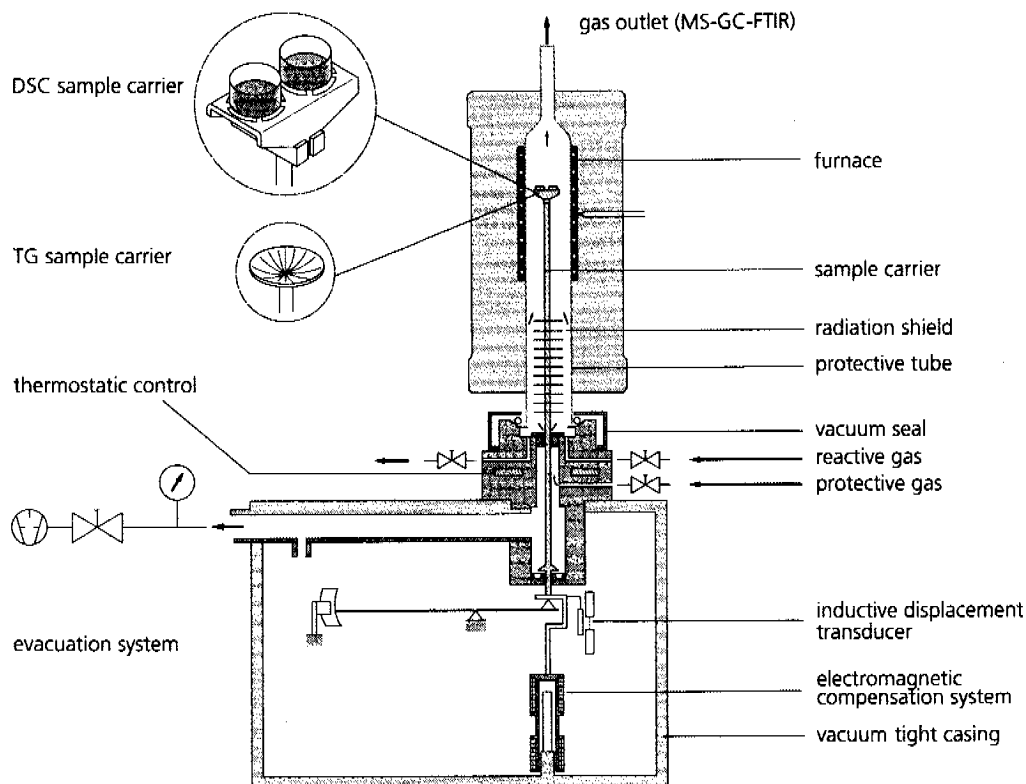


Fig. 2-1: Scheme of thermoanalyzer: Netzsch STA 449 C Jupiter®

Characteristic for the instrument are the extremely stable and reproducible TG (drift < 1  $\mu\text{g}/\text{h}$ ) and DSC baselines. The applied STA 449 allows measurements to be conducted over the range of room temperature up to 1650 °C. User-exchangeable TG, TG/DTA or TG/DSC sample holders are available for this apparatus, shown in Figure 2-2. Each sensor can be configured with different thermocouples, allowing optimization of sensitivity, time constant and atmosphere for every application. The range of the applied sample mass can be chosen from milligrams up to 5 g (TG high volume crucible). However for TG/DSC experiments the amount of investigated sample was in the range of ca. 30 mg. Furthermore, flat TG-crucibles with a large diameter

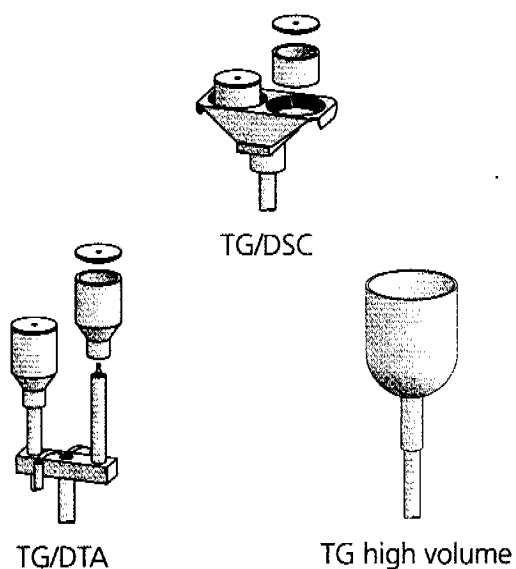


Fig. 2-2: Different sample holders and crucibles for the specific system.

(o.d.=16.4 mm) were applied when investigating adsorption phenomena, in order to minimize diffusion problems caused by thick layer of the sample (cf. chapter 5 and 6).

## 2.2 Hyphenated Evolved Gas Analysis

In order to analyze the gases leaving the STA 449, the thermoanalyzer was connected by a heated (optionally up to 230 °C, mainly 200 °C was supplied) transfer-line to a Bruker Vector 22 FTIR spectrometer. The coupling of TA-FTIR is presented in Figure 2-3.

The FTIR spectrometer is equipped with a MCT detector and an especially developed low-volume gas cell (8.7 ml) with a 123 mm path length and ZnSe windows. To avoid condensation of low volatile compounds the cell was

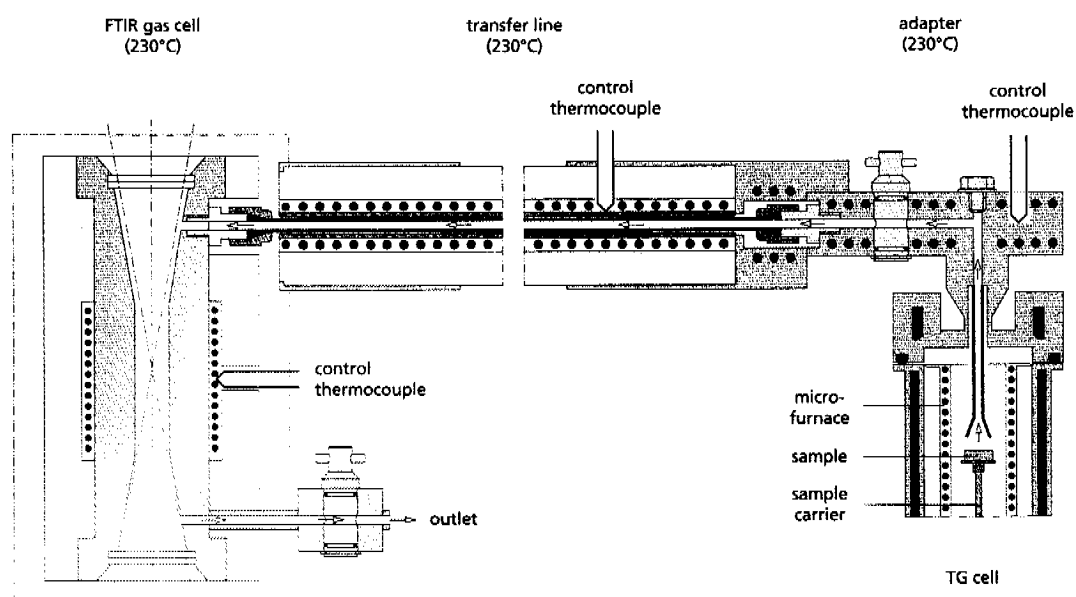


Fig. 2-3: Scheme of coupling TA-FTIR

heated to a constant temperature of 200 °C. The whole FTIR compartment was continuously purged by nitrogen and additionally molecular sieves from CU Chemie Uetikon AG were used to minimize the water and carbon dioxide background in the recorded spectra. The resolution of the collected spectra was generally set to 4  $\text{cm}^{-1}$ , but can be varied between 1 and 32  $\text{cm}^{-1}$  and co-addition of 4 scans per spectrum was normally applied.

Gases leaving the FTIR spectrometer were passed through a heated (optionally up to 230 °C) capillary to a Pfeiffer Omni Star GSD 301 O mass spectrometer. Additionally the TA-MS coupling was applied, in which Balzers quadrupole mass spectrometer QMG 420 was connected to the Netzsch STA 409 thermoanalyzer (cf. Chapter 5). The scheme of TA-MS coupling is presented in Figure 2-4.

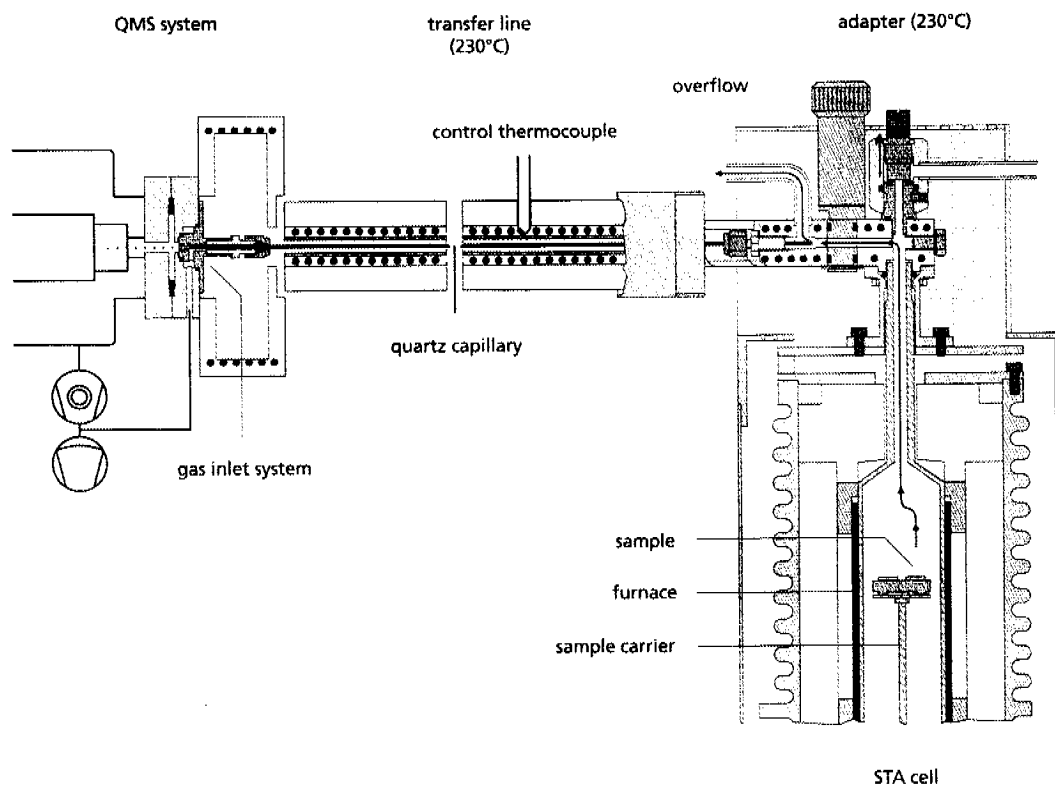


Fig. 2-4: Scheme of coupling TA-MS

## 2.3 Pulse Thermal Analysis

For the gas injections a home-made device was placed before the thermoanalyzer. It contains a rotary sample valve enabling a carrier gas to purge the loop of a given volume, which had been previously filled with the calibration gas of known composition. In order to quantify the FTIR or MS signals, pulses of a known volume were injected before and/or after the decomposition of the investigated sample. The scheme of the PulseTA<sup>®</sup> system is presented in Figure 2-5. The flow rate of the gas, passing through the *balance* chamber and over the *sample* was controlled by mass flow controllers 1 and 2, Brook's model 5850E, based on a thermal mass flow sensing technique.

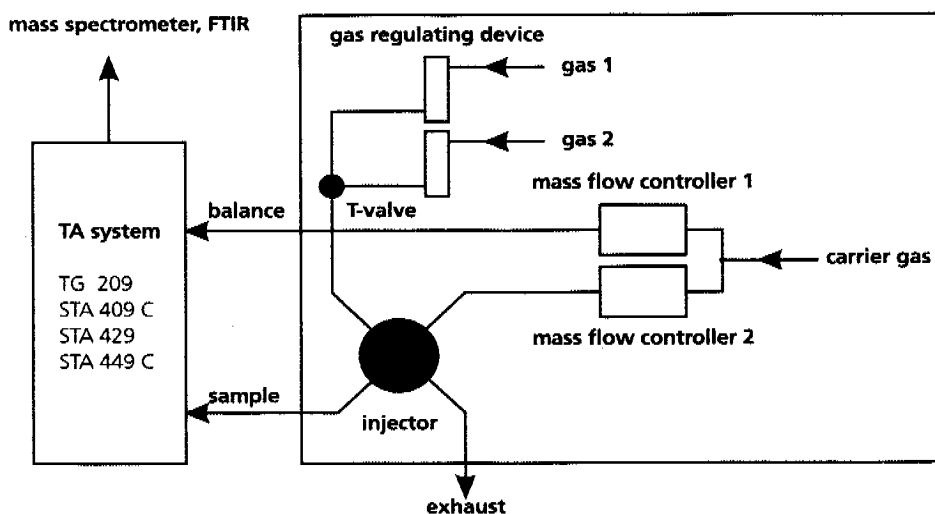


Fig. 2-5: Scheme of PulseTA<sup>®</sup>: principle of injection of gases into the carrier gas stream.

For injections of the liquids another home-made device consisting of a T-port tube was applied, which allows quantifying the evolved gases on the same experimental set up. An illustration of the whole TA-FTIR-MS system is shown in Figure 2-6. The T-port tube heated to ca. 100 °C was closed with a septum on the top (cf. no. 6 Figure 2-6), enabling the injections of liquids or dissolved solids with a syringe. Another injection port was installed on the top of the thermoanalyzer (cf. no. 7 Figure 2-6), allowing injections of liquids after the thermoanalyzer, therefore not being in contact with the sample and passing directly to the FTIR cell. This device was especially used for dissolved solids and liquids possessing higher boiling points (>150 °C) in order to avoid condensation on cold spots in the thermoanalyzer. Injections at these two different locations (before and after TA) results in totally different peak shapes, illustrated in Figure 2-7. The flow rate for injections after the thermoanalyzer has to be relatively low, because the residence time in the transfer line is very short, which, in turn, results in a very sharp and narrow FTIR signal compared to the



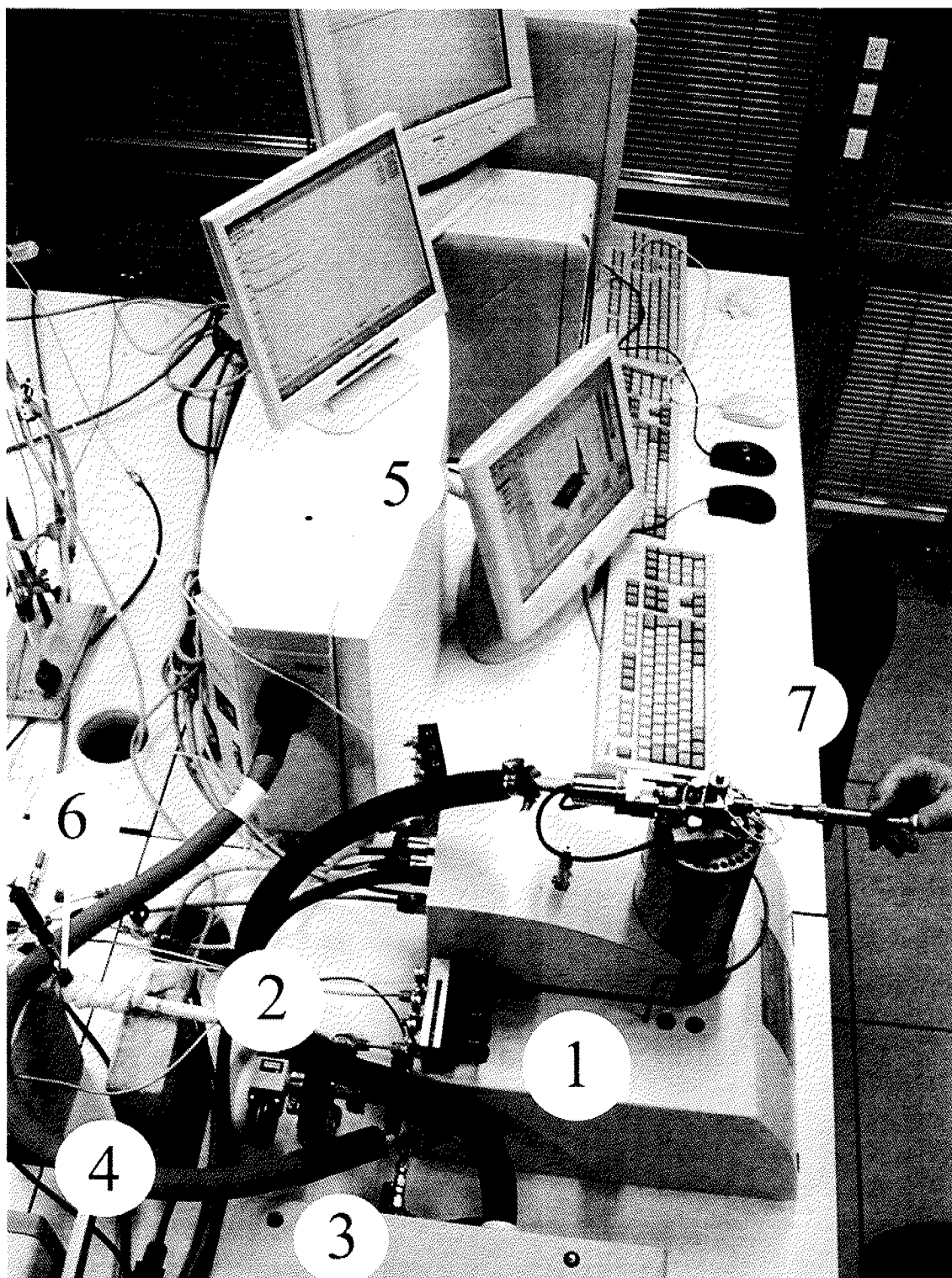
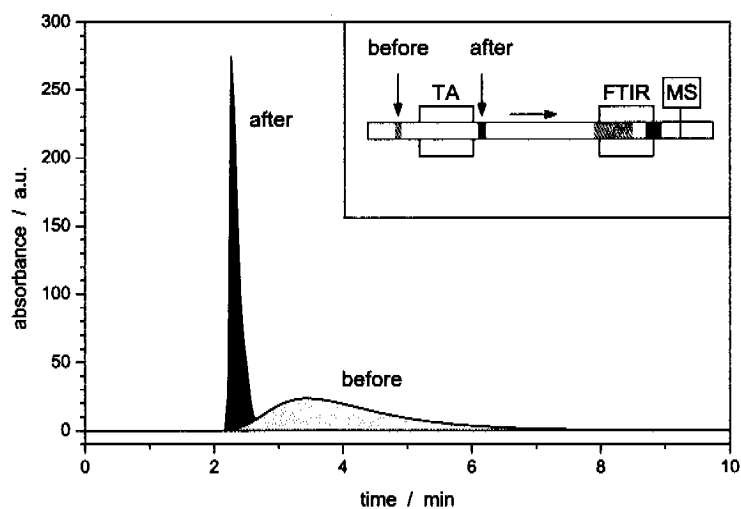


Fig. 2-6: Picture of the whole TA-FTIR-MS system, detail view. 1: thermoanalyzer, 2: transferline TA-FTIR, 3: FTIR spectrometer, 4: transferline FTIR-MS, 5: MS, 6: liquid injection port before TA, 7: liquid injection port after TA.



**Fig. 2-7:** Methanol pulses injected before (cf. no. 6 Figure 2-6) and after (cf. no. 7 Figure 2-6) the thermoanalyzer. Injected volume: 1 $\mu$ l. Inset: scheme of the experimental set up and the places of injection are marked by arrows.

one obtained by injection before the TA. In that case, the injected gas has to pass through a much larger volume (TA) and the FTIR response has a longer tailing due to prominent backmixing phenomena occurring in the TA-chamber.

Seite Leer /  
Blank leaf

Seite Leer /  
Blank leaf

## Quantitative Calibration of FTIR Spectroscopic Signals

### 3.1 Introduction

The main advantage of the coupled techniques TA-MS and TA-FTIR is the identification of gaseous products, which together with the thermal effects (DTA) and mass changes (TG), allows interpreting the course of the investigated reactions. The qualitative analysis is routinely done by comparing recorded spectra with key fragment ions and their relative intensities for known elements and compounds (MS) and with reference spectroscopic signals (FTIR). The development of TA-FTIR and TA-MS hyphenated techniques have been reviewed in the past [1–3]. The first application of coupling thermogravimetric and spectroscopic analysis was reported in 1969 by Kiss [4]. He has monitored the content of water and ammonia in evolved gases formed during the decomposition of ammonium paramolybdate and paratungstate and the dehydration of copper sulfate. The water molecules after passing over calcium carbide were transformed into acetylene and the amount of the generated acetylene was measured.

A variety of efforts [5–7] were made in the following years to gain benefits from coupling complementary techniques. Compared to other methods of

evolved gas analysis (EGA), FTIR is fast, sensitive and can detect almost all molecules except homonuclear diatomic gases.

In the strive for extending the opportunities of coupled techniques, successful quantification has been achieved recently, applying FTIR [8–10] or MS [8,11–14] spectrometry. Such quantification is especially important when investigating multistage decomposition reactions, or, when two or more gases evolve simultaneously. In such cases the thermoanalytical methods alone fail for the quantitative description of the investigated process and have to be coupled with MS or FTIR enabling quantitative and qualitative determination of the evolved gases.

The conventional method of quantification of FTIR spectra is based on time-consuming calibration, which requires the preparation and measuring of reference mixtures with varying concentrations. Therefore several expensive gas standards and an accurate flow control are required to obtain reliable values of concentrations in the FTIR gas cell. Moreover, due to the influence of several experimental parameters on the intensity of FTIR signal (as e.g. change of the baseline), the calibration has to be frequently repeated. In order to avoid these problems, pulse calibration techniques were investigated by Guardia and coworkers [15,16]. They developed a direct and simultaneous application to quantify different fluids, e.g. butyl acetate, toluene and methyl ethyl ketone based on the use of vapor phase FTIR measurements. However, these experiments were only carried out with FTIR spectrometer without coupling it to the thermoanalyzer. First quantification of evolved gases based on the pulse technique combined with TG systems was performed by Maciejewski et al. [12,13]. Quantification of the FTIR signals in the FTIR-TA system was targeted in this chapter by decomposing a known amount of solids with known stoichiometry of the decomposition process and by injection of liquids into the TA-FTIR sys-

tem. The extension to FTIR-TA coupled technique was achieved by Marsanich et al. [17,18]. They applied also the gas-pulse calibration using ammonia, carbon monoxide and carbon dioxide. They introduced the vaporization technique for calibration of the FTIR signals by liquids samples using the vaporization technique. The applied procedure enabled indirect quantification of evolved gases. The injections (calibrations) were not carried out *in situ*, that is during the same experimental run in which the decomposition of the investigated samples was studied.

The opportunity of injecting a known amount of a particular gas or liquid into the carrier gas stream provides a quantitative calibration by relating the FTIR signal to the injected quantity of probe species. A linear relation between spectral absorbance at a given wavenumber and low concentration of gaseous compounds is postulated by Lambert-Beer's law:  $A_{\nu} = c \cdot d \cdot \epsilon_{\nu}$ , where  $A$  is the integral absorbance over a wavenumber interval  $\nu$  ( $\text{cm}^{-1}$ ),  $c$  the concentration of the absorbing species ( $\text{mol l}^{-1}$ ),  $d$  the optical path length (cm) and  $\epsilon_{\nu}$  the integral molar absorption coefficient ( $\text{l mol}^{-1} \text{cm}^{-1}$ ). Three different methods of quantifications in coupled TA systems have been applied so far. They are based on calibration by:

- Decomposing solids with well-known stoichiometric reaction e.g. calcium carbonate [12,14], calcium oxalate [12,14,19,20] or sodium bicarbonate [12,19] in TG-MS systems.
- Injection of a known amount of the calibration compound into the carrier gas stream flowing through the thermoanalyzer and evolved gas analysis device (MS [12] or FTIR [17,18]).
- Vaporization of known amounts of liquids in the thermoanalyzer itself [18,21].

In order to extend and validate the opportunities of quantification of evolved gases in TA-FTIR systems, we present the results of *in situ* calibrations applying

different techniques and using gases, liquids and solids. Additionally, the influence of experimental parameters such as the concentration of the analyzed species, temperature and flow rate of carrier gas on the FTIR signals was investigated. Furthermore, the PulseTA<sup>®</sup> [13] developed in our group was expanded to new applications, involving liquid components. This new technique, in contrast to the known vaporization methods, is based on isothermal or non-isothermal calibration, which allows *in situ* calibration before the reaction (decomposition) of the target compound has already started.

## 3.2 Experimental

Experiments were carried out on a Netzsch TG 209 and STA 449 analyzer equipped with two pulse devices enabling injection of a certain amount of one or two different gases or gaseous mixtures into the carrier gas stream flowing through the system [13]. The experimental set up is depicted in Figure 2-5 in Chapter 2. The amount of injected gas could be changed from 0.01 to 2.0 ml. Volumes of 0.25, 0.5, 1.0 and 2.0 ml were mainly used.

Additionally two heated injection ports were installed before and after (on the top of) the thermoanalyzer allowing injections of liquids with a Hamilton syringe CR-700-20. The amount of injected liquid was usually in the range from 1 to 10  $\mu\text{l}$ .

The flow rate was controlled by mass flow controllers, Brook's model 5850E, based on a thermal mass flow sensing technique. A helium (purity 99.999%, PanGas) carrier gas flow rate of  $50 \text{ ml min}^{-1}$  was used. The thermoanalyzer was connected by a heated (ca.  $200 \text{ }^\circ\text{C}$ ) transfer-line to a Bruker Vector 22 FTIR spectrometer (Figure 2-6 in Chapter 2).



The FTIR apparatus is equipped with a MCT detector and a specifically developed low-volume gas cell (8.7 ml) with a 123 mm path length and ZnSe windows. To avoid condensation of low volatile compounds the cell was heated to a constant temperature of 200 °C. The whole FTIR compartment was continuously purged by nitrogen and additionally molecular sieves were used to minimize the water and carbon dioxide background in the recorded spectra. The resolution of the collected spectra was set to 4 cm<sup>-1</sup> and co-addition of 4 scans per spectrum was applied. As a consequence spectra were recorded with a temporal resolution of about 6 s, depending on the integration methods. The IR acquired interferograms constantly during the time of the test, and the residence time of the injected species in the gas cell was about 10 s (flow rate: 50 ml min<sup>-1</sup>). In this way, the spectra of all gases were averaged, without cutting peaks of the calibration pulses, which would lower the accuracy of the quantification of the evolved species.

### 3.2.1 Pulse Calibration

For the gas injections a home-made device was placed before the thermoanalyzer. It contains a rotary sample valve enabling a carrier gas to purge the loop of a given volume, which had been previously filled with the calibration gas of known composition. In order to quantify the FTIR signals, pulses of a known volume were injected before and/or after the decomposition of the investigated sample. For injections of the liquids another home-made device consisting of a T-port tube was applied, which allows quantifying the evolved gases on the same experimental set-up. The T-port tube heated to ca. 100 °C was closed with a septum on the top, enabling the injections of liquids or dissolved solids with a syringe. Another injection port was installed on the top of the ther-

moanalyzer, allowing injections of liquids after the thermoanalyzer, therefore not being in contact with the sample and passing directly to the FTIR cell. This device was especially used for dissolved solids and liquids possessing higher boiling points ( $>150\text{ }^{\circ}\text{C}$ ) in order to avoid condensation on cold spots in the thermoanalyzer. The carrier gas flow was set to  $20\text{ ml min}^{-1}$ . The flow rate has to be relatively low, because the residence time in the transfer line is very short, which, in turn, results in a very sharp and narrow FTIR signal compared to the one obtained upon injection before the thermoanalyzer. In that case, the injected gas has to pass through a much larger volume (TA) and FTIR response has a longer tailing due to prominent backmixing phenomena occurring in the TA-chamber.

### 3.2.2 Pinhole Calibration

This method was used to calibrate the FTIR spectra when making calibration with organic liquids or water. Usually 25 mg of the investigated liquid was placed in the crucible closed by the lids with pinholes with different diameters (0.1, 0.5, 1 and 2 mm). The heating and flow rate were  $10\text{ K min}^{-1}$  and  $50\text{ ml min}^{-1}$ , respectively.

### 3.2.3 Differential Calibration

Last method allows carrying out the calibration of the FTIR signal and investigation of the decomposition (or desorption) process during one run. The set up consists of two crucibles: the first contains the liquid used for the calibration and the second one the investigated sample. The quantification is based on the FTIR signal obtained during vaporization of the liquid at low, constant temperature ( $25\text{--}50\text{ }^{\circ}\text{C}$ ) or during a non-isothermal run carried out with low heat-

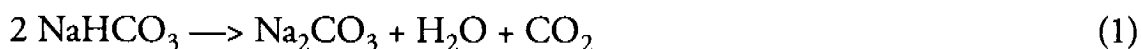
ing rate up to a temperature lying significantly below the decomposition temperature of the solid sample. The rate of vaporization can be changed in a very broad range by varying the temperature and the pinhole diameter. The experiments were normally performed applying an isothermal period of about 30 min followed by the decomposition period with a heating rate of  $10 \text{ K min}^{-1}$ . The sample mass of the calibrated liquid was in the range of 10–25 mg and the mass of decomposed sample was 100–200 mg. In order to avoid overlapping of the calibration and measuring processes, it was important that the liquid reference material used for the calibration had fully evaporated during the isothermal run, before beginning of the decomposition of the solid. The carrier gas flow was set to  $25\text{--}50 \text{ ml min}^{-1}$ .

### 3.3 Results and Discussion

We have investigated the three methods of calibration of FTIR signals described above. The presented examples describe the application of both, gases and liquids in the calibration procedure.

#### 3.3.1 Quantification of FTIR Signals Using Gases

The application of PulseTA<sup>®</sup> for quantitative interpretation of FTIR signals is illustrated by comparing results obtained by means of thermogravimetry and FTIR in a simultaneous PulseTA<sup>®</sup>-FTIR experiment. 36.15 mg of  $\text{NaHCO}_3$  was decomposed under helium with a heating rate of  $10 \text{ K min}^{-1}$ . The decomposition of sodium bicarbonate occurs according to Eq. 1:



In order to quantify the FTIR signal of  $\text{CO}_2$ , two 1 ml pulses of  $\text{CO}_2$  were injected before and after the decomposition of  $\text{NaHCO}_3$  (Figure 3-1A). The

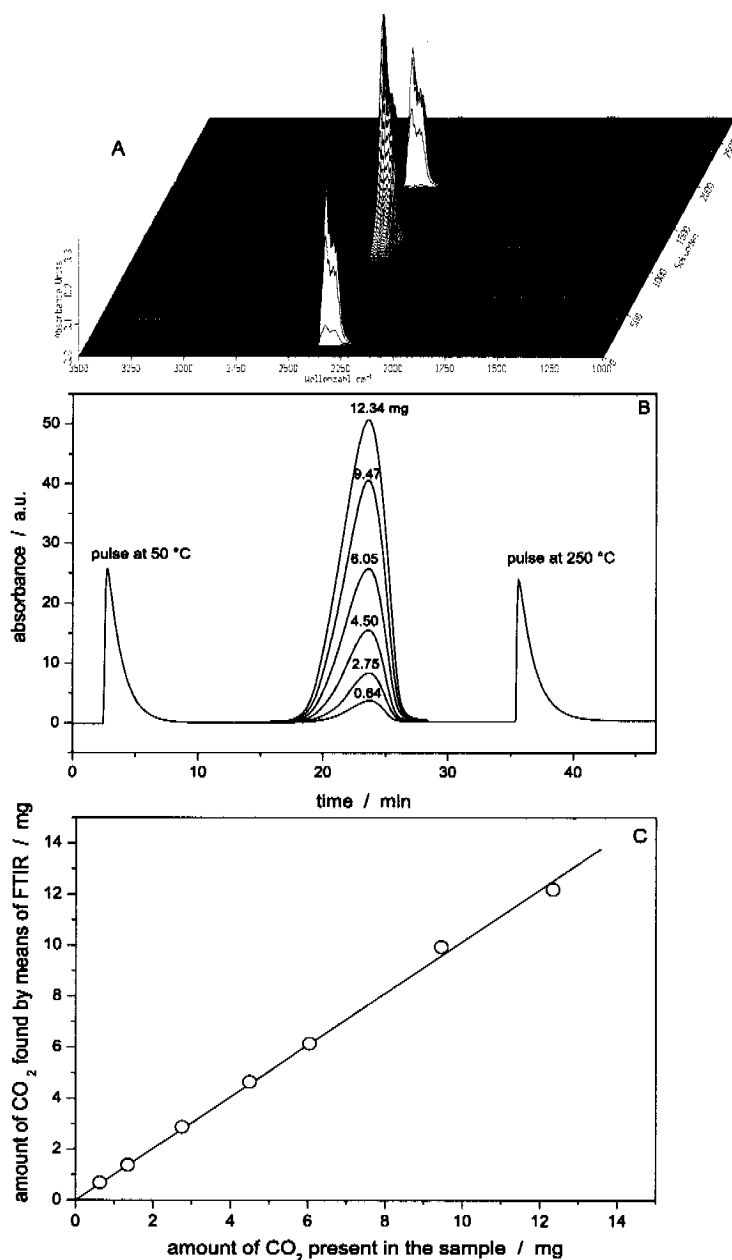


**Fig. 3-1:** A: 3-D FTIR-diagram of the calibration (2 pulses) and the evolved gases during the decomposition of  $\text{NaHCO}_3$ . B: Relationship between amount of evolved  $\text{CO}_2$  in the sample and intensity of  $\text{CO}_2$  traces recorded in TA-FTIR system. C: Amount of  $\text{CO}_2$  found by FTIR as a function of amount of  $\text{CO}_2$  present in the sample.

mean value of the integral intensities of the injected pulses was 1727 a.u., while the integral intensity of the signal of the evolved CO<sub>2</sub> was 9236 a.u. The temperature of the injected gas was 28 °C. The amount of CO<sub>2</sub> formed during the decomposition calculated from these data corresponds to 9.52 mg, which agrees well with the stoichiometric value of 9.47 mg, confirming the accuracy of the quantification method. In order to check the dependence between the intensity of FTIR signals and amount of evolved species, different amounts of NaHCO<sub>3</sub> were decomposed. The resulting CO<sub>2</sub> traces are presented in Figure 3-1B.

Figure 3-1C shows the relation between the amount of evolved CO<sub>2</sub> derived from FTIR signals and the amount of CO<sub>2</sub> present in the sample. The obtained linear dependence between the integral intensities of CO<sub>2</sub> traces (peak areas) and amount of evolved gas has been hold in a wide range: in the presented case from 0.64 to 12.34 milligrams of evolved CO<sub>2</sub>.

The influence of the temperature (in the TA chamber) on the shape and intensity of the FTIR signals was investigated. At each temperature two pulses of CO<sub>2</sub> have been injected into the carrier gas stream; the integral intensity  $I$  (Eq. 2) was independent of the temperature (50 °C: 101/100 a.u., 350 °C: 101/99 a.u., 950 °C: 101/98 a.u.).

$$I = \int_{t_1}^{t_2} \left[ \int_{\nu_1}^{\nu_2} A(\nu) d\nu \right] dt \quad (2)$$

The results confirmed the conclusion by Maciejewski et al. [12] for the TA-MS system that in the range room temperature up to 1000 °C the shape of the spectra is slightly changing but the integral intensities remain constant. Note that at higher temperature the backmixing and diffusion in the TA are

enhanced which in turn affects the residence time distribution of the calibration gas.

The comparison of the integration of CO<sub>2</sub> and NH<sub>3</sub> signals at different wavenumbers presented in Table 3-1 and Table 3-2 clearly illustrates the potential source of errors in the calibration, resulting from application of too strong vibrational signals. For species giving very intensive signals as e.g. CO<sub>2</sub>, it is relative easy to leave the range where linearity of the Lambert-Beer relationship is guaranteed (cf. chapter 4). Best correlation was obtained at 3600 cm<sup>-1</sup> for CO<sub>2</sub> ( $r^2 = 0.9998$ ), whereas the band at 2350 cm<sup>-1</sup> gave also

**Table 3-1:** Pulse calibration: FTIR integral intensity recorded during injections of CO<sub>2</sub>. Slopes of linear regression through zero were normalized to 1 in order to simplify comparison of the values, gained by different integration methods for CO<sub>2</sub> (1: 2350 cm<sup>-1</sup>) and (2: 3600 cm<sup>-1</sup>).

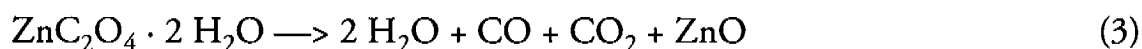
Loops / ml	CO <sub>2</sub> (1)	CO <sub>2</sub> (2)	RSD (1) / %	RSD (2) / %
0.25	0.28	0.26	10.5	3.1
0.50	0.56	0.52	9.3	3.1
0.75	1.03	1.00	3.0	0.4
2.00	1.96	1.99	-1.5	-0.3
Linear correlation $r^2$			0.9952	0.9998

**Table 3-2:** Pulse calibration: FTIR integral intensity recorded during injections of NH<sub>3</sub>. Integration methods for NH<sub>3</sub> (1: 950 cm<sup>-1</sup>) and (2: 1630 cm<sup>-1</sup>).

Loops / ml	CO <sub>2</sub> (1)	CO <sub>2</sub> (2)	RSD (1) / %	RSD (2) / %
0.25	0.27	0.25	9.6	-9.8
0.50	0.54	0.52	7.3	-3.6
0.75	1.10	1.02	9.6	-6.9
2.00	1.94	1.98	-3.0	2.3
Linear correlation $r^2$			0.9909	0.9994

good results ( $r^2 = 0.9952$ ).  $\text{NH}_3$  measurements showed good correlation at  $1630\text{ cm}^{-1}$  ( $r^2 = 0.9994$ ), but at  $950\text{ cm}^{-1}$  the linear dependence was slightly poorer ( $r^2 = 0.9909$ ).

The possibility of the exact quantification of FTIR signals by means of PulseTA<sup>®</sup> increases significantly the potential of the coupled TA-FTIR method. A further application of PulseTA<sup>®</sup> for the quantification of evolved gases is illustrated by the results obtained for the decomposition of zinc oxalate dihydrate (Eq. 3):



To calibrate the FTIR signals, 1 ml pulses of CO and CO<sub>2</sub> were injected before decomposition into the carrier gas stream. The traces of CO and CO<sub>2</sub> pulses were normalized in order to compare the integral intensities of traces of CO and CO<sub>2</sub> formed during decomposition. The resulting curves, presented in Figure 3-2, indicate that the amounts of both evolved species are equal. This agrees well with the reaction stoichiometry (Eq. 3). Note that confirmation of this stoichiometry is difficult when applying conventional mass spectrometry. Due to the fragmentation of CO<sub>2</sub> species the determination of the composition of CO and CO<sub>2</sub> mixture needs very time consuming calibration of the MS signals and accurate determination of the fragmentation pattern of CO<sub>2</sub> molecules in the applied mass spectrometer. The use of tabulated data of CO<sub>2</sub> fragmentation for calibration purposes without their experimental corroboration can lead to uncertain results due to overlapping of current ions of  $m/z=28$  resulting from the presence of CO and fragmentation of CO<sub>2</sub>.

The gas-pulse calibration method is a single point *in situ* calibration, where calibration and investigated reaction are performed in the same experimental

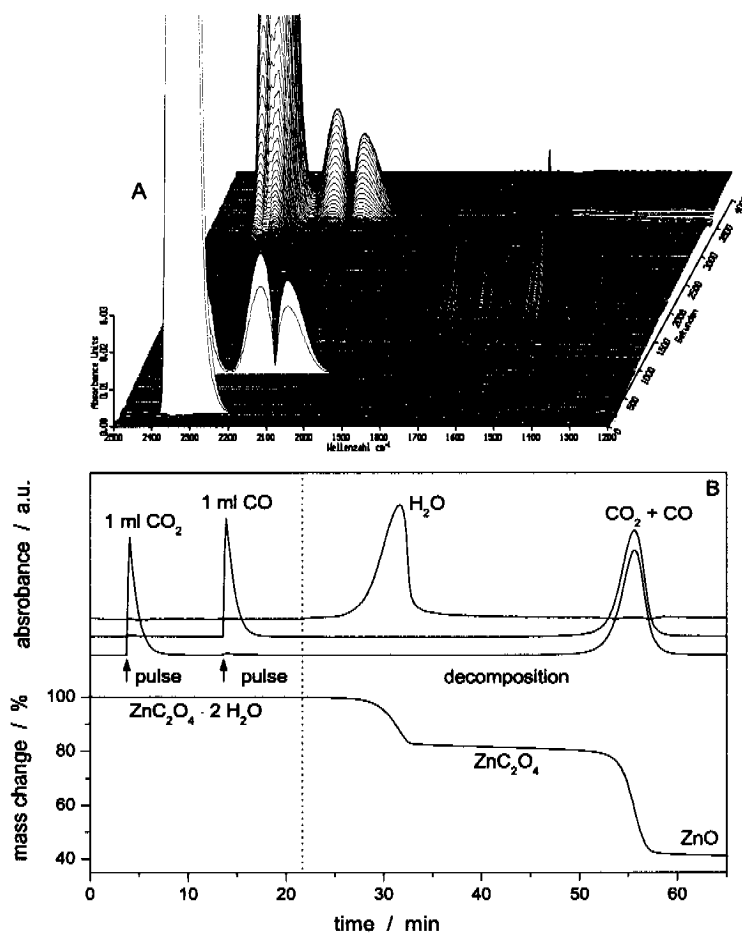


Fig. 3-2: A: 3-D FTIR-diagram of the calibration (1 pulse:  $\text{CO}_2$ , second pulse:  $\text{CO}$ ) and the evolved gases during the decomposition of  $\text{ZnC}_2\text{O}_4 \cdot 2 \text{H}_2\text{O}$ . B: Normalized  $\text{CO}$  and  $\text{CO}_2$  traces obtained during calibration (injection of 1 ml  $\text{CO}$  and  $\text{CO}_2$ ) and decomposition of  $\text{ZnC}_2\text{O}_4 \cdot 2 \text{H}_2\text{O}$ ; TG curve is shown in the lower part of the plot.

run. This enables quantification of the spectroscopic signals without taking into account several parameters such as flow rate and kind of the carrier gas, rate of the FTIR data acquisition or other experimental factors. In order to carry out the quantification in the linear range, where the Lambert-Beer' law is obeyed, the calibration should be made with the smallest possible amounts of injected calibration gases. Additionally, the amount of the analyzed substance should be chosen in such a way that the amount of evolved gases are similar to



those used for the calibration, especially if adsorption bands with high intensity are used.

Marsanich et al. [17] also found a linear relationship between FTIR signals and the amount of injected gases with pulse calibration for  $\text{NH}_3$ ,  $\text{CO}_2$  and  $\text{CO}$  (0-35 mol). In contrast to our strategy, they did not inject the gases into the carrier gas flow passing through the TGA system. They applied a separate gas stream that was directly passed to the FTIR cell.

The *in situ* method described in this chapter was later applied for the quantification of  $\text{NO}_2$ ,  $\text{NO}$  and  $\text{NH}_3$  during the selective catalytic reduction of  $\text{NO}$  by  $\text{NH}_3$  over manganese-cerium mixed oxides (cf. chapter 6).

### 3.3.2 Quantification of FTIR Signals by Liquids

For gases the quantification of FTIR signals is possible either by conventional calibration (varying concentrations of target gases) or, as described above, by the injection of a known amount of the calibrating gas into the carrier gas stream. For the quantification of FTIR signals by the liquids we applied several methods, pulse calibration and two methods based on the evaporation of liquids: pinhole and differential calibrations. These methods were studied by applying different organic liquids and water.

#### Pulse Calibration

In order to extend the opportunities of quantifying FTIR signals, the possibility of injection of liquids into the carrier gas stream was studied. The signals resulting from the injection of pulses of ethanol into the carrier gas stream are shown in Figure 3-3A. In order to check the dependence between amount of injected liquid and resulting intensity of FTIR signals, the amount of ethanol was changed from 5 to 80  $\mu\text{l}$ . The traces of ethanol obtained by applying dif-

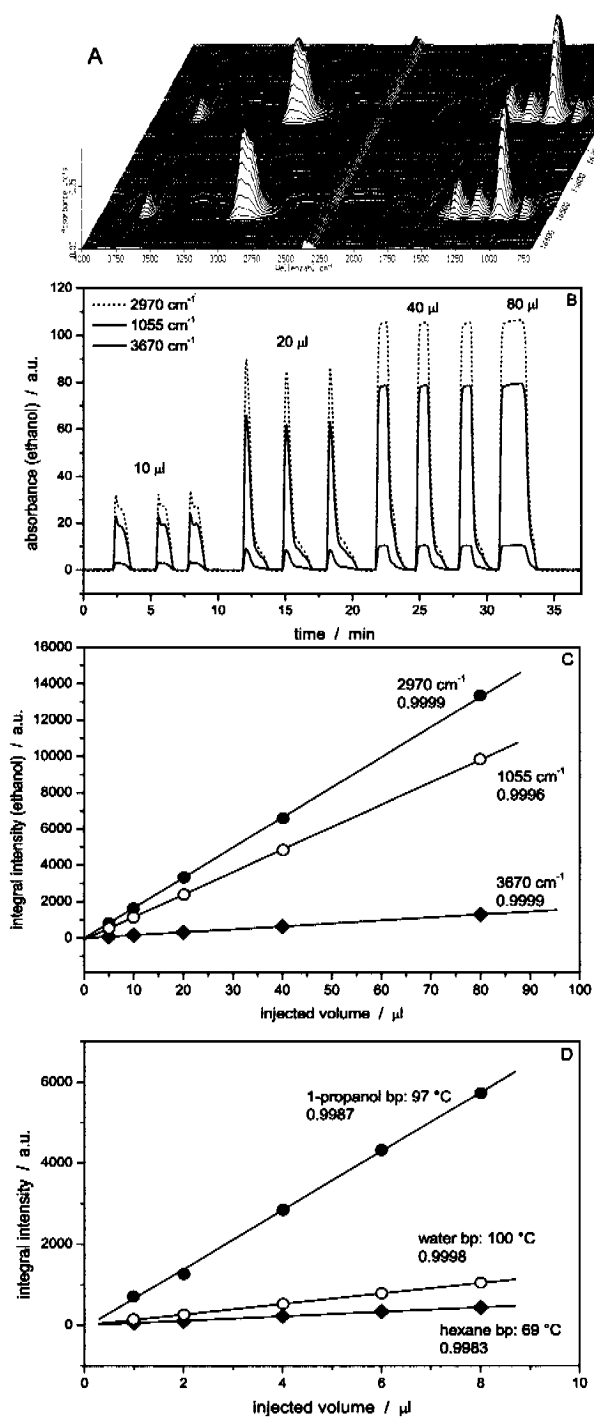


**Fig. 3-3:** A: 3-D FTIR-diagram of the calibration of ethanol (1 pulse: 5  $\mu$ l). B: ethanol traces due to different integration methods at three characteristic wavenumbers for ethanol (1055, 2970 and 3670  $\text{cm}^{-1}$ ). C: Linear dependence between the integral intensity of the FTIR signals on the amount of injected ethanol. D: Linear dependence between the intensity of the FTIR signals on the amount of injected liquids (1-propanol, water and hexane).

ferent integration modes at the characteristic wavenumbers are shown in Figure 3-3B. The averaged integral intensities of the signals as a function of injected volumes are presented in Figure 3-3C. The applied integration modes for the characteristic bands for ethanol revealed a linear relationship: best correlations were obtained at  $3670\text{ cm}^{-1}$  ( $r^2 = 0.9999$ ) and at  $2970\text{ cm}^{-1}$  ( $r^2 = 0.9999$ ), whereas the linearity obtained with the band at  $1055\text{ cm}^{-1}$  was slightly less perfect ( $r^2 = 0.9996$ ).

Other calibrations (injection from one to eight  $\mu\text{l}$ ) were performed with hexane (b.p.  $69\text{ }^\circ\text{C}$ ), 1-propanol (b.p.  $97\text{ }^\circ\text{C}$ ) and water (b.p.  $100\text{ }^\circ\text{C}$ ). The linear dependence between amount of injected liquid and integral intensity of FTIR signal (peak area) enables the quantification of FTIR data (Figure 3-3D). It is worth mention that the injection of various gases or liquids allows also creating own libraries facilitating identification of gaseous products evolving during reaction or desorption.

The quantification of the FTIR spectra by injecting liquids was extended to binary organic mixtures. Figure 3-4A-B show FTIR spectra of binary mixtures of methanol and methyl formate and their characteristic traces due to integration of the bands at  $1030$  and  $1180\text{ cm}^{-1}$ , respectively. Figure 3-4C shows a linear dependence of the intensity of the FTIR signals on the amount of injected liquids (methanol and methyl formate), and finally, Figure 3-4D depicts the dependence of the FTIR absorbance ratio on the mass ratio of methanol in the mixture (wt.%). These results corroborate that if the selected characteristic FTIR bands of two or more investigated compounds do not overlap, the quantification of the resulting spectra is also possible in the case of binary mixtures. Of course, as mentioned by Barontini et al. [22], it is necessary to take into account possible factors influencing the composition of the gaseous phase during evaporation of liquids (as e.g. formation of azeotropes). It

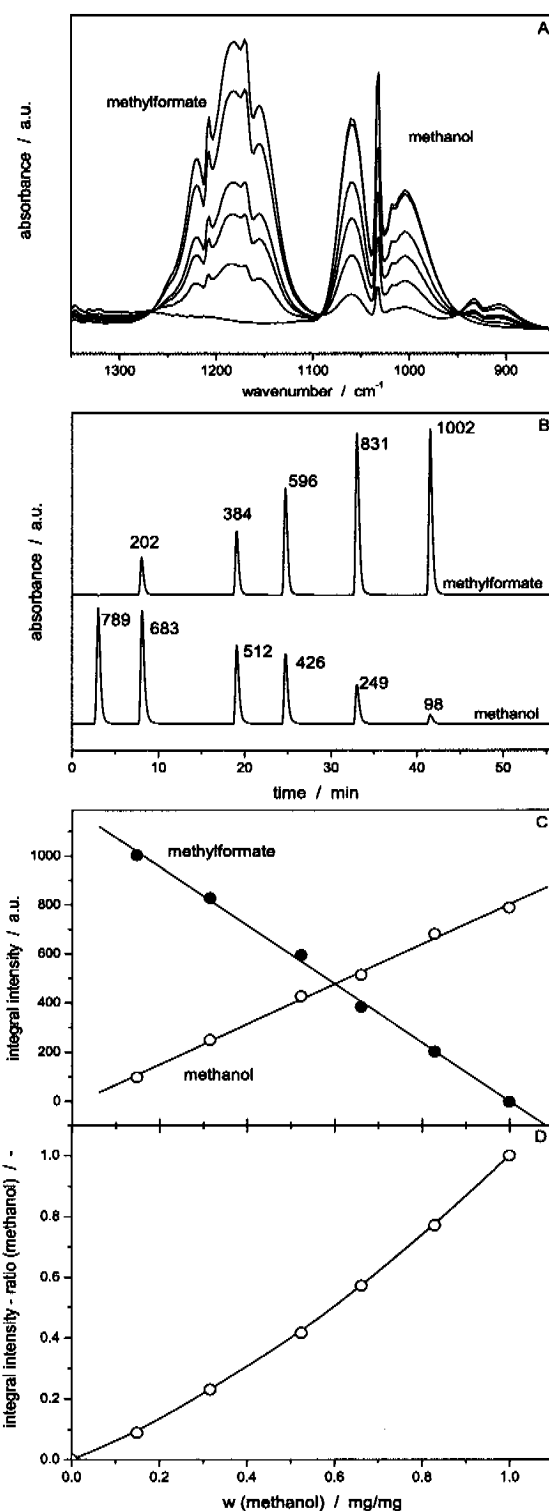


**Fig. 3-4:** A: FTIR spectra of binary liquid mixtures of methanol and methylformate. B: methanol and methylformate traces as a function of the mixtures composition. C: The dependence between the integral intensity of the FTIR signals on the mixture composition. D: resulted FTIR absorbance ratio vs. mass ratio ( $w$ ) of methanol in the binary mixtures.

is in principle possible to obtain the vapor-liquid equilibrium data, but a serious limitation is the poor mixing (natural convection only). Note, that sample stirring is not possible in the commonly used TA-FTIR systems.

As an example of quantification of FTIR spectra by pulse calibration with liquids, we present the determination of the amount of water evolved during the decomposition of sodium bicarbonate and dehydration of copper sulfate pentahydrate.

Figure 3-5A shows the water traces recorded during two calibration pulses and decomposition of 106.5 mg  $\text{NaHCO}_3$  according to reaction (1). The

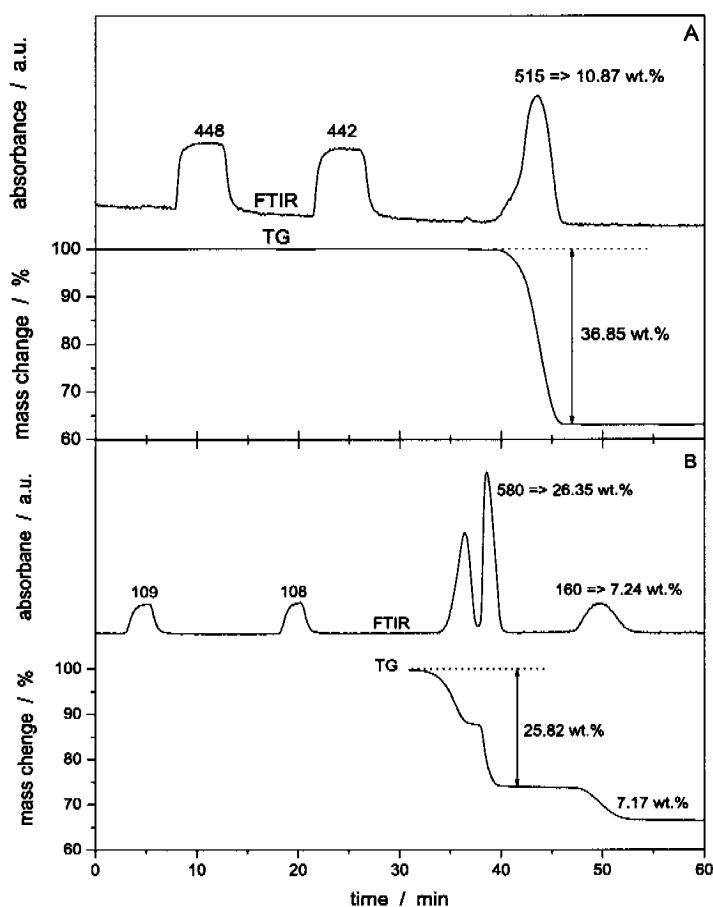


**Fig. 3-5:** Pulse calibration: water-traces recorded during decomposition of 106.5 mg  $\text{NaHCO}_3$  (A) and 48.9 mg  $\text{CuSO}_4 \cdot 5 \text{H}_2\text{O}$  (B). Heating rate:  $10 \text{ K min}^{-1}$ , carrier gas:  $50 \text{ ml min}^{-1}$ , Injected water volumes:  $10 \mu\text{l}$  (A),  $2.5 \mu\text{l}$  (B).

mean value of the integral intensities of the injected pulses was 445 a.u., while the integral intensity of the signal of the evolved H<sub>2</sub>O was 515 a.u. The amount of injected water was 10.0 mg (ca. 10 μl). The amount of H<sub>2</sub>O formed during the decomposition calculated from these data corresponded to 10.87 wt.%, which agrees well with the stoichiometric value of 10.69 wt.%, confirming the accuracy of the quantification method. The stoichiometry of the decomposition was corroborated by the TG analysis: the observed mass loss due to the evolution of CO<sub>2</sub> and H<sub>2</sub>O was 36.85 wt%, while the stoichiometric value amounts to 36.90 wt.%.

Figure 3-5B shows the water traces recorded during two calibration pulses and dehydration of 48.9 mg CuSO<sub>4</sub> · 5 H<sub>2</sub>O. At lower temperatures the dehydration of the pentahydrate occurred in two steps; the observed mass loss corresponded to 25.82 wt.% and agreed well with the evolved amount of water found by means of FTIR (26.35 wt.%).

During the further dehydration at about 220 °C (between 48 and 52 min) the residual water molecules evolved (dehydration of monohydrate), as confirmed by experimental and stoichiometric mass losses (7.17 and 7.21 wt.%, respectively). The amount of water determined from the FTIR traces by comparing the integral intensity of the injected 2.41 mg (ca. 2.5 μl) water and the intensity of the decomposition peak was 7.24 wt.% which is in accord with the gravimetric results and the reaction stoichiometry.

### **Pinhole Calibration**

During the pinhole calibration the compound is not injected into the carrier gas stream, but placed into the thermoanalyzer and vaporized isothermally or by a linear heating ramp. For liquid mixtures (cf. binary mixtures) it is impor-

tant to select a characteristic wavenumber interval to avoid overlapping of related absorption bands.

Figure 3-6 shows the mass losses and FTIR signals recorded during vaporization of acetone (A), ethanol (B), water (C) and hexanol (D) from the pans with different pinhole sizes. Due to the low boiling points of acetone and ethanol remarkable mass losses were recorded immediately after starting measurement. In this case, especially when working without lid or using larger pinhole sizes, it is difficult to determine an accurate mass loss during evaporation (cf. Figure 3-6A) because a certain amount of the substance will evaporate even

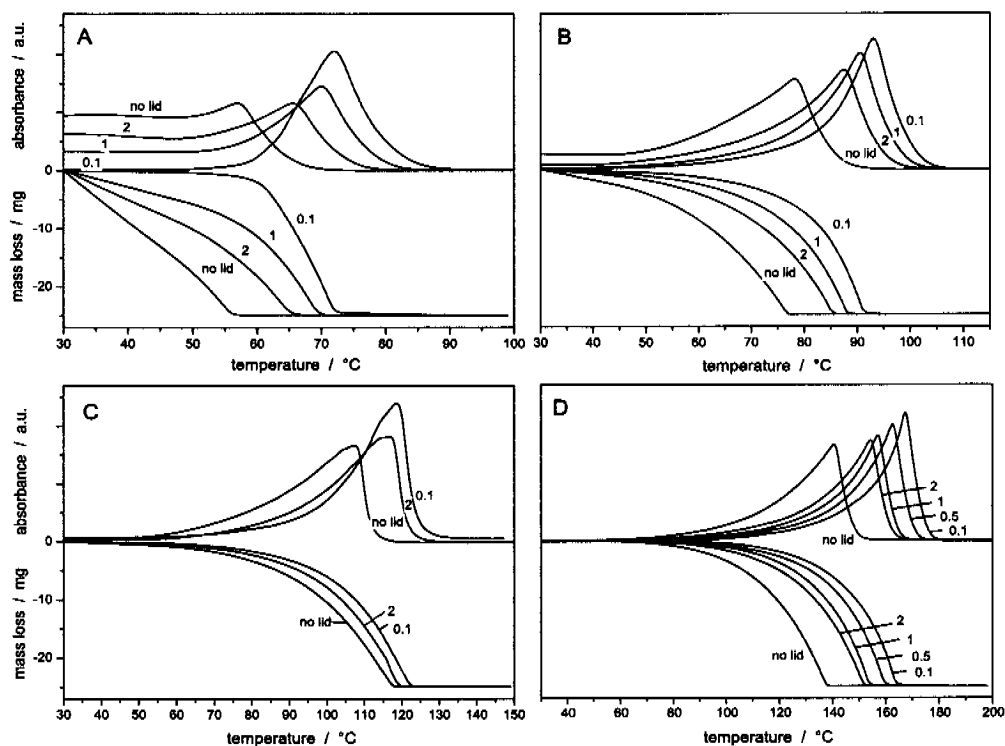


**Fig. 3-6:** Pinhole calibration of acetone (A), ethanol (B), water (C) and hexanol (D), sample mass: 25 mg, heating rate: 10 K min<sup>-1</sup>, flow rate: 50 ml min<sup>-1</sup>, pinhole diameters are indicated on the curves.

at room temperature, which in turn, will disallow finding the relationship between the amount of evaporated liquid and intensity of FTIR traces. A lid with a pinhole size of 0.1 mm was necessary to prevent the acetone vaporization at room temperature and obtain the FTIR trace, which started at the baseline and enabled proper integration of the recorded peak. For ethanol a pinhole size of 2.0 mm was enough and for water and hexanol even no lids were necessary to achieve accurate calibration. To avoid uncertainty caused by the mass loss in the beginning of the experiment due to the high evaporation rate (vapor pressure) of some liquids, the amount of the calibrating substance used was higher than 25 mg. During experiment settling and some isothermal part of the temperature ramp the mass loss of the sample was not recorded. The calibration measurements were started exactly when the mass of the calibration liquid, measured by the internal TA balance, was precisely 25.0 mg.

The detailed results of the pinhole calibrations are listed in Table 3-3. The relative standard deviation (RSD) was smaller than 4% for all four liquids with boiling points ranging from 56 °C (acetone) to 154 °C (hexanol). The vaporization at low temperatures at the beginning of the experiment or even before its start, which can introduce a significant error during the pinhole calibration

**Table 3-3:** Pinhole calibration: FTIR integral intensity recorded during vaporization of 25 mg of different liquids (acetone, ethanol, water and hexanol) from pans covered by lids with various pinhole sizes. Peak areas were determined at their characteristic wavenumber and normalized to an average of 100 a.u.

Sample	0.1 mm	0.5 mm	1.0 mm	2.0 mm	no lid	RSD / %
acetone	98.7	-	101.1	101.5	98.6	1.52
ethanol	97.2	-	99.1	102.8	100.9	2.38
water	102.0	-	-	98.8	99.2	1.78
hexanol	104.2	102.7	94.8	98.1	100.2	3.73



procedure, was also reported by Slager and Prozonic [21]. They found that for highly volatile compounds (e.g. acetone and methanol) significant evaporation occurred before the TGA run was actually started.

The carrier gas flow is a crucial factor in the calibration procedure, that affects intensity and shape of the recorded signals. Low flow rate leads to higher maximum intensity of the observed spectra, but increases the residence time of the evaporated molecules in the TA-FTIR system and leads to more prominent backmixing, resulting in significant tailing of the signals. This phenomenon can cause difficulties in the evaluation of the integral intensities of the recorded signals when the reaction or desorption does not occur in a single stage due to overlapping signals. The influence of the flow on the shape and intensity of spectroscopic signals has been analyzed quantitatively by some of us for the MS-TA system [11]. In order to study this influence on the calibration by the pinhole method, experiments were carried out with different carrier gas flow rates. The real progress of the evaporation is reflected by the derivative TG curve (DTG) that indicates the rate of the mass change. This progress has been compared to the recorded FTIR spectra which allowed to investigate the changes of the shape of the recorded spectroscopic signals as a function of the carrier gas flow rate.

Figure 3-7 shows the quantification of the FTIR signals using pinhole (2.0 mm) calibration of ethanol when varying the carrier gas flow rate. 25 mg sample of ethanol was heated with  $10 \text{ K min}^{-1}$ . All DTG and FTIR curves were normalized in order to allow comparison of flow rate influence on the shape of the FTIR signals. The results presented in Figure 3-7 clearly indicate that low carrier gas flow rate leads to increase of the residence time in the TG-FTIR system and results in a long tailing of the recorded FTIR traces due to prominent backmixing (cf. the comparison of the real rate of the evaporation process rep-

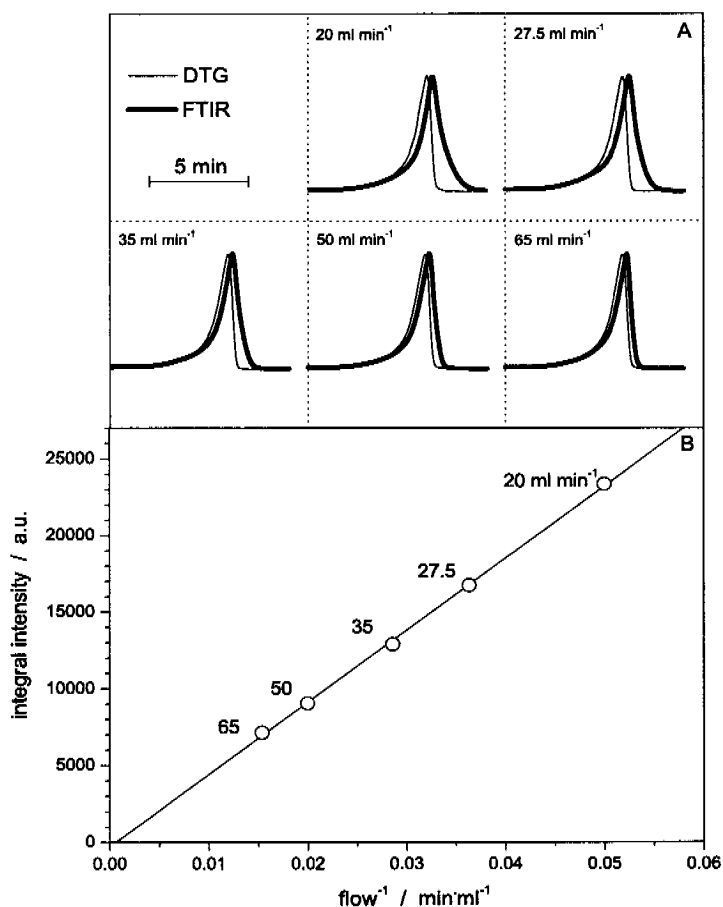


**Fig. 3-7:** A: Pinhole calibration of ethanol with varying carrier flow rate, sample size: 25 mg, heating rate: 10 K min<sup>-1</sup>, DTG (thin) and FTIR (thick lines). B: The relationship between the integral intensity and the reciprocal flow defined as the ratio of injected volume (1 ml) to the flow rate of carrier gas (ml min<sup>-1</sup>), which are marked on the data.

resented by DTG curve to the delayed FTIR traces for the flow of 20 ml min<sup>-1</sup>). However, there exists a linear relationship between FTIR absorbances and the reciprocal values of the flow rate (Figure 3-7B). A detailed study of the influence of mass transfer (by convection and diffusion) on the relation between thermoanalytical and mass spectrometric curves was reported by Roduit et al. [11].

Although, the best accordance between DTG and FTIR traces was found for the highest flow rate of 65 ml min<sup>-1</sup>, in further experiments generally a flow

rate of  $50 \text{ ml min}^{-1}$  was used. This flow rate proved to be a good compromise to achieve high analytical sensitivity and sampling frequency allowing discrimination of different TG-steps in a narrow temperature window.

De la Guardia and coworkers [23] found that the carrier gas flow rate is a critical parameter in vapor phase FTIR spectrometric analysis which affects the analytical sensitivity and the sampling frequency. They selected a nitrogen flow rate of  $50 \text{ ml min}^{-1}$ , which allows a  $20 \text{ h}^{-1}$  sampling frequency. Marsanich et al. [17] used a similar flow rate ( $60 \text{ ml min}^{-1}$ ) in his studies with the same FTIR gas cell volume (8.7 ml) and FTIR path length (123 mm). Generally, it can be stated that a higher diffusivity of the evolving species in the carrier gas requires a higher minimal carrier gas flow rate to minimize the differences between thermoanalytical (e.g. TG or DTG) and FTIR signals.

The main disadvantage of pinhole-calibration beside uncontrolled mass loss, as mentioned above, lies in the fact that the calibration and decomposition can not be done in one experimental run. As shown by Slager et al. [21], using this method temperatures up to the boiling point of the calibrating substance are necessary to obtain the dependence between mass loss and integral intensity of the FTIR signal required for the calibration. Application of such high temperatures can, however, affect the process to be investigated, if one wants to follow it *in situ*. Therefore we developed and applied another method in our laboratory, which will be discussed next.

### Differential Calibration

The differential calibration is based on the isothermal or non-isothermal vaporization of a liquid compound at different temperatures, with low heating rates and simultaneous monitoring, in differential time periods, corresponding mass losses and intensities of FTIR signals. Figure 3-8A shows the principle of this

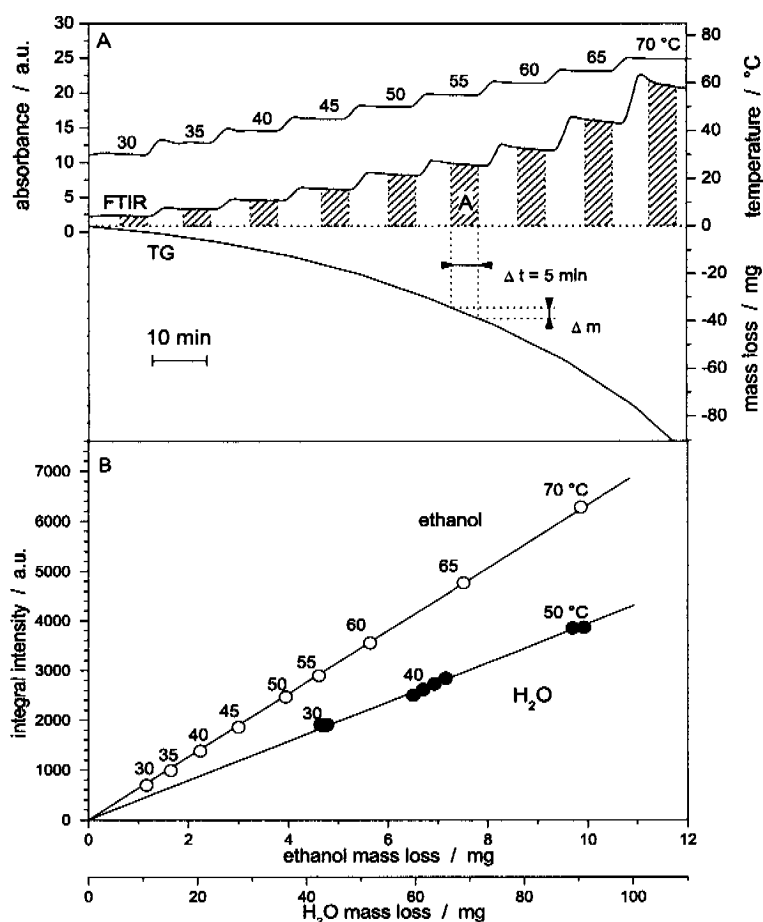


**Fig. 3-8:** A: Differential calibration of ethanol at various temperatures. Interval time: 5 min, flow rate: 50 ml min<sup>-1</sup>. B: Linear dependence between the integral of absorbance over a specified time (5 min ethanol and 10 min water) on the amount of evolved liquids during the same time interval. Corresponding temperatures are indicated on the temperature curve. Crucible diameter was 7.5 mm for ethanol and 17.0 mm for water calibration.

method applied for isothermal calibration with ethanol at temperatures between 30 and 70 °C. The integral absorbances were measured during constant time intervals (5 min) and plotted against the mass loss  $\Delta m$  recorded during the same time intervals by the TG signal. This dependence is presented in Figure 3-8B where additionally the same relationship for water collected during the longer time intervals (10 min) is depicted. The very good regression coeffi-

coefficients obtained for ethanol ( $r^2 = 0.99998$ ) and water ( $r^2 = 0.9975$ ) indicate the high accuracy of the applied calibration technique.

The correlation of the integral intensity of the FTIR signal with the exact amount of evaporated liquid measured by thermobalance in arbitrarily chosen periods of time allowed the extension of the method for the simultaneous calibration and measurement of evolved species in one experimental set-up. Depending on the flow rate, the time lag between the beginning of the reaction (observed on DTG curve) and the appearance of the FTIR signals was in the range of 4.3 s (for flow of  $65 \text{ ml min}^{-1}$ ) to 14.1 s (flow of  $20 \text{ ml min}^{-1}$ ). Data collection occurred during a few minutes after steady state of the mass loss and FTIR signals had been reached. The 5.6 seconds delay (flow:  $50 \text{ ml min}^{-1}$ ) between the real course of the reaction (DTG curve) and that of measured FTIR signals did not influence the calibration results. At low flows the back-mixing became prominent leading to some tailing of the FTIR traces, but the calibration was not significantly affected by this phenomenon. The target sample and the calibration sample are placed in two separate pans which are weighed continuously as during conventional thermogravimetric runs. The first calibration period is performed in the isothermal mode at relatively low temperature. During this period the relationship between the intensity of the FTIR signal and the amount of evaporated liquid can be determined in a few differential time periods which increases the accuracy of the calibration. After total evaporation of the calibration liquid, which is indicated by the end of the mass loss on the TG curve, the second experimental stage is started, during which the temperature in the system is raised according to the chosen temperature ramp.

This *in situ* calibration is shown in Figure 3-9 which depicts the quantification by FTIR of the evolved water formed during dehydration of sodium bicar-

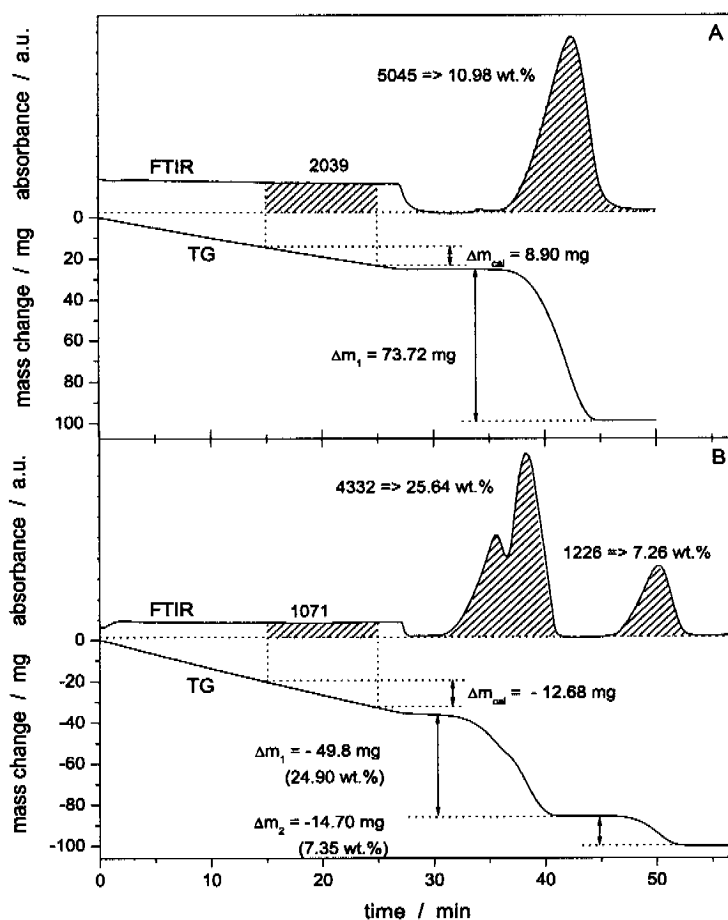


**Fig. 3-9:** Differential calibration: water-traces recorded during decomposition of 200 mg NaHCO<sub>3</sub> (A) and 200 mg CuSO<sub>4</sub> · 5 H<sub>2</sub>O (B). Heating rate: 10 K min<sup>-1</sup>, carrier gas: 25 (A), 50 (B) ml min<sup>-1</sup>. The mass of water used for the calibration at 50 °C was ca. 25 mg (A) and 35 mg (B). Interval time: 10 min. Crucible diameter: 7.5 mm.

bonate and copper sulfate pentahydrate. Figure 3-9A shows the water trace recorded during mass calibration and decomposition of 200 mg NaHCO<sub>3</sub> according to reaction (Eq. 1). The integral of the FTIR absorbance over the interval of 10 min was 2039 a.u., while the integral intensity of the signal of the evolved H<sub>2</sub>O was 5045 a.u. The amount of evolved water during the calibrating stage was 8.90 mg. The amount of H<sub>2</sub>O formed during the decomposition calculated from these data corresponds to 10.98 wt.%, which agrees well with the

stoichiometric value of 10.69 wt.%, corroborating the very good accuracy of the differential quantification method.

Figure 3-9B shows water traces recorded during differential calibration and decomposition of 200 mg  $\text{CuSO}_4 \cdot 5 \text{H}_2\text{O}$ . At the first step of decomposition the observed mass loss corresponded to 24.90 wt.% and agreed well with the evolved amount of water found by FTIR (25.64 wt.%).

During the decomposition starting at about 220 °C (45 min), the water corresponding to the monohydrate evolved: the observed mass loss agrees well with the stoichiometric value (7.35 wt.% vs. 7.21 wt.%, respectively). The amount of water determined from FTIR traces based on calibration data was 7.26 wt.% (mass loss due to release of 12.68 mg of water results in FTIR signal with an integral intensity 1071 a.u).

### 3.3.3 Quantification of FTIR Signals Using Solids

Some of the methods described above for the calibration of FTIR signals could also be applied with solid calibration materials. In this case, before injection into the TG-FTIR system the calibration substance must be dissolved in a solvent that possesses different characteristic FTIR bands than the calibration substance.

Figure 3-10A shows the spectra recorded during decomposition of acetylsalicylic acid (ASA or aspirin) at 260 °C under dry and wet conditions, and the spectra of the main products from IR-library: acetic acid, salicylic acid (SA) and phenol. The bands used for the quantification were  $1800 \text{ cm}^{-1}$  (acetic acid) and  $3300 \text{ cm}^{-1}$  (SA).

Figure 3-10B depicts the acetic acid and SA traces recorded during decomposition of 21.5 mg aspirin under dry and wet (saturation of the carrier gas by

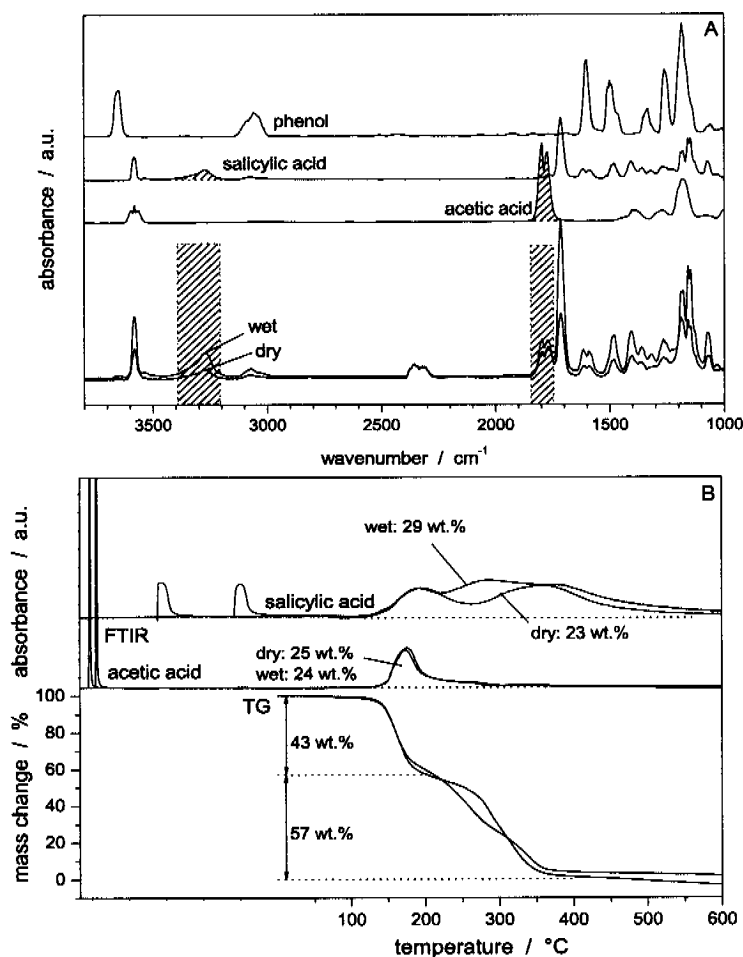


**Fig. 3-10:** A: Extracted spectra recorded during decomposition of aspirin at approximately  $260^{\circ}\text{C}$  under wet (thick line) and dry conditions. The window of the characteristic wavenumber is marked and used for further time-resolved traces. B: Acetic acid and salicylic acid traces recorded during decomposition of 21.5 mg aspirin under wet and dry conditions and calibration pulses injected before decomposition: Injections were done after the TA, immediately before the FTIR-transfer-line.

purging through water at  $30^{\circ}\text{C}$ ) conditions. For the calibration a solution of 10 mg SA dissolved in 100 ml ethanol was used. Two  $\mu\text{l}$  of acetic acid and two  $\mu\text{l}$  of the SA/ethanol mixture were injected after the thermoanalyzer in order to avoid the crystallization of SA in the TA chamber. Gravimetric traces (TG) show clearly a two-step-decomposition of aspirin under dry conditions (43 and 57 wt.% for the first and second step, respectively), whereas during the reaction



under wet conditions the decomposition steps are not so well resolved. Acetic acid is evolved mainly in a first step, at higher temperature (ca. 260 °C) the main decomposition product is SA and at about 360 °C additionally the evolution of phenol is observed. The amount of evolved SA found by means of FTIR under wet conditions (29 wt.%) was slightly higher than under dry conditions (23 wt.%). However, the amounts of the acetic acid were almost the same (24 and 25 wt.%) for both conditions. Robeiro et al. [24] reported also a mass loss in two consecutive steps, between 120 and 400 °C. The first step up to 260 °C occurred with a loss of 42.8% followed by 57.2% in the second step, which agrees with our results. They attributed the first mass loss to the evolution of acetic acid and evaporation of ASA and SA. They identified the evaporation process by means of chromatography but were not able to quantify it.

To characterize the influence of the gas flow on the FTIR spectra of the SA in the same TG-FTIR system, salicylic acid was heated under nitrogen with different flow rates and pressures by Jackson et al. [25], who found considerable peak broadening because of the high boiling point of salicylic acid. With higher flow rate the IR responses would be narrower, but in TGA system high carrier flow rates can generate instability problems of the balance. The fact, that we injected the SA directly on the top of the thermoanalyzer just before the heated transfer-line (200 °C) to the FTIR spectrometer and kept the flow rate high (50 ml min<sup>-1</sup>), leads to accurate quantification and avoids condensation of SA on possible cold spots in the system. This procedure slightly lowers the accuracy of the data acquisition due to the sharpness of the peaks caused by the high flow rate and the short distance between injection position and IR cell (cf. acetic acid peaks in Figure 3-10B), but condensation or resublimation of SA would result in much larger error than some peak cutting in the calibration segment.

### 3.3.4 Comparison of the Calibration Methods

Table 3-4 compares the results of the quantification of the FTIR spectra using two *in situ* methods, pulse calibration (PC) and differential calibration (DC). The comparison is based on the amounts of water evolved during decomposition of sodium bicarbonate and copper sulfate pentahydrate. Both compounds decompose with well-known stoichiometry and the thermogravimetric curves recorded simultaneously allow comparing the accuracy of the applied procedures used for the quantification of the spectroscopic signals.

**Table 3-4:** Comparison between gravimetric and spectroscopic results of water evolution obtained by pulse calibration (PC) or differential calibration (DC) during the decomposition of sodium bicarbonate and copper sulfate pentahydrate. The relative standard deviation (RSD) is calculated based on TG and FTIR results.

Sample	step	method	stoich.	TG	FTIR	RSD / %
NaHCO <sub>3</sub>	1	PC	10.69	-	10.87	1.68 <sup>a</sup>
NaHCO <sub>3</sub>	1	DC	10.69	-	10.98	2.71 <sup>a</sup>
CuSO <sub>4</sub> · 5 H <sub>2</sub> O	1	PC	28.84	25.82	26.35	2.05
CuSO <sub>4</sub> · 5 H <sub>2</sub> O	1	DC	28.84	24.90	25.64	2.97
CuSO <sub>4</sub> · 5 H <sub>2</sub> O	2	PC	7.21	7.17	7.24	0.98
CuSO <sub>4</sub> · 5 H <sub>2</sub> O	2	DC	7.21	7.35	7.26	1.22

<sup>a</sup> RSD is related to the stoichiometric expected value.

The relative standard deviation (RSD) is calculated based on TG and FTIR results, except the decomposition of sodium bicarbonate, where TG results are not taken into account because CO<sub>2</sub> and water evolved simultaneously, i.e. in the same temperature range. Here the RSD is related to the expected stoichiometric value only. All deviations between gravimetric and spectroscopic results are lower than 3% which corroborates the good accuracy

of the applied methods. The fact that both these methods could be applied *in situ*, in one experimental run, underlines their potential. They offer a much less time-consuming calibration procedure than generally applied. The opportunity of injecting the fluid before or after the thermoanalyzer widens the application range of the hyphenated TG-FTIR technique. Fluids, injected before the TA, can react with the sample (allowing e.g. the investigation of adsorption or gas-solid reactions), whereas injection after the TA allows simple quantitative analysis of the evolved species.

The pinhole calibration method significantly extends the scope of liquid calibration. The results presented in this study confirmed its applicability for quantification of volatile compounds. The use of different diameters of the pinhole and different temperature ramps during calibration provides the opportunity of calibrating FTIR signals with liquids having very different evaporation rate (vapor pressure) at room temperature. Slager and Prozonic [21] achieved calibrations for methanol, xylene, dimethyl formamide and dimethyl acetamid with this method using a constant flow rate, however, changing experimental parameters (e.g. flow rate) limits this application. We showed that the amount found by means of FTIR absorbance is proportional to the reciprocal of the flow rate.

Another serious limitation of the pinhole method is its application with substances possessing very low boiling point as e.g. acetone. Part of the calibration agent evaporates already during sample handling and experiment settling, rendering the relation between the amount of evaporated liquid and the FTIR integral signal inaccurate.

The differential method, described in this paper, further extends the opportunities of liquid calibrations by the vaporization methods described by Slager and Marsanich et al. [18,21]. Especially high volatile materials (e.g. acetone,

ethanol) can be applied without any limitations for quantification with this method. For the calibration, the experimental data from only a certain, arbitrarily chosen differential time interval are taken, omitting the ill-defined start of the experiment, where already significant mass losses may occur before the TA-FTIR data are collected.

### 3.4 Conclusions

The methods of quantification of FTIR signals based on the pulse and differential techniques, described in this work, allow *in situ* applications and easy and less time-consuming calibration procedure which can be used in different studies, such as the quantification of adsorption phenomena (cf. chapter 5), gas-solid reactions (cf. chapter 6) and decomposition of solids. The main advantages of the pulse and differential calibration methods compared to the commonly used quantification of the FTIR spectra are: simplicity, accuracy and very good reproducibility. The fact that both the calibration and experiment can be performed in a single run significantly decreases the influence of artefacts and minimizes experimental errors (e.g. shift of the base-line in FTIR cell, influence of changes in the carrier gas flow, etc.) which can bias the quantification based on FTIR spectra. The described calibration methods widen the application range of the TG-FTIR technique, which is a very sensitive and reliable tool for characterizing reactions involving solids and gases such as complex decomposition reactions. The extension of the quantification by applying liquid and solid-liquid solutions opens up further opportunities in the area of quantification of spectroscopic signals in coupled TG-FTIR-MS systems.

### 3.5 References

- [1] S. Materazzi, R. Curini, G. D'Ascenzo, A.D. Magri, *Thermochim. Acta* 264 (1995) 75.
- [2] S. Materazzi, *Appl. Spectrosc. Rev.* 33 (1998) 189.
- [3] S. Materazzi, *Appl. Spectrosc. Rev.* 32 (1997) 385.
- [4] A.B. Kiss, *Acta Chim. Acad. Sci. Hung.* 61 (1969) 207.
- [5] C.A. Cody, L. Dicarlo, B.K. Faulseit, *Am. Lab.* 13 (1981) 93.
- [6] P.B. Roush, J.M. Luce, G.A. Totten, *Am. Lab.* 15 (1983) 90.
- [7] J.O. Lephardt, *Appl. Spectrosc. Rev.* 18 (1982) 265.
- [8] M. Mittleman, *Thermochim. Acta* 166 (1990) 301.
- [9] L.C.K. Liaw, T.C.K. Yang, D.S. Viswanath, *Appl. Spectrosc.* 51 (1997) 905.
- [10] M.F. Cai, R.B. Smart, *Energy Fuels* 7 (1993) 52.
- [11] B. Roduit, J. Baldyga, M. Maciejewski, A. Baiker, *Thermochim. Acta* 295 (1997) 59.
- [12] M. Maciejewski, A. Baiker, *Thermochim. Acta* 295 (1997) 95.
- [13] M. Maciejewski, C.A. Muller, R. Tschan, W.D. Emmerich, A. Baiker, *Thermochim. Acta* 295 (1997) 167.
- [14] J. Wang, B. McEnaney, *Thermochim. Acta* 190 (1991) 143.
- [15] E. Lopez-Anreus, S. Garrigues, M. de la Guardia, *Analyst* 123 (1998) 1247.
- [16] A. Perez-Ponce, F.J. Rambla, J.M. Garrigues, S. Garrigues, M. de la Guardia, *Analyst* 123 (1998) 1253.
- [17] K. Marsanich, F. Barontini, V. Cozzani, L. Petarca, *Thermochim. Acta* 390 (2002) 153.

- [18] F. Barontini, K. Marsanich, V. Cozzani, *J. Therm. Anal. Cal.* 78 (2004) 599.
- [19] M. Muller-Vonmoos, G. Kahr, A. Rub, *Thermochim. Acta* 20 (1977) 387.
- [20] B.H. Li, R.D. Gonzalez, *Catal. Lett.* 54 (1998) 5.
- [21] T.L. Slager, F.M. Prozonic, *Thermochim. Acta* 426 (2005) 93.
- [22] F. Barontini, E. Brunazzi, V. Cozzani, in *Proc. 5th SKT 2003*, Netzsch, Selb, Germany, 2003, p. 37.
- [23] A. Perez-Ponce, J.M. Garrigues, S. Garrigues, M. de la Guardia, *Analyst* 123 (1998) 1817.
- [24] Y. Asakura Ribeiro, A.C.F. Caires, N. Boralle, M. Ionashiro, *Thermochim. Acta* 279 (1996) 177.
- [25] R.S. Jackson, A. Rager, *Thermochim. Acta* 367 (2001) 415.

Seite Leer /  
Blank leaf

Seite Leer /  
Blank leaf



# Influence of Measuring Conditions on the Quantification of FTIR Spectroscopic Signals

## 4.1 Introduction

A disadvantage of classical thermal analysis (TA) is that gases released from the probe sample during the measurement are normally not analyzed. This shortcoming can be overcome by coupling TA with mass spectrometry (MS) or Fourier-Transform-Infrared (FTIR) spectroscopy, as it was shown in the previous chapter.

Besides the identification of evolved gases, their quantification by FTIR [1–6] or MS [4,7–9] spectrometry has been addressed. The common method of quantification of spectrometric signals is time-consuming and requires the application of gaseous mixtures with well-defined composition. First quantification of evolved gases based on the pulse technique combined with TA systems was reported by Maciejewski et al. [8,10]. The extension to FTIR-TA coupled technique was investigated in Chapter 3 by decomposing solids with known stoichiometry of the decomposition process and by injection of liquids into the TA-FTIR system. Marsanich et al. [11] applied the gas-pulse calibration using ammonia, carbon monoxide and carbon dioxide. They introduced

the vaporization technique of liquid samples for calibration of the FTIR signals. Similar procedure was applied also by Slager and Prozonic [12].

Quantification using MS combined with the pulse calibration technique is facilitated by the fact that the linear relationship between the observed intensities of the ion current and the amount of the analyzed species is hold in a wide concentration range. Furthermore the MS data acquisition time is generally short and recording evolved gases can be achieved with a high time resolution. In contrast, quantification of evolved gases in TA-FTIR systems is complicated by the fact that the Lambert-Beer's law is often valid only in a small concentration range, and consequently the amount of injected gas by the single-point calibration must closely match that evolved during decomposition. Additionally the data acquisition time in FTIR is only comparable with that applied in MS when choosing poor spectral resolution (e.g.  $32\text{ cm}^{-1}$ ). The other parameters such as e.g. residence time in the IR-cell are also important for achieving high accuracy in data collection.

A closer look on the experimental conditions applied in the various reported TA-FTIR studies indicates that in certain cases the conditions deviate significantly from the optimal settings for quantification of FTIR traces. Some experimental conditions used for TA-FTIR investigations are listed in Table 4-1 [4,6,12–20]. Comparison of acquisition time and residence time describes the precision and completeness of the recorded traces: values of this ratio below or equal one indicate a big likelihood that each molecule could be detected and contributed to the integral intensity of recorded traces. Values above one indicate that most likely some of the target molecules did not contribute to the signal thereby lowering the accuracy of quantification. This is especially important, if pulse calibration is applied, resulting in generally sharp peaks, which can result in the situation that under extreme conditions (high

**Table 4-1:** Comparison of TA-FTIR systems with different measuring conditions.

Apparatus	Ref.	Reso- lution cm <sup>-1</sup>	Co- adding scans	Acq. time s	Flow rate ml min <sup>-1</sup>	Vol. IR cell ml	Resid. time s	Quot. Acq. t/ Resid. t
Bruker IFS 28	[13]	4	10	~10	15	8.7	34.8	0.3
Perkin Elmer	[14]	8	4	~4	89	~10	~7	0.6
Digilab FTS 60	[4]	8	16	~5	50	6	7.2	0.7
Bruker Equinox	[15]	4	16	9.5	60	8.7	8.7	1.1
Bruker Equinox	[16]	4	-	17.5	35	8.7	14.9	1.2
IBM IR 85	[17]	-	-	30	-	556	25	1.2
Digilab FTS 7	[6]	8	16	13	10	6	7.2	1.8
Midac / Nicolet	[12]	4	32-45	60	100	30	18	3.3
Nicolet Magna	[18]	16	3	~3	50	0.49	0.6	5
Bruker Vector 22	[19]	2	16	75	100	19.7	11.8	6.4
Perkin Elmer	[20]	-	-	~60	95	4.8	3	20

quotient of acquisition time divided per residence time) the pulses are not fully recorded.

Preliminary investigations clearly indicated a significant influence of improper experimental settings on the accuracy of the quantification of IR spectra by the pulse technique. The importance of this aspect for proper application of FTIR in combined TA-FTIR systems has prompted us to study systematically the influence of the experimental conditions on the quantitative interpretation of FTIR traces.

## 4.2 Experimental

Experiments were carried out on a Netzsch STA 449 analyzer equipped with two pulse devices enabling injection of a certain amount of one or two different gases or gaseous mixtures into the carrier gas stream flowing through the system (Figure 2-5 in Chapter 2). Volumes of 0.25, 0.5, 1.0 and 2.0 ml were mainly used.

Additionally the option of bypassing the thermoanalyzer by injecting species after the thermoanalyzer (into the transfer-line) was used, which enabled calibration without contact of the calibrating pulse with the investigated sample. This alternative method results in much sharper signals and therefore calibration is less accurate (*vide infra*).

The carrier gas flow rate was controlled by mass flow controllers, Brook's model 5850E, based on a thermal mass flow sensing technique. Helium and argon (purity 99.999%, PanGas) were used as carrier gases with flow rates from 12.5 to 200 ml min<sup>-1</sup>. The thermoanalyzer was connected by a heated (ca. 200 °C) transfer-line to a Bruker Vector 22 FTIR spectrometer. Gases leaving the FTIR spectrometer were passed through a heated (ca. 200 °C) capillary to a Pfeiffer Omni Star GSD 301 O mass spectrometer.

The FTIR spectrometer is equipped with a MCT detector and an especially developed low-volume gas cell (8.7 ml) with a 123 mm path length and ZnSe windows. To avoid condensation of low volatile compounds the cell was heated to a constant temperature of 200 °C. The whole FTIR compartment was continuously purged by nitrogen and additionally molecular sieves were used to minimize the water and carbon dioxide background in the recorded spectra. The resolution of the collected spectra was set between 1 and 32 cm<sup>-1</sup> and co-addition of 4 scans per spectrum was applied. As a consequence spectra

were recorded with a time resolution of about 2-20 s, depending on the integration methods and applied FTIR spectral resolution.

MS measurements were performed directly after the FTIR chamber resulting in similar temporal traces of the evolved species. The few characteristic mass to charge ratios (e.g. for  $\text{CO}_2$  and  $\text{H}_2\text{O}$   $m/z=44$  and 18, respectively) were monitored versus temperature or time in the multiple ion detection mode. Data acquisition time was relatively short, generally about 2 s. Such an acquisition time could only be applied on cost of low resolution i.e.  $32\text{ cm}^{-1}$  in the FTIR system.

$\text{NaHCO}_3$  (p.a. Merck) and  $\text{CuSO}_4 \cdot 5\text{ H}_2\text{O}$  (Fluka AG) were used as reference samples with well known stoichiometry of the decomposition. In order to check the behavior of the system in a wide range of  $\text{CO}_2$  concentrations the sample mass of  $\text{NaHCO}_3$  was varied between 2 and 420 mg, while the sample mass of  $\text{CuSO}_4 \cdot 5\text{ H}_2\text{O}$  was 50 mg.

For the gas injections a home-made device was placed before the thermoanalyzer. It contains a rotary sample valve enabling a carrier gas to purge the loop of a given volume, which had been previously filled with the calibration gas of known composition. In order to quantify the FTIR signals, pulses of a known volume were injected generally before the decomposition of the investigated sample. A standard heating rate of  $10\text{ K min}^{-1}$  was applied for all decompositions.

### 4.3 Results and Discussion

From preliminary investigations it emerged that the following experimental parameters can affect the accuracy of the quantification of FTIR signals: sam-

ple mass, place of the injection of the calibrating gas, carrier gas flow, resolution of the spectrometer and accordingly acquisition time in the IR cell. FTIR data were compared with the simultaneously gained MS data, which allowed significant optimization of the various parameters and led to increase of the accuracy of the FTIR quantification method.

### 4.3.1 Influence of Sample Mass and Concentration of the Target Gas

The application of PulseTA<sup>®</sup> for quantitative interpretation of FTIR signals is based on the Lambert-Beer's-Law. Figure 4-1 shows the pulse calibration using the example of CO<sub>2</sub> where different amounts of the gas were injected into the TA-FTIR-MS system. CO<sub>2</sub> traces were monitored using two characteristic

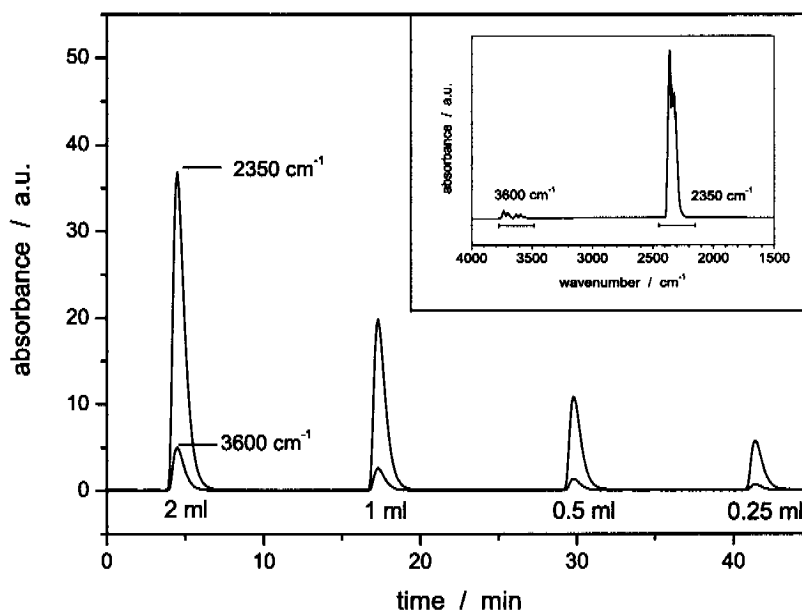


**Fig. 4-1:** Pulse calibration: intensity of CO<sub>2</sub> signals recorded in TA-FTIR system for the characteristic wavenumbers 2350 cm<sup>-1</sup> and 3600 cm<sup>-1</sup>, respectively. Carrier gas: 100 ml min<sup>-1</sup> He, resolution: 4 cm<sup>-1</sup>. Inset: IR-spectrum of CO<sub>2</sub>.

wavenumber regions, namely  $2450\text{--}2150\text{ cm}^{-1}$  (asymmetric stretch, peak- $2350\text{ cm}^{-1}$ ), which is widely applied for identification and quantification purposes and  $3780\text{--}3480\text{ cm}^{-1}$  (overtone band, peak- $3600\text{ cm}^{-1}$ ), which shows much lower FTIR intensity, and interferes with water bands in the same region. The integral intensities  $I$  (Eq. 2 in Chapter 3) resulting from calibration pulses are shown in Figure 4-2.

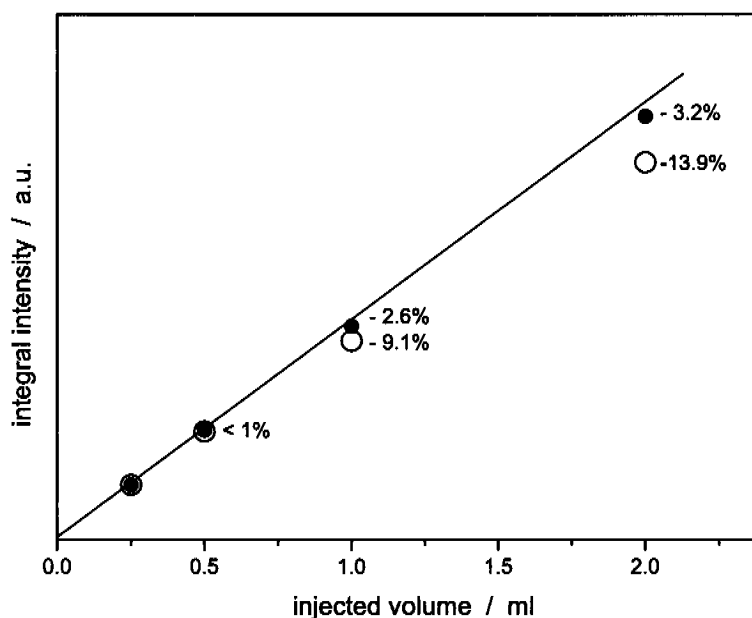


**Fig. 4-2:** Relationship between injected volume and integral intensity of evolved  $\text{CO}_2$  measured in TA-FTIR system for different IR regions: solid circles:  $3600\text{ cm}^{-1}$  and open circles:  $2350\text{ cm}^{-1}$ .

The absorbance of the evolved  $\text{CO}_2$  was much larger for the traces recorded at  $2350\text{ cm}^{-1}$  than at  $3600\text{ cm}^{-1}$  and this led to a significant deviation from linearity during injections of higher amounts of  $\text{CO}_2$ . Integral intensities observed for 2 ml injections deviated by 13.9% from the linear dependence for

the traces recorded for  $2350\text{ cm}^{-1}$ , whereas for  $3600\text{ cm}^{-1}$  only small non-linearity was observed ( $-3.2\%$ ).

Figure 4-3 shows the relationship between the mass of the decomposed sample ( $\text{NaHCO}_3$ ) and the integral intensity of evolved  $\text{CO}_2$  as determined using the TA-FTIR system. The traces gained at  $2350\text{ cm}^{-1}$  show a linear dependence between integral intensity of the signal and mass up to 50 mg (13 mg of evolved  $\text{CO}_2$ ). Quantification based on the band at  $3600\text{ cm}^{-1}$ , however, could be achieved even up to 400 mg sample (ca. 105 mg  $\text{CO}_2$ ) with a spectral resolution of  $4\text{ cm}^{-1}$  and a carrier flow rate of  $50\text{ ml min}^{-1}$  He. For sample masses over 100 mg (ca. 26 mg of evolved  $\text{CO}_2$ ) no linear relationship was obtained using the signal at  $2350\text{ cm}^{-1}$  biasing quantification.

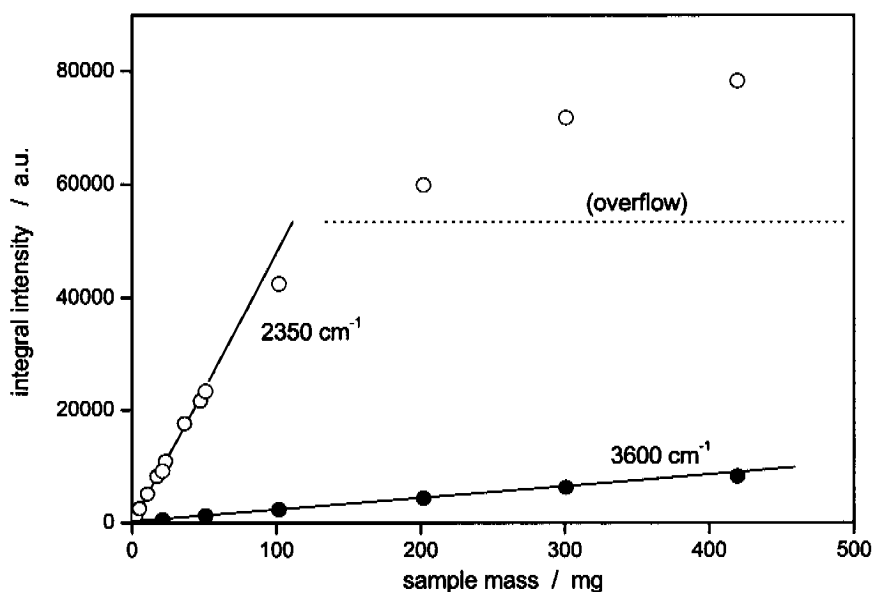
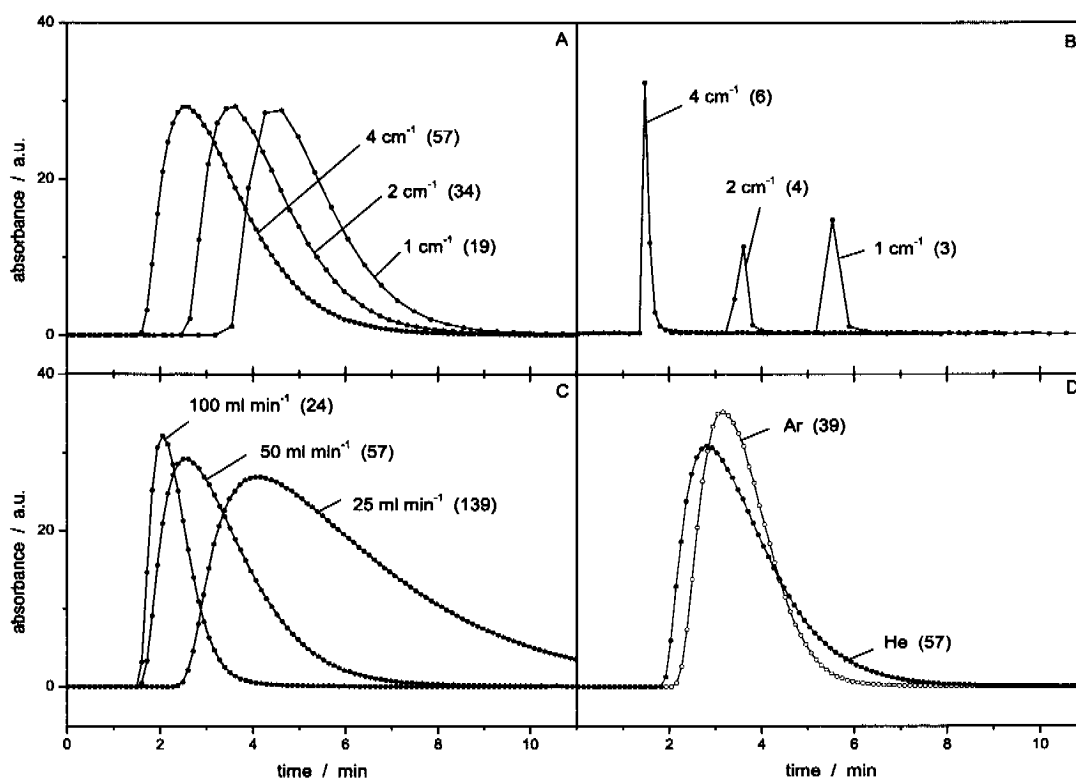


Fig. 4-3: Relationship between the mass of the investigated sample ( $\text{NaHCO}_3$ ) and integral intensity of evolved  $\text{CO}_2$  measured in TA-FTIR system: solid circles:  $3600\text{ cm}^{-1}$  and open circles:  $2350\text{ cm}^{-1}$ . Carrier gas:  $50\text{ ml min}^{-1}$  He, resolution:  $4\text{ cm}^{-1}$ .



### 4.3.2 Influence of Parameters of Data-Acquisition and Carrier Gas

Figure 4-4 illustrates the influence of the parameters of data acquisition and other experimental conditions on the shape and intensity of CO<sub>2</sub> traces recorded using the TA-FTIR system after injection of 1 ml CO<sub>2</sub>. Figure 4-4a shows pulses recorded with different spectral resolutions. Generally the injection was made before the thermoanalyzer, but in the case where contact of the injected gas with the investigated sample has to be avoided, the calibrating gas can be injected into the carrier gas by-passing the TA chamber. This procedure



**Fig. 4-4:** Influence of the experimental conditions on the shape and intensity of CO<sub>2</sub> traces recorded in TA-FTIR system after injection of 1 ml CO<sub>2</sub>. Numbers of recorded data points (> 1% of maximal intensity) are given in brackets. A: Carrier gas: 50 ml min<sup>-1</sup> He, injection before TA, (CO<sub>2</sub> traces at 2350 cm<sup>-1</sup>). B: Carrier gas: 50 ml min<sup>-1</sup> He, injection after TA, (CO<sub>2</sub> traces at 3600 cm<sup>-1</sup>). C: Carrier gas: 100, 50 and 25 ml min<sup>-1</sup> He, injection before TA, resolution 4 cm<sup>-1</sup>, (CO<sub>2</sub> traces at 2350 cm<sup>-1</sup>). D: Carrier gas: 50 ml min<sup>-1</sup> He and Ar, injection before TA, resolution 4 cm<sup>-1</sup>, (CO<sub>2</sub> traces at 2350 cm<sup>-1</sup>).

leads to much sharper peaks (Figure 4-4B) with a huge maximal intensity which allows quantification using only the weaker signal at  $3600\text{ cm}^{-1}$ . Due to the small distance between injection and detecting sensor the number of recorded data points at the same carrier gas flow (marked in brackets) was much lower than in the case where the injected gas passed through the relatively large volume of the TA chamber resulting in dilution of the injected gas. The influence of the carrier gas flow on the shape and intensity of FTIR signal is presented in Figure 4-4C. The number of recorded data points increases with decreasing flow rate leading additionally to lowering of the maximal concentrations in the FTIR cell. The tailing of the signal can be caused not only by lowering the carrier gas flow but also by the application of different carrier gas. The results presented in Figure 4-4D show that  $\text{CO}_2$  pulses in helium result in broader peaks (larger tailing) than in argon due to higher diffusivity of the investigated gas in helium. Application of helium enables the collection of significantly more data-points which results in better description of the real traces of the evolved gas. Similar dependence was observed by Roduit et al. by quantitative calibration of mass spectrometric signals [7]. They found that due to the much higher diffusivity of  $\text{CO}_2$  in helium compared to argon, the mixed-flow zone in the TA chamber significantly increases leading to peak broadening. However, the maximal concentration due to injections of certain amount of  $\text{CO}_2$  into the carrier gas is smaller in helium than in argon.

Figure 4-5 illustrates the relationship between IR-resolution, the acquisition time and the residence time of injected molecules. Figure 4-5A shows the  $\text{CO}_2$  and NO spectra recorded with different spectral resolutions between 1 and  $32\text{ cm}^{-1}$ . The application of high spectral resolution ( $2\text{ cm}^{-1}$ ) allows quantification of specific mixtures where the vibrational signals of both gases overlap as e.g. acetylene and hydrogen cyanide. For NO, at higher resolution, even dif-

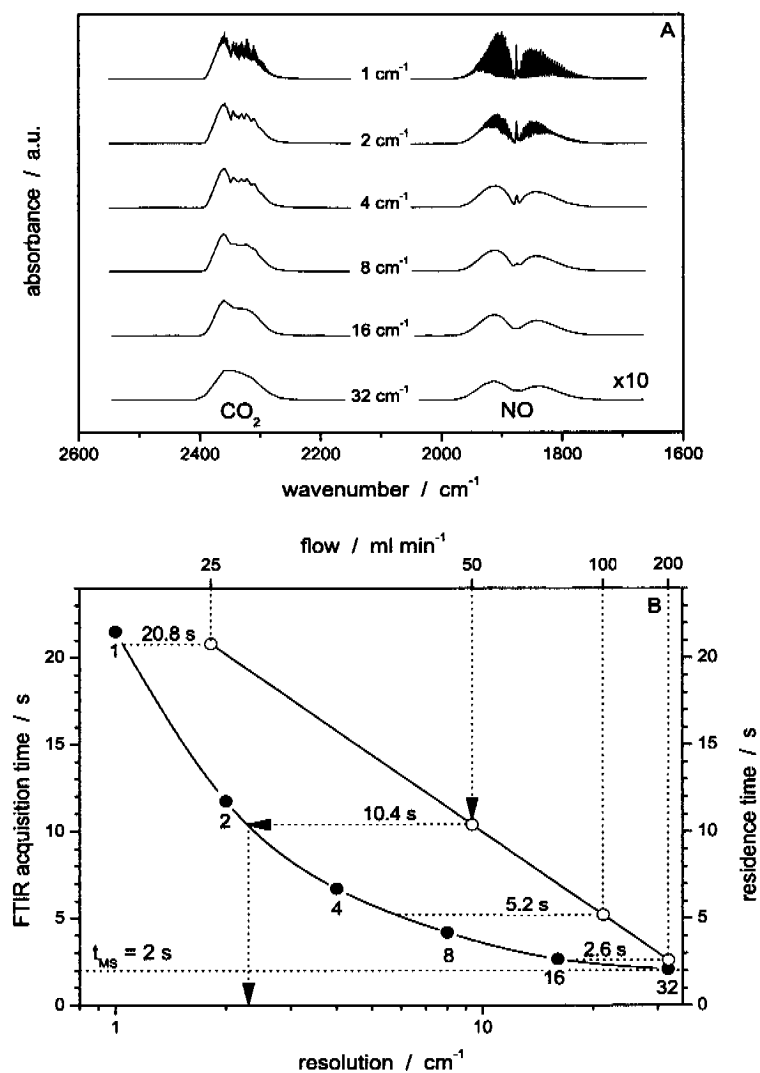


**Fig. 4-5:** Influence of selected spectral resolution of FTIR: A: CO<sub>2</sub> and NO spectra recorded with different spectral resolutions. Intensities of NO spectra are scaled up (x10). Concentration of both gases: ca. 1% in He. B: Relationship between acquisition time, spectral resolution and residence time (FTIR chamber) in TA-FTIR system. Number of averaged scans: 4.

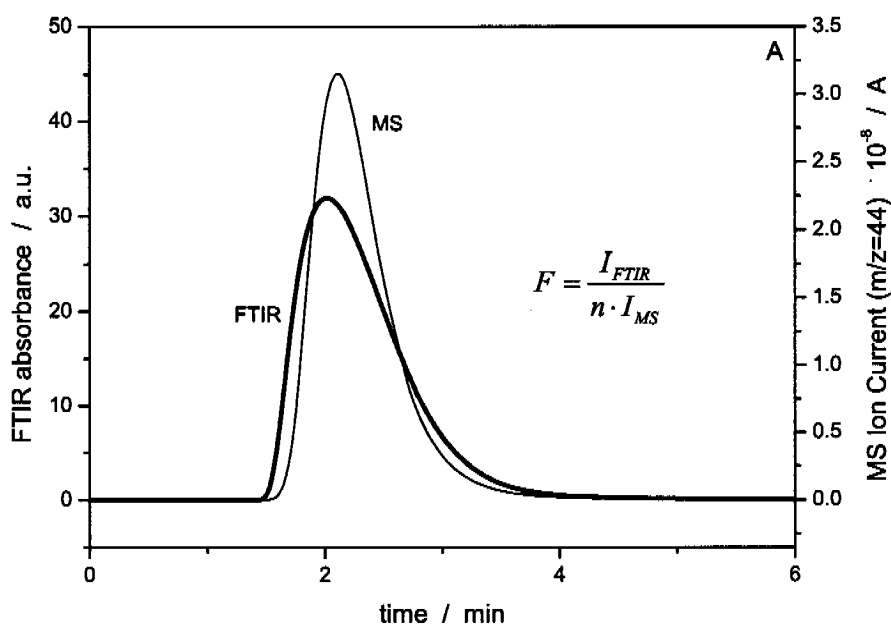
ferentiation between isotopes is possible. However, the application of high resolution has a significant drawback in dynamic TA experiments. In order to increase the accuracy of quantification at a given flow rate, the acquisition time has to be decreased, which can only be achieved by lowering the spectral resolu-

tion, as shown in Figure 4-5B. High resolution, as e.g.  $1\text{ cm}^{-1}$ , results in a temporal acquisition of 21.5 s, and low resolution as  $32\text{ cm}^{-1}$  in 2.1 s, the latter is comparable to the acquisition time of mass spectrometric signals used for quantification in this study.

The acquisition time has to be strictly correlated with the mean residence time of the evolved gas in the FTIR gas cell. For too long acquisition time it is impossible to quantify properly the analyzed species. The mean residence time in the gas cell estimated by the quotient between the volume of the IR cell compartment and the carrier gas flow through the system, is shown as an upper line in Figure 4-5B (carrier gas flow: reciprocal scale). The comparison of both dependences presented in this figure allows choosing a maximal resolution required for a good description of the traces, enabling accurate quantification. For example, when using a carrier flow rate of  $50\text{ ml min}^{-1}$  (residence time 10.4 s), the resolution should not be higher than  $4\text{ cm}^{-1}$ . For higher resolutions, i.e. 2 or  $1\text{ cm}^{-1}$ , data acquisition needs a time larger than 10.4 s (11.7 s and 21.5 s, respectively), therefore when using a flow of  $50\text{ ml min}^{-1}$  part of the target gas species will not be accounted for, leading to erroneous quantification.

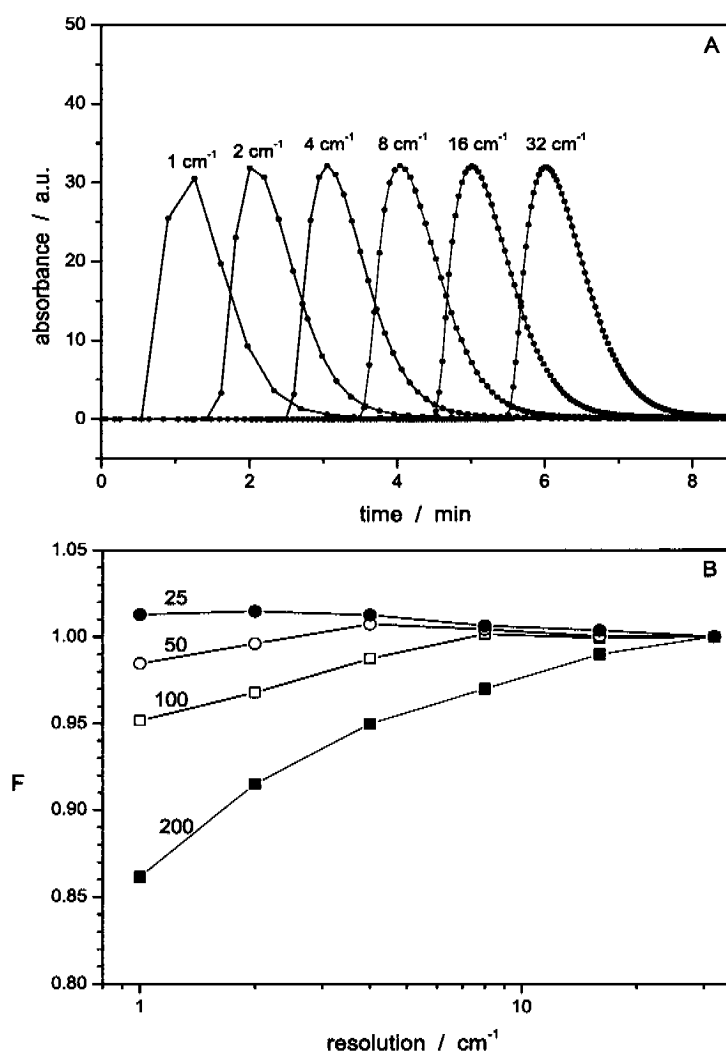
When investigating the influence of the experimental conditions on the integral intensity of FTIR signals one has to apply an independent reference allowing exact comparison of signals obtained in different experiments. In our studies, parallel to the IR technique, we applied mass spectrometry. In all experiments we compared the data obtained by both techniques. As reported in our previous studies [8,10] the integral intensities of MS signals are almost independent of experimental conditions, as also corroborated in the present study. This observation allowed us to use the MS signal as a reference for interpretation of the intensity of IR signals obtained under different conditions.

In order to compare the FTIR results obtained by using different experimental set-ups with the MS results, we introduced the ratio  $F$  as illustrated in Figure 4-6.  $F$  is the normalized ratio between integral intensities of FTIR and MS signals and provides a reasonable criterion for the correctness of the quantitative FTIR analysis. Figure 4-6 shows the integral intensities of 1 ml  $\text{CO}_2$  injected in He recorded by FTIR and MS. For the FTIR signal recorded using a low resolution of  $32 \text{ cm}^{-1}$  where the largest amount of data points are collected and a corresponding MS signal the factor  $F$  is deliberately set to 1. Note that acquisition times in this case were almost the same for both techniques (2.1 s for FTIR and 2 s for MS).



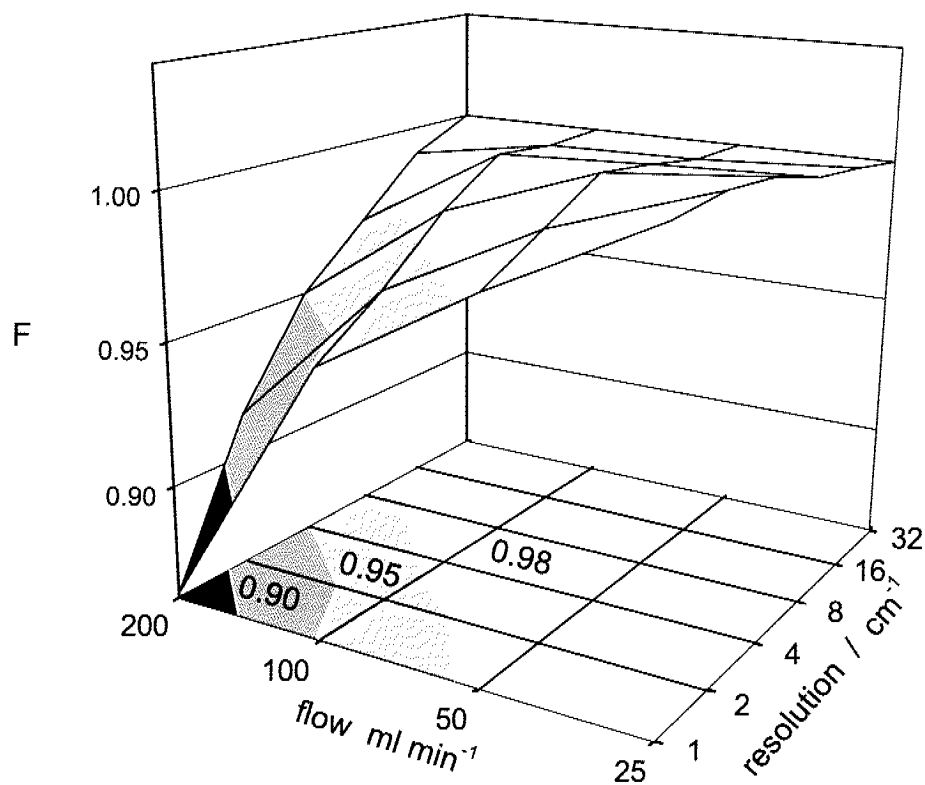
**Fig. 4-6:** Integral intensity  $I$  of 1 ml  $\text{CO}_2$  injected in He measured by FTIR (thick line) and MS, respectively.  $F$  is the normalized ratio between integral intensity of FTIR and MS signals. For FTIR signal measured with a resolution of  $32 \text{ cm}^{-1}$  and the corresponding MS signal,  $F$  is set to 1.

Figure 4-7A shows the influence of the resolution on the shape of the FTIR signal recorded during injections of 1 ml CO<sub>2</sub> to a carrier gas flow of 100 ml min<sup>-1</sup>. High resolution (i.e. 1 cm<sup>-1</sup>) results in smaller integral intensity due to the low number of collected data points, which leads to a decrease of the



**Fig. 4-7:** A: Influence of the spectral resolution (and data acquisition time) on the shape of FTIR signal recorded during injections of 1 ml CO<sub>2</sub> at a flow rate of 100 ml min<sup>-1</sup>. B: Relationship between ratio F (FTIR/MS signal) and resolution for different carrier gas flows (indicated in ml min<sup>-1</sup> on the curves).

value of  $F$ . In Figure 4-7B the observed relationship between ratio  $F$  and resolution for different carrier gas flows is shown. Especially for high carrier gas flows high spectral resolutions are not recommended because the resulting data acquisition time (cf. Figure 4-5B) differs significantly from the corresponding residence time in the IR compartment, which leads to a significant loss of data points. Figure 4-8 shows the dependence of  $F$  on the flow rate and resolution.  $F$  decreases not only with increasing the spectral resolution (which decreases the temporal resolution of data acquisition), but also with increasing the flow rate. Proper collection of FTIR data is only achieved when the acquisition time is in the range of the residence time of the gas in IR cell ( $F$  is above 0.98). As an



**Fig. 4-8:** 3-D illustration of dependence of  $F$  on the flow rate and resolution. The areas in which the  $F$  value in the plane "flow rate vs. resolution" lays in the range  $<0.90$ ,  $0.90-0.95$ ,  $0.95-0.98$  and above  $0.98$ , respectively, are marked.

example, when using a resolution of  $4\text{ cm}^{-1}$  the gas flow should not be higher than  $130\text{ ml min}^{-1}$ .

In order to quantify evolved gases in the TA-FTIR system with high spectral resolutions ( $1$  or  $2\text{ cm}^{-1}$ ) only low flow rates ( $< 50\text{ ml min}^{-1}$ ) can be used. The data presented in Table 4-1 (last column) indicate that in some cases this important parameter has not been taken into account when setting the experimental parameters in TA-FTIR investigations.

A further illustration showing that improper selection of the experimental settings can lead to erroneous quantification of FTIR spectra is presented in Figure 4-9, which shows the influence of the carrier gas flow on the shape of FTIR signals recorded during calibration (injection of  $1\text{ ml CO}_2$ ) and decomposition of  $20\text{ mg NaHCO}_3$ . The maximal intensities of the decomposition

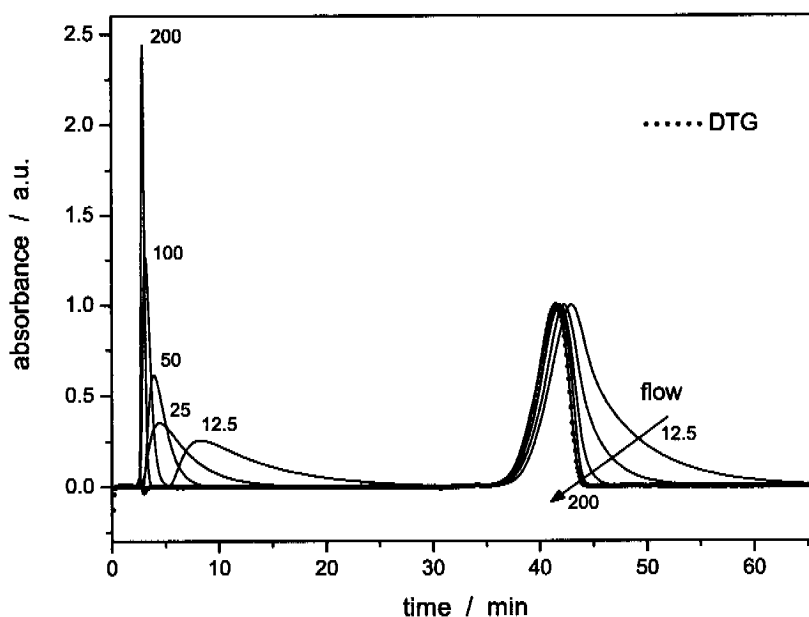


**Fig. 4-9:** Influence of the carrier gas flow on the shape of FTIR signals measured during calibration (injection of  $1\text{ ml CO}_2$ ) and decomposition of  $20\text{ mg NaHCO}_3$ . The intensities of the decomposition traces are normalized. Carrier gas flow rates are indicated on the curves ( $\text{ml min}^{-1}$ ).



traces are normalized. With increasing flow rate the calibration peaks become sharper and the value of their maximal concentration increases significantly compared to the decomposition traces. On the other hand, lower flow rates (25 or 50  $\text{cm}^{-1}$ ) show a larger tailing, as clearly emerges from calibrating and decomposition traces. The quantification of the FTIR traces presented in Figure 4-9 is shown in Figure 4-10. This figure depicts the dependence of the integral intensities of the calibration and decomposition signals on the carrier gas flow. The amount of  $\text{CO}_2$  evolved from the sample determined by comparison of integral intensities of calibration and decomposition peaks is shown in the upper part of the plot. The deviation from the stoichiometric amount can

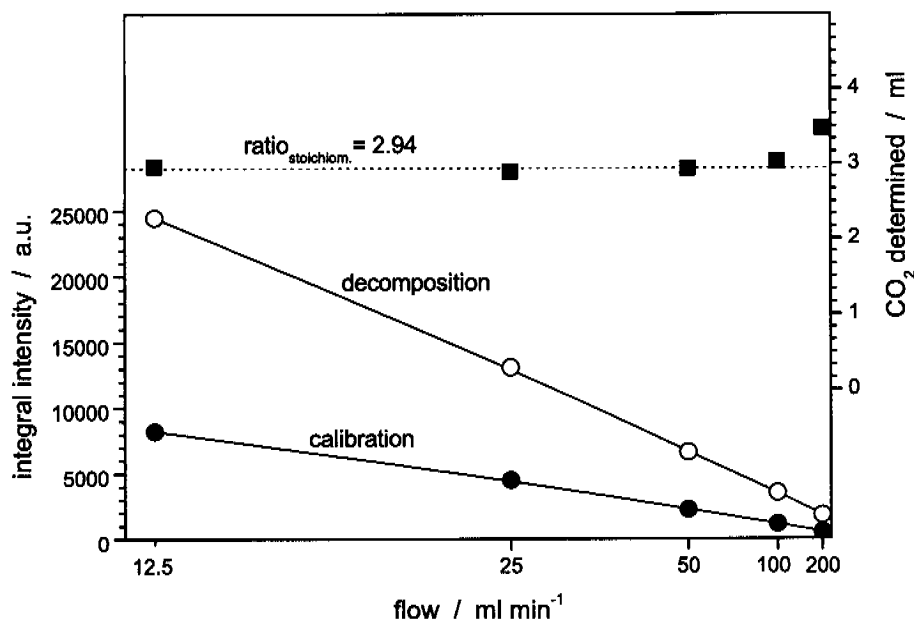


**Fig. 4-10:** Dependence of the integral intensities of the calibration and decomposition signals on the carrier gas flow. The amount of evolved  $\text{CO}_2$  determined from the comparison of calibration (solid circles) and decomposition (open circles) signals is presented in the upper part of the Figure. The stoichiometric value for the sample mass 20 mg  $\text{NaHCO}_3$  and injection of 1 ml  $\text{CO}_2$  amounts to 2.94.

easily be seen when increasing the flow rate, which of course influences much more the narrow peaks obtained during calibration than the relatively broad signals resulting from the decomposition.

However, application of low carrier gas flows has, in certain cases, also a disadvantage, e.g. when multistage reactions have to be investigated. Lower flow rate increases the tailing of the signal. This phenomenon is clearly visible in Figure 4-9: The lower the flow rate, the more the real course of the reaction represented by the differential thermogravimetric curve (DTG, dotted line) differs from those represented by spectrometric signals. This aspect is clearly visible also in Figure 4-11 depicting the multistage dehydration of copper sulfate pentahydrate. The results illustrate the difficulty in separation of the two consecutive dehydration stages occurring in the range 60–120 °C. The water

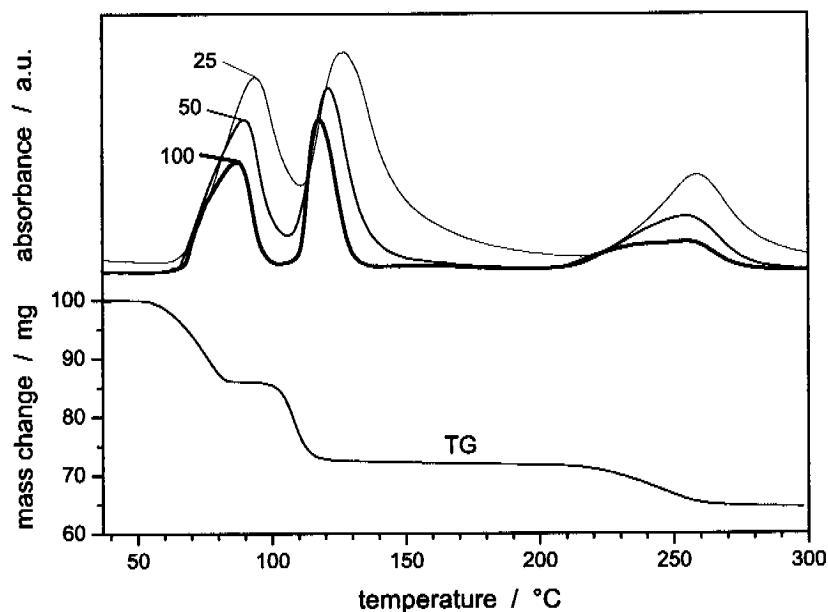


**Fig. 4-11:** Water traces during dehydration of 50 mg  $\text{CuSO}_4 \cdot 5 \text{H}_2\text{O}$  measured at different carrier gas flows. Heating rate:  $10 \text{ K min}^{-1}$ , carrier gas: He, flow rates are indicated on the curves ( $\text{ml min}^{-1}$ ). Corresponding TG traces are shown in the lower part.

traces recorded using carrier gas flows of 25 and 50 ml min<sup>-1</sup> cannot be quantified properly due to partial overlap. In contrast, using a carrier gas flow of 100 ml min<sup>-1</sup> the contribution of these peaks can be determined. Note that better splitting of these two peaks can also be achieved by e.g. decreasing the heating rate, however that lowers the concentration of the detected gas in the system and consequently the accuracy of quantification.

An example indicating how the procedure of the quantification of FTIR spectra by pulse calibration with gases can be influenced by different experimental parameter settings is given in Figure 4-12, which presents the CO<sub>2</sub>

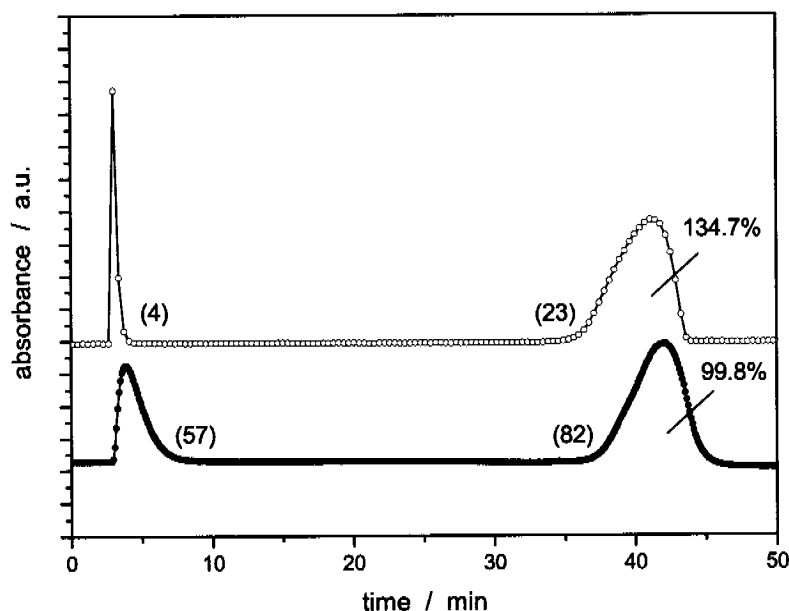


**Fig. 4-12:** Example of quantification of FTIR traces by pulse technique during decomposition of 20 mg NaHCO<sub>3</sub>. Numbers of recorded data points (> 1% of maximal intensity) are given in brackets. **A** (open circles): Carrier gas 200 ml min<sup>-1</sup> Ar, resolution 1 cm<sup>-1</sup>, (pulse: 4 points). Calculated amount of CO<sub>2</sub> in the sample amounted to 134.7% of the stoichiometric value. **B** (solid circles): Carrier gas 50 ml min<sup>-1</sup> He, resolution 4 cm<sup>-1</sup>, (pulse: 57 points). 99.8% of CO<sub>2</sub> was determined.

traces recorded during calibration pulses and decomposition of  $\text{NaHCO}_3$  according to the following reaction (Eq. 1):



**Table 4-2:** Results of the pulse calibration technique with different experimental set-ups A and B reported in Figure 4-12.  $\text{CO}_2$  amounts (%) quantified by MS and FTIR related to stoichiometric value are given. F is the normalized ratio between integral intensity of FTIR and MS calibration signal (decomposition peaks were normalized).

Set-up	MS / %	FTIR / %	F / -
A (open circles)	102.9	134.7	0.76
B (solid circles)	99.2	99.8	0.99

Table 4-2 compares the results of the quantification of the FTIR and MS recorded traces shown in Figure 4-12 using pulse calibration with significantly different experimental parameters. The comparison is based on the calculated amounts of  $\text{CO}_2$  evolved during decomposition of sodium bicarbonate related to the stoichiometric value. Experiment A (open circles) shows the error that had been introduced when unsuitable parameters were used: the sharp pulse observed using high spectral resolution ( $1 \text{ cm}^{-1}$ ) and high carrier gas flow rate ( $200 \text{ ml min}^{-1} \text{ Ar}$ ) led to a large error in the FTIR quantification. Due to the low temporal resolution (collection of only 4 points during injection) and the high maximal intensity significantly lower values of the integral intensities of the calibration pulse were found resulting in overestimation of the amount of  $\text{CO}_2$  originating from the decomposition reaction.

Experiment B (solid circles) was performed under optimized conditions as regards quantification: a flow rate of  $50 \text{ ml min}^{-1}$  was chosen and spectral reso-

lution was set to  $4\text{ cm}^{-1}$ , which provided 57 data points during the calibration pulse and led to a more accurate determination of the evolved  $\text{CO}_2$  trace. MS and FTIR results obtained using proper experimental conditions (B) corroborated that high accuracy of the quantification of spectral signals can be achieved with both TA-MS and TA-FTIR.

We have shown the importance of choosing adequate experimental conditions, in order to quantify evolved gases by the pulse technique. Several parameters such as carrier flow rate, injection location, amount of injected gas and data acquisition time resulting from the spectral resolution have to be taken into account when setting the experimental conditions optimal for calibration of FTIR signals. We hope that the present study helps the practitioner to improve the quantification of evolved components in combined TA-FTIR investigations.

## 4.4 Conclusions

Quantification of evolved gases during thermal analysis by the pulse technique using MS or FTIR spectroscopy requires careful optimization of the experimental settings. Quantification based on FTIR is strongly affected by the chosen experimental parameters, whereas MS analysis is only little affected. The most important factors to be considered in gas quantification by means of TA-FTIR are: the choice of the spectral resolution and carrier gas flow rate. High spectral resolution leads to poor time resolution. Low carrier gas flow rate leads to poor separation of the reaction steps during multistage decompositions, as shown for the dehydration of  $\text{CuSO}_4 \cdot 5\text{H}_2\text{O}$ . The application of a TA-FTIR-MS system with properly chosen experimental conditions allows an easy and

less time-consuming *in situ* calibration procedure which can be used in different studies, such as the quantification of adsorption phenomena (cf. chapter 5), gas-solid reactions (cf. chapter 6) and decomposition of solids (cf. chapter 3).

## 4.5 References

- [1] S. Materazzi, R. Curini, G. D'Ascenzo, A.D. Magri, *Thermochim. Acta* 264 (1995) 75.
- [2] S. Materazzi, *Appl. Spectrosc. Rev.* 33 (1998) 189.
- [3] S. Materazzi, *Appl. Spectrosc. Rev.* 32 (1997) 385.
- [4] M. Mittleman, *Thermochim. Acta* 166 (1990) 301.
- [5] L.C.K. Liaw, T.C.K. Yang, D.S. Viswanath, *Appl. Spectrosc.* 51 (1997) 905.
- [6] M.F. Cai, R.B. Smart, *Energy Fuels* 7 (1993) 52.
- [7] B. Roduit, J. Baldyga, M. Maciejewski, A. Baiker, *Thermochim. Acta* 295 (1997) 59.
- [8] M. Maciejewski, C.A. Muller, R. Tschan, W.D. Emmerich, A. Baiker, *Thermochim. Acta* 295 (1997) 167.
- [9] J. Wang, B. McEnaney, *Thermochim. Acta* 190 (1991) 143.
- [10] M. Maciejewski, A. Baiker, *Thermochim. Acta* 295 (1997) 95.
- [11] K. Marsanich, F. Barontini, V. Cozzani, L. Petarca, *Thermochim. Acta* 390 (2002) 153.
- [12] T.L. Slager, F.M. Prozonic, *Thermochim. Acta* 426 (2005) 93.
- [13] E. Post, S. Rahner, H. Mohler, A. Rager, *Thermochim. Acta* 263 (1995) 1.

- [14] I. Pitkanen, J. Huttunen, H. Halttunen, R. Vesterinen, *J. Therm. Anal. Cal.* 56 (1999) 1253.
- [15] F. Barontini, K. Marsanich, V. Cozzani, *J. Therm. Anal. Cal.* 78 (2004) 599.
- [16] R.S. Jackson, A. Rager, *Thermochim. Acta* 367–368 (2001) 415.
- [17] R. Bassilakis, R.M. Carangelo, M.A. Wojtowicz, *Fuel* 80 (2001) 1765.
- [18] A. Perez-Ponce, J.M. Garrigues, S. Garrigues, M. de la Guardia, *Analyst* 123 (1998) 1817.
- [19] A.I. Balabanovich, A. Hornung, D. Merz, H. Seifert, *Polym. Degrad. Stab.* 85 (2004) 713.
- [20] W.M. Groenewoud, W. de Jong, *Thermochim. Acta* 286 (1996) 341.

Seite Leer /  
Blank leaf



## Gas Adsorption Studied on Zeolites

### 5.1 Introduction

In this chapter an important application of PulseTA<sup>®</sup> in catalytic research is described. Using hyphenated simultaneous thermal analysis–mass spectrometry, the quantity of adsorbed gas and their heat of adsorption with differential scanning calorimetry (DSC) is studied.

A very frequently used method for characterizing heterogeneous catalysts is gas adsorption, which includes the processes involved whenever a gas (adsorptive) is brought into contact with a solid (adsorbent). The determination of the amount of adsorbed species and the various thermal effects combined with the above process provide information on the amount and nature of active surface sites. The selective chemisorption, i.e. formation of a strongly bound adsorbed monolayer, allows the determination of the metal surface area and metal dispersion of supported catalysts. Dispersion is expressed as the ratio of the total number of metal atoms accessible on the surface to the total number of metal atoms in the sample.

The measurement of gas uptake is carried out by static methods such, as volumetry and gravimetry, as well as with dynamic flow techniques such as gas chromatography or gas thermal conductivity [1]. In volumetry, the catalyst, previously pretreated and evacuated, is contacted by a known quantity of the adsorbate gas. The amount of adsorbed gas is determined by measuring the

pressure after the adsorption equilibrium is established. Successive doses of gas allow the determination of the adsorption isotherm, i.e. the amount of adsorbed gas versus the equilibrium pressure. Volumetry combined with calorimetry allows the determination of the heat of adsorption, which helps in understanding the nature of the catalytically active sites [2–4]. In the gravimetric method, the amount of adsorbed gas is measured by weighing the sample. Recently, a new, so called tapered element oscillating microbalance (TEOM) technique has been developed that offers a method for measuring mass changes in a fixed bed reactor while reaction gases are passed through the sample. The mass is determined by monitoring the frequency changes of the tapered oscillating element [5,6]. In contrast to conventional microbalances, none of the probe molecules bypass the sample holder, however, as reported by Rebo et al. [7], the maximum adsorbed amounts determined by TEOM correspond well with values obtained in conventional gravimetric systems.

Dynamic methods of measuring adsorption are faster and more convenient than static methods because they do not require vacuum systems. In the continuous flow technique, the pretreated catalyst is flushed by an inert gas at a temperature sufficient for desorbing all adsorbed species. After cooling to the required temperature, the flow is switched to the adsorbate gas until the downstream detector (generally a thermal conductivity cell) shows a constant gas phase composition. After purging with an inert gas, the adsorptive is once more switched on to investigate possible reversible adsorption.

An interesting modification of the conventional gravimetric method has been recently reported by Brown and Rhodes [8]. A combined TG-DSC instrument was equipped with a pneumatically operated three-way valve, which permitted switching between a pure carrier gas and a blend of 5% reactive gas in the carrier gas. The sample was dosed with the adsorptive in a con-

trolled stepwise fashion by repeatedly switching the composition of the gas phase over the adsorbent.

Proper selection of temperature, when investigating adsorption phenomena, is a prerequisite irrespective of the technique used. The choice of temperature always involves a compromise between high and low. High temperatures reduce the time needed to achieve thermodynamic equilibrium between the adsorbed probe molecules and the active surface sites, whereas low temperatures lead to a higher coverage of the surface [4]. On the other hand, too low adsorption temperatures do not allow sufficient mobility of physisorbed molecules and thus do not ensure that energetically stronger active sites would be populated before weaker sites begin to fill [9].

Adsorbate molecules should be mobile enough at the adsorption temperature so that each dose of adsorptive can interrogate all of the available adsorption sites. The mobility of the adsorbed molecules can be checked by temperature-programmed desorption (TPD), which has become a very common technique for catalyst characterization [10]. The information collected from TPD studies contains the type and amount of desorbed species and indicates the temperature range of the desorption process, this being related to the bond energies between adsorbate and the surface.

In common practice, the determination of the amount of adsorbed species, the heat of adsorption and the study of the desorption require different experimental equipments. Here we demonstrate that pulse thermal analysis [11] makes it possible to study all these phenomena using the same experimental set-up. Results of ammonia adsorption measurements by means of the pulse technique are compared to corresponding data derived from volumetric measurements.

## 5.2 Experimental

Experiments were carried out on Netzsch STA 409 thermoanalyzer equipped with a pulse device (Netzsch) enabling injection of a certain amount of one or two different pure gases or gaseous mixtures into the carrier gas stream flowing through the system. The amount of injected gas could be changed from 0.01 to 10 ml. Mainly 0.25, 0.50 and 1.0 ml volumes were used. The flow rate was controlled by mass flow controllers, Brooks's model 5850E, based on a thermal mass flow sensing technique. The thermoanalyzer was connected by a heated (ca. 200 °C) stainless steel capillary to a Balzers quadrupole mass spectrometer QMG 420. The amount of the adsorbents varied from ca. 25–30 mg for DSC measurements (Pt crucible, o.d.=6.8 mm, volume 0.085 ml) to 20–400 mg (alumina crucible, o.d.=16.4 mm, volume 1.0 ml) in the experiments where the influence of the bed thickness on the adsorption process was investigated.

In order to compare the results obtained by the pulse technique with those from a conventional method, volumetric measurements with the same reactants were carried out on Micromeritics ASAP 2010 system. After measuring the first adsorption isotherm at 200 °C, the system was evacuated in order to remove the physisorbed ammonia and a second isotherm was measured. The amount of chemisorbed ammonia was calculated from the difference between these isotherms, according to the generally applied procedure [12].

The zeolites, ZSM-5 and mordenite, used as adsorbents, are crystalline aluminosilicates made up of tetrahedrally coordinated Al and Si atoms bonded through bridging oxygens. ZSM-5 has a three-dimensional pore structure with interconnected channels of dimensions 0.53 nm x 0.57 nm and 0.55 nm. Mordenite possesses a two-dimensional channel system with dimensions 0.67 nm x 0.70 nm and small perpendicular pores with dimensions 0.29 nm x

0.57 nm [13]. The zeolites were received in the Na form from Chemie Uetikon AG. After calcination at 500 °C they were ion exchanged at 90 °C with 1 M  $\text{NH}_4\text{NO}_3$  and heated in air to 500 °C for 2h to obtain the H-form. Before the adsorption experiments samples were heated in the thermoanalyzer to 500 °C to remove the gases adsorbed during handling, then they were cooled down to the measuring temperature and equilibrated until no mass change was detectable. Ammonia (purity 99.98%, PanGas) and helium or argon (purity 99.999%) were used as adsorptive and carrier gases, respectively.

Additionally, silica-titania aerogel [14] and a commercial nickel catalyst (Engelhard Ni-5256 E3/64) were used as adsorbents.

### 5.3 Results

Figure 5-1 shows the mass changes of the H-ZSM-5 zeolite at 200 °C resulting from a series of ammonia pulses, and illustrates the typical features of the pulse technique. Strong, virtually irreversible adsorption (chemisorption) of the injected ammonia occurred during pulses 1–3, pulse 4 resulted in both strong and weak (reversible) adsorption phenomena, whereas during pulses 5 and 6 only weak adsorption (physisorption) took place. The mass gain at steady state, indicated by  $\theta$  in Figure 5-1, where no further mass changes were detectable, represents the amount of chemisorbed ammonia. The second part of the experiment depicts the temperature range of the desorption process (TPD). The weight loss at temperatures above 550 °C is due to the evolution of residual water from the zeolite, the desorption of ammonia occurs in the range 205–550 °C, as confirmed by monitoring the  $m/z = 15$  mass spectrometric signal.

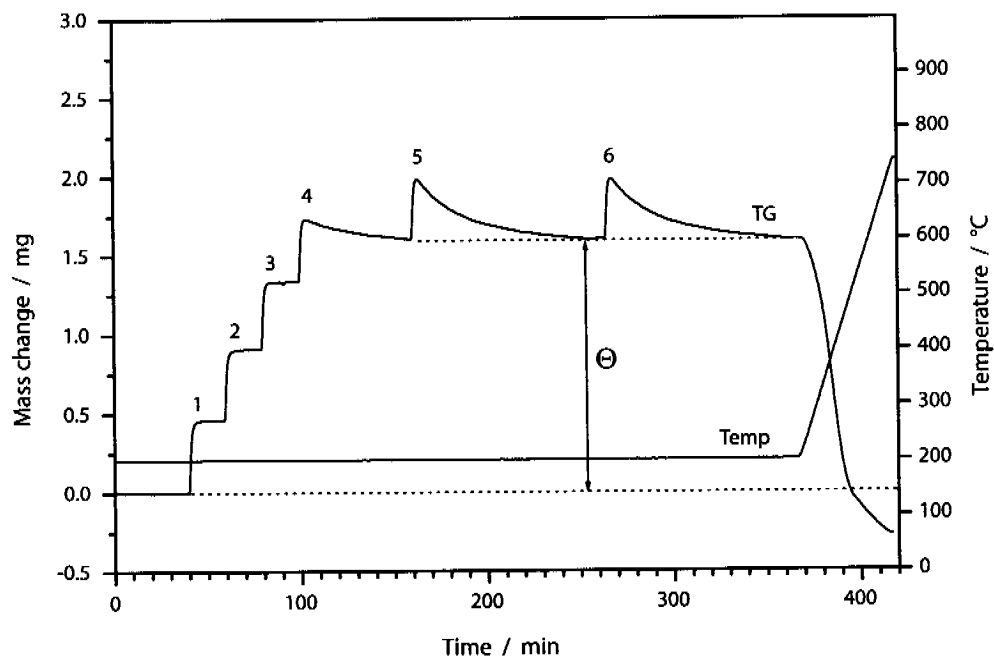


**Fig. 5-1:** Mass changes of H-ZSM-5 zeolite after exposure to a series of pulses of 1 ml ammonia at 200 °C. The desorption after the 6th pulse was initiated by heating at a rate of 10 K min<sup>-1</sup>. The amount of chemisorbed ammonia is marked as  $\theta$ .

In the following, experimental parameters which have the greatest influence on the adsorption process under dynamic conditions, were investigated. These parameters embrace: thickness of the adsorbent bed in the crucible, temperature and carrier gas flow.

### 5.3.1 Influence of Thickness of Adsorbent Bed

The conditions for mass transport in the experimental set-up used are not optimal for the gas-solid interaction. As in all typical thermoanalyzers the gas does not flow through the sample bed, this can influence the kinetics of the adsorption due to diffusional limitations. In order to study the influence of diffusion effects and to check the reproducibility of the method, the sample mass was

varied over a range from 10 to 400 mg. Figure 5-2A shows that the specific amount of chemisorbed ammonia at 200 °C, related to 1 g of adsorbent, is independent of the sample mass i.e. the bed thickness, provided the same kind of crucible was used (open symbols in Figure 5-2A). The use of the DTA crucible with its different geometry (smaller diameter), resulting in a thicker bed and lower amount of zeolite, did not influence the amount of chemisorbed ammonia (solid symbols). However, the thickness of the bed significantly

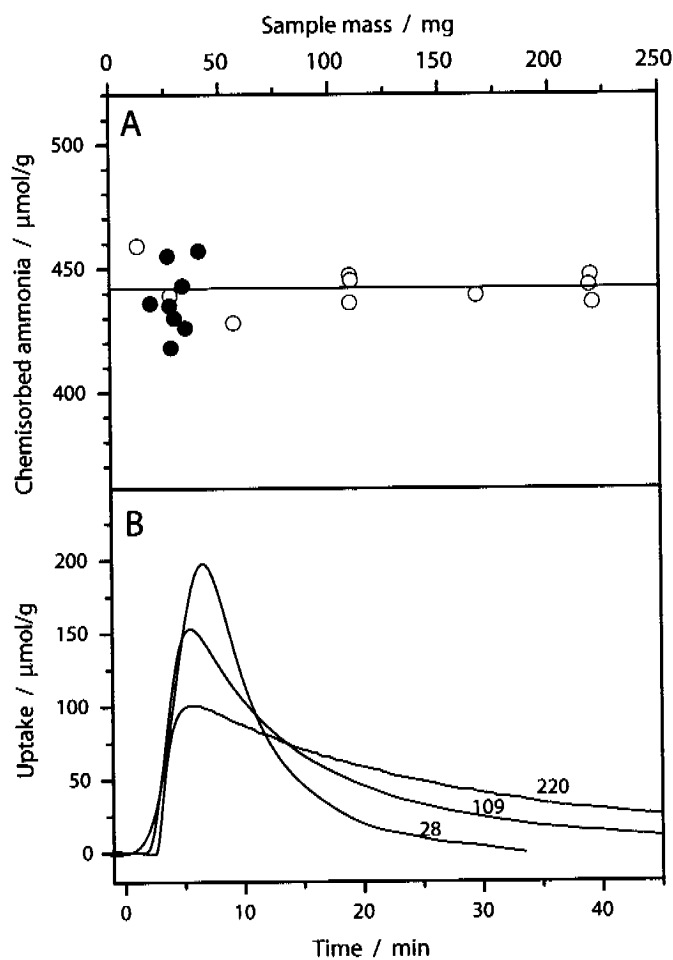


**Fig. 5-2:** Influence of the mass of adsorbent (zeolite H-ZSM-5) on: (A) Amount of chemisorbed ammonia (solid circles present the results obtained in DSC crucibles), B: Rate of desorption of physisorbed species. Masses of zeolite are indicated on curves. He flow:  $50 \text{ ml min}^{-1}$ , heating rate:  $10 \text{ K min}^{-1}$ .

affected the desorption process of physisorbed ammonia. Figure 5-2B presents the influence of the sample mass (indicated in mg on the curves) on the desorption of physisorbed ammonia at 200 °C. The changes of the adsorption uptake indicate that the thicker the bed, the higher is the time required for total desorption at a constant carrier gas flow.

### 5.3.2 Influence of Temperature

Figure 5-3A shows the dependence of the amount of strongly adsorbed ammonia on temperature for H-ZSM-5, as determined by the PulseTA<sup>®</sup> method (solid circles). For comparison, corresponding results measured by the volumetric method at 143 °C [15,16], 150 °C [4,17,18], 200 °C [4,17], 250 °C and 300 °C [4,17,18] are also shown (open circles). The influence of temperature on the desorption rate of the physisorbed species is presented in Figure 5-3B.

The temperature dependence of the amount of chemisorbed species is very similar for both methods. The observed differences can, at least partly, be attributed to the different origin of the H-ZSM-5 samples and the evacuation procedure applied during the volumetric measurements. In order to compare the results of both methods for the same sample, the amount of ammonia chemisorbed on H-ZSM-5 at 200 °C was measured volumetrically. The results are presented in Figure 5-4 and indicated (open diamond) in Figure 5-3A. This experiment demonstrates that for the same sample the difference between the results obtained by the two methods is below 5%. In volumetry, the evacuation of the system, necessary for the determination of the physisorbed species, can lead to removal of a small amount of chemisorbed ammonia. This behavior is illustrated by the results presented in Table 5-1 which compares the amount of adsorbed ammonia on different adsorbents measured with both techniques.



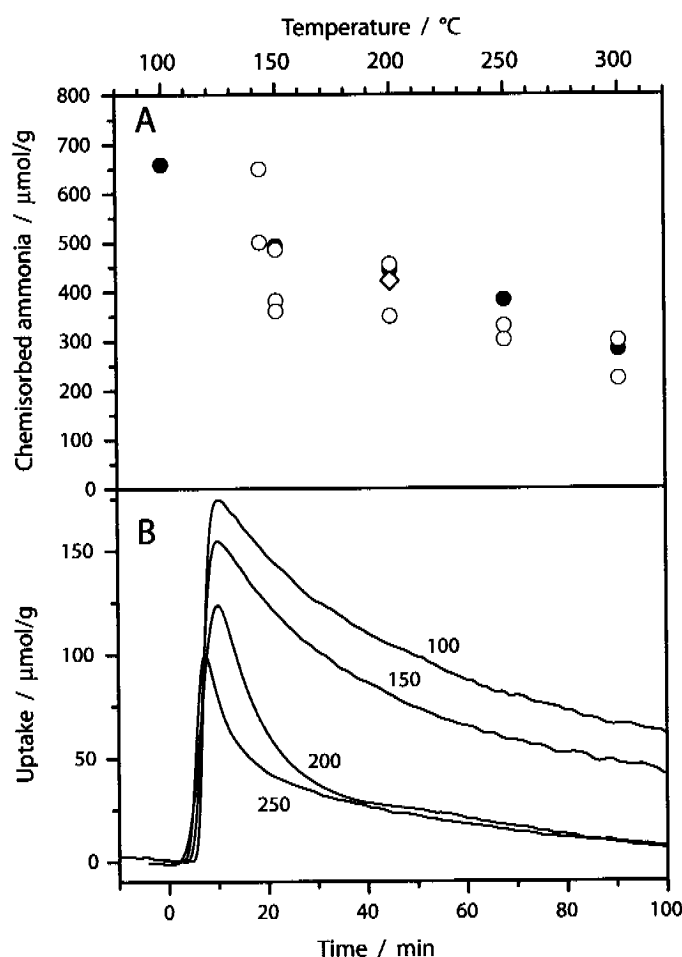


**Fig. 5-3:** Influence of temperature on: (A) Amount of chemisorbed ammonia, solid circles indicate results obtained by PulseTA<sup>®</sup>; open circles represent volumetric results reported in the literature. Open diamond indicates our volumetric measurement. (B) Rate of desorption of physisorbed species, temperatures in centigrades are marked on curves. Helium flow:  $50 \text{ ml min}^{-1}$ , heating rate:  $10 \text{ K min}^{-1}$ , sample mass:  $113.5 \text{ mg}$ .

The difference between chemisorbed amounts of ammonia determined by PulseTA<sup>®</sup> and volumetry, is especially apparent in the case where the adsorption strength between adsorbate and adsorbent is weak, resulting in desorption at lower temperatures, as observed with the titania-silica aerogel. Figure 5-5 compares the TPD curves, represented by the mass spectrometric signals of  $m/z = 15$ , for H-ZSM-5 and the aerogel. This particular  $m/z$  ratio for ammonia has been chosen, instead of the stronger  $m/z = 17$  signal, to exclude the contri-

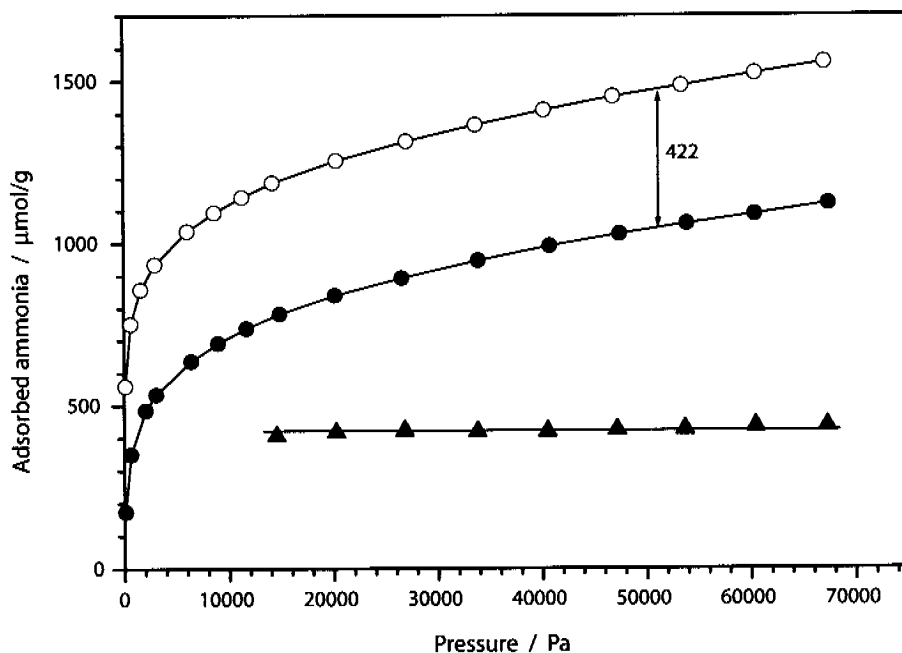


**Fig. 5-4:** Volumetric measurement of amount of ammonia chemisorbed on H-ZSM-5 zeolite at 200 °C. Open circles represent the first adsorption isotherm, the second isotherm, measured after evacuation, is given by solid circles. The triangles show the difference between both isotherms.

**Table 5-1:** Ammonia adsorption on various catalyst materials<sup>a</sup>

Sample	$T_{\text{ads}} / ^\circ\text{C}$	$\theta_{\text{vol}} / \mu\text{mol g}^{-1}$	$\theta_{\text{grav}} / \mu\text{mol g}^{-1}$
H-ZSM-5	200	422	442
Silica-titania aerogel	50	689	1123
Ni-5256 E3/64	50	449	528
H-mordenite	200	-	1830

<sup>a</sup> Uptakes (coverages) determined by conventional volumetric method ( $\theta_{\text{vol}}$ ) and PulseTA<sup>®</sup> gravimetry ( $\theta_{\text{grav}}$ ).

bution resulting from the fragmentation of water, especially important at higher temperatures.

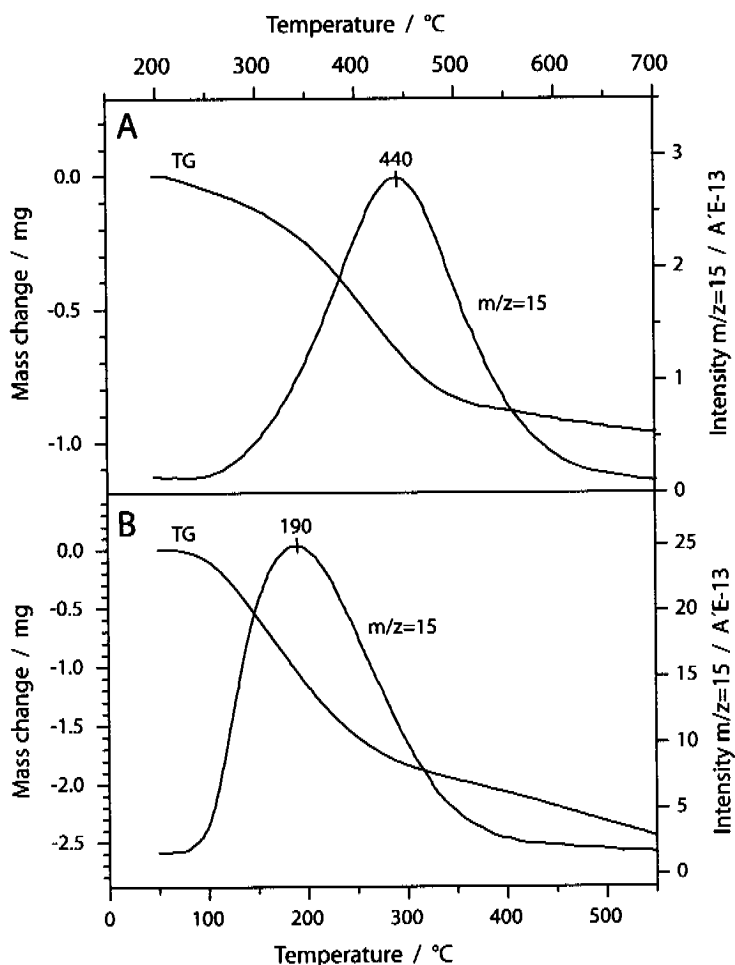
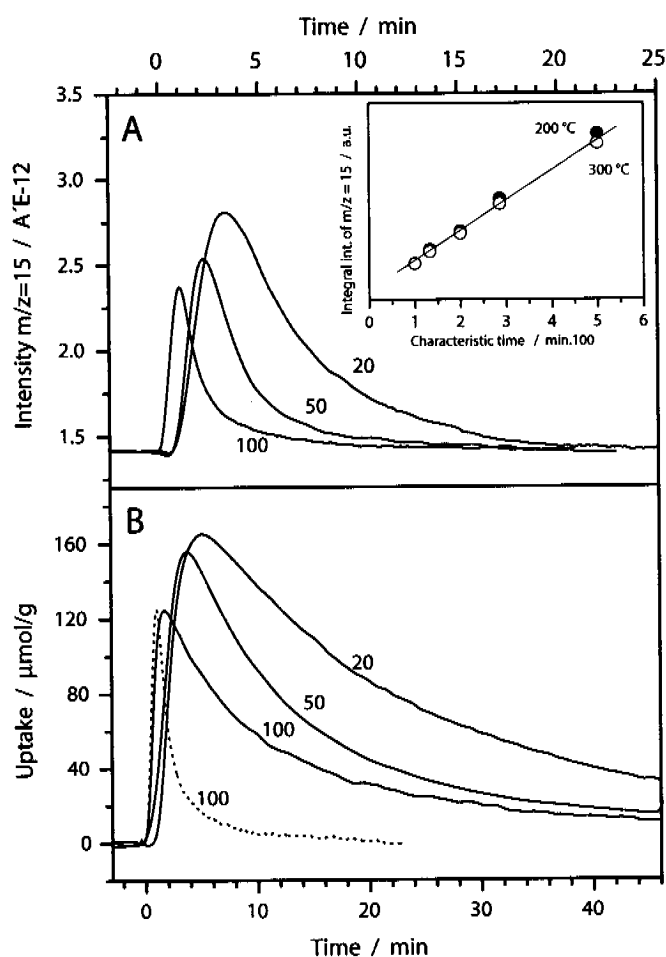


Fig. 5-5: Desorption of chemisorbed ammonia ( $m/z = 15$ ) from: (A) H-ZSM-5 zeolite and (B) silica-titania aerogel. Heating rate:  $10 \text{ K min}^{-1}$ , helium flow:  $50 \text{ ml min}^{-1}$ .

### 5.3.3 Influence of Carrier Gas Flow

During adsorption measurements carried out with the PulseTA<sup>®</sup> technique, the contact between adsorptive and adsorbent occurs only during a relatively short time after the injection of the adsorptive into the carrier gas stream. A change of carrier gas flow significantly influences the time in which the injected species are in contact with the solid and the rate of desorption of physisorbed species. In order to illustrate this behavior, the carrier gas flow was changed between  $20$  and  $100 \text{ ml min}^{-1}$ , and  $1 \text{ ml}$  pulses of ammonia were injected at

200 and 300 °C into helium. The resulting  $m/z = 15$  signals, measured for an empty reactor, are shown in Figure 5-6A. Figure 5-6B presents the dependence of the desorption of physisorbed ammonia at 200 °C (compare to the 6th pulse in Figure 5-1) on the carrier gas flow. The dashed line represents the change of ammonia concentration in an empty reactor for a flow of  $100 \text{ ml min}^{-1}$  using the same time-scale as for the desorption curves.



**Fig. 5-6:** Influence of carrier gas flow (in  $\text{ml min}^{-1}$  indicated on curves) on: **A:** Response signal ( $m/z=15$ ) of 1 ml pulse of injected ammonia in an empty reactor and, **B:** Rate of desorption of physisorbed ammonia at 200 °C. The dashed line represents the change of the ammonia concentration for a flow of  $100 \text{ ml min}^{-1}$  using the same time-scale as for the desorption curves. The inset in Figure 5-6A presents the dependence of the integral intensity of  $m/z = 15$  signal on the characteristic time (defined in text).

The relationship between the integral intensity of the mass spectrometric signal  $m/z = 15$  and the characteristic time [19], defined as the ratio of injected volume of adsorptive to carrier gas flow rate, is shown in the inset in Figure 5-6A for experiments at 200 °C (solid circles) and 300 °C (open circles).

### 5.3.4 Determination of the Adsorption Heat

The goal of the final set of experiments was to check if it is possible to determine the thermal effects that occur during adsorption, in relation to the amount of chemisorbed adsorptive, simultaneously measured by thermogravimetry. The difficulties in determination of the thermal effects resulting from the interaction of an adsorptive with an adsorbent lie in the accurate measurement of the heat evolved and the amount adsorbed. The results presented above indicate that the determination of the amount of chemisorbed species is possible using a standard thermobalance when it is equipped with a pulse device that enables the injection of a known amount of adsorptive into the carrier gas stream. The procedure allows the quantification of both chemi- and physisorbed species. Moreover, it is also possible to investigate the desorption process.

The experimental set-up used for determining the amount of adsorbed species allowed measurements without significant diffusional constraints. The thickness of the adsorbent bed was decreased by spreading the solid in a thin layer in a large alumina crucible. Furthermore, helium was used as a carrier gas in order to increase the rate of diffusion during adsorption and desorption of the physisorbed species. Albeit favorable for mass transfer, these conditions were not optimal for determining thermal effects. Hence it was necessary to check if the change in experimental parameters, optimal for DSC measure-

ments, were suitable for measuring the heat of adsorption, in relation to the amount of adsorbed species.

The DSC measurements were carried out in a platinum crucible with a sample mass of 25–30 mg. Helium, used for the TG measurements, was replaced by argon. Under normal conditions the thermal conductivity of Ar is 0.0176, and for He it is  $0.1511 \text{ W m}^{-1} \text{ K}^{-1}$ . Helium is not recommended for DSC measurements because it lowers the intensity of DSC signals, due to its high thermal conductivity. Preliminary experiments, with indium as a standard, have shown that the integral intensity of the melting peak (measured as area below the baseline) is 2.6 times smaller for helium than for argon. On the other hand, the use of argon as a carrier gas increases the buoyancy effect and reduces the rate of diffusion due to its higher density and lower diffusion coefficient. The normal densities of He and Ar and the diffusion coefficients of ammonia in He and Ar at 200 °C are:  $0.1785 \text{ g l}^{-1}$ ,  $1.7837 \text{ g l}^{-1}$ ;  $9.27 \cdot 10^{-5} \text{ m}^2 \text{ s}^{-1}$  and  $2.45 \cdot 10^{-5} \text{ m}^2 \text{ s}^{-1}$ , respectively.

Quantitative calibration of the DSC signals was carried out by the standard procedure of measuring the enthalpy changes of a synthetic sapphire cylinder (NBS Standard Reference Material 720). Typical thermal effects recorded during the adsorption of ammonia are presented in Figure 5-7. The first pulse of  $\text{NH}_3$  leads to strongly bound (chemisorbed) ammonia only, whereas the third one is characteristic for weakly bound (physisorbed) ammonia. The physisorbed ammonia desorbs completely (note the endothermic effect of the desorption) after ca. 25–30 min. During the second pulse, both processes chemi- and physisorption are discernible. By decreasing the amount of injected gas it was possible to follow the interdependence between the adsorption heat and the uptake (coverage). Figure 5-8 depicts the adsorption of ammonia on H-ZSM-5 (A) and H-mordenite (B). The results listed in Table 5-2 indicate that

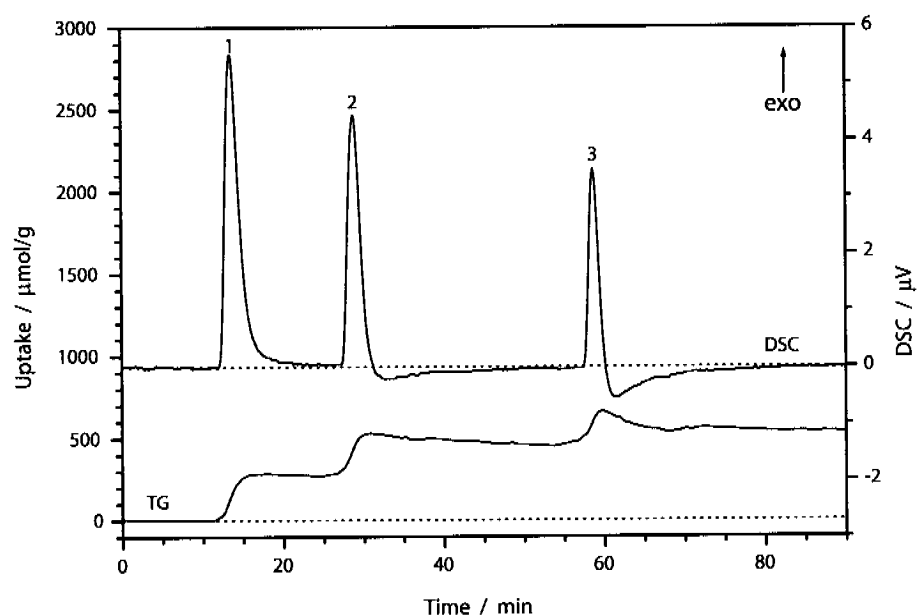


**Fig. 5-7:** DSC and TG signals occurring during adsorption of ammonia at 50 °C on nickel catalyst. Argon flow, 50 ml min<sup>-1</sup>, ammonia pulse, 1.0 ml, mass of adsorbent, 31.6 mg.

**Table 5-2:** Ammonia adsorption on zeolites, H-ZSM-5 (a) and H-mordenite (b) at 200 °C

$\theta_a / \mu\text{mol g}^{-1}$	$\Delta H_a / \text{kJ mol}^{-1}$	$\theta_b / \mu\text{mol g}^{-1}$	$\Delta H_b / \text{kJ mol}^{-1}$
0–187	138.2	0–484	141.4
187–328	136.3	484–916	141.2
328–436	135.6	916–1277	135.9
		1277–1615	137.2

for both zeolites the adsorption heat is only weakly dependent on the coverage, as has been reported in the literature (see [20]).

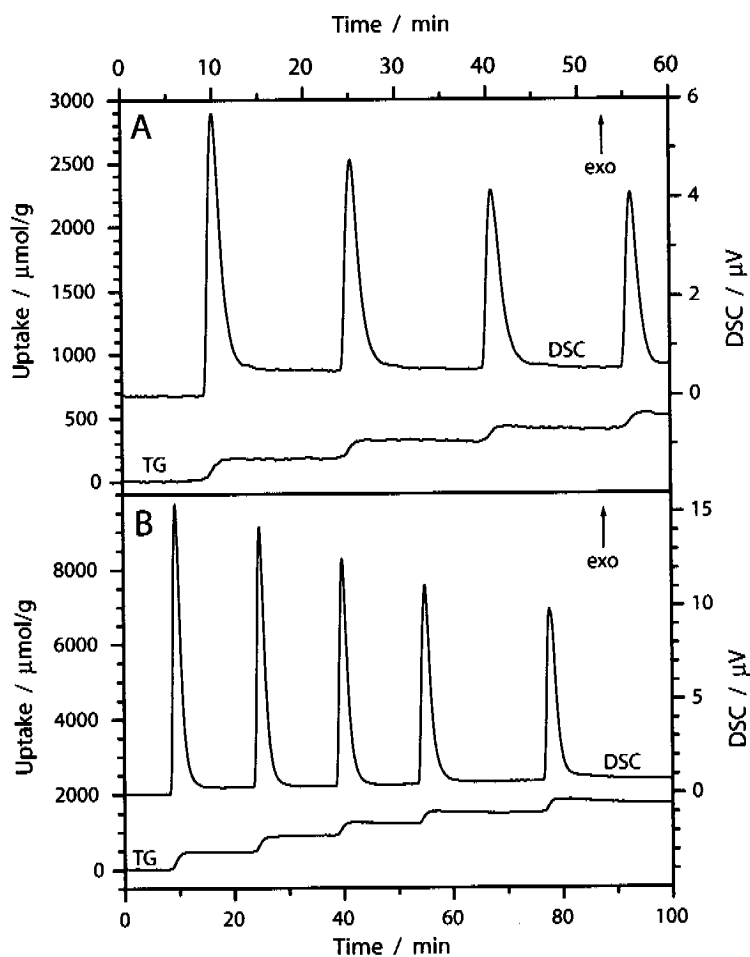


**Fig. 5-8:** DSC and TG signals occurring during adsorption of ammonia at 200 °C on zeolites: A: H-ZSM-5, B: H-mordenite. Adsorption heats determined for different coverage ranges are listed in Table 5-2.

## 5.4 Discussion

The method for determining the amount of adsorbed probe molecules used in this study differs from the commonly used volumetric and gravimetric methods. The main difference are:

- Typical thermoanalytical experiments (TG, DSC) focus on the desorption processes only, the adsorbent is usually exposed to an atmosphere containing the probe molecules beforehand [21–24]. Pulse thermal analysis allows



to study both, adsorption and desorption processes in the same experimental set-up.

- Contrary to the normal volumetric procedure, the adsorption process is investigated under atmospheric pressure.
- The contact between solid and adsorptive is limited to the short duration of the pulse.

Despite the above differences, the results on ammonia adsorption of this study agree well with those reported in the literature. Both the amount of chemisorbed ammonia and the heat of adsorption agree well with the values reported for H-ZSM-5 and H-mordenite having similar Si/Al ratios, i.e. 25 and 8, respectively. The amount of chemisorbed ammonia at 200 °C, as determined by PulseTA<sup>®</sup>, is 442  $\mu\text{mol g}^{-1}$ , whereas the values reported in the literature vary from 384 [4] through 420 [25] to 450  $\mu\text{mol g}^{-1}$  [2]. The heats of ammonia adsorption, determined for the two zeolites, also agree with those reported in the literature. For both samples, the differential heats of adsorption are constant up to a coverage of one molecule of ammonia per aluminium site [26], therefore the integral heats derived here can easily be compared with the reported differential values. The adsorption heat found in this study for H-ZSM5 is 138  $\text{kJ mol}^{-1}$  for coverages 0–187  $\mu\text{mol g}^{-1}$ , and 135.6  $\text{kJ mol}^{-1}$  for coverages 328–436  $\mu\text{mol g}^{-1}$ . Parillo et al. [9] report 145  $\text{kJ mol}^{-1}$  (0–400  $\mu\text{mol g}^{-1}$ ) and 150  $\text{kJ mol}^{-1}$  [20] (between zero and one ammonia molecule per aluminium site), Auroux [4] found 140  $\text{kJ mol}^{-1}$  in the same range and Cardonna-Martinez et al. [2] 143  $\text{kJ mol}^{-1}$ . For H-mordenite, our value, 141  $\text{kJ mol}^{-1}$ , for the coverage 0–484  $\mu\text{mol g}^{-1}$  is also comparable to the heats reported: 132–146  $\text{kJ mol}^{-1}$  [2], and 160  $\text{kJ mol}^{-1}$  [20].

Unfavorable mass transfer conditions, induced by the fact that carrier gas does not flow through the adsorbent bed in the applied thermoanalytical system, were not a severe limitation for the adsorption measurements. This

emerges from the present study and a comparison of conventional gravimetric results (carrier gas not flowing through the bed) with data reported in the studies using the TEOM method (gases pass through the bed). The similarity of the results [7] confirms that the final state of chemisorption is unaffected by the non optimal contact between gas and solid.

The total amount of chemisorbed gas per unit mass of adsorbent does not depend on the pulse volume or the amount of solid sample used (see Figure 5-2A). These parameters mainly influence the physisorption process, as illustrated in Figure 5-9. Complete coverage of the surface can be reached between one (Figure 5-9B) and 13 pulses (Figure 5-9D), depending on the ratio between the amount of injected probe molecules and the mass of the solid. In the second case it is possible to measure the differential heats of adsorption if the evolved heat during one pulse is greater than ca. 150–200 mJ. The thermal effects presented in Figure 5-8A are between 760 and 530 mJ for the first and third pulses, respectively.

Even at the relatively high temperature of 200 °C, a fraction of the probe molecules in the last few pulses before saturation are physisorbed. For a particular adsorptive the rate of physisorption depends mainly on the thickness of the adsorbent bed (diffusion limitation) and the flow and kind of carrier gas. The rate of desorption decreases with increasing thickness of the adsorbent layer, and increases with higher flow rate of the carrier gas. However, even for small masses and high flows, the time of desorption of the physisorbed species is in the order of 30–40 min. The six minute periods of desorption, as applied by Brown and Rhodes [8], would be much too short to fully remove all physisorbed species in our experiments.

Monitoring physisorption *in situ* seems to be a necessary prerequisite for a better understanding of the observed adsorption phenomena. The amount of

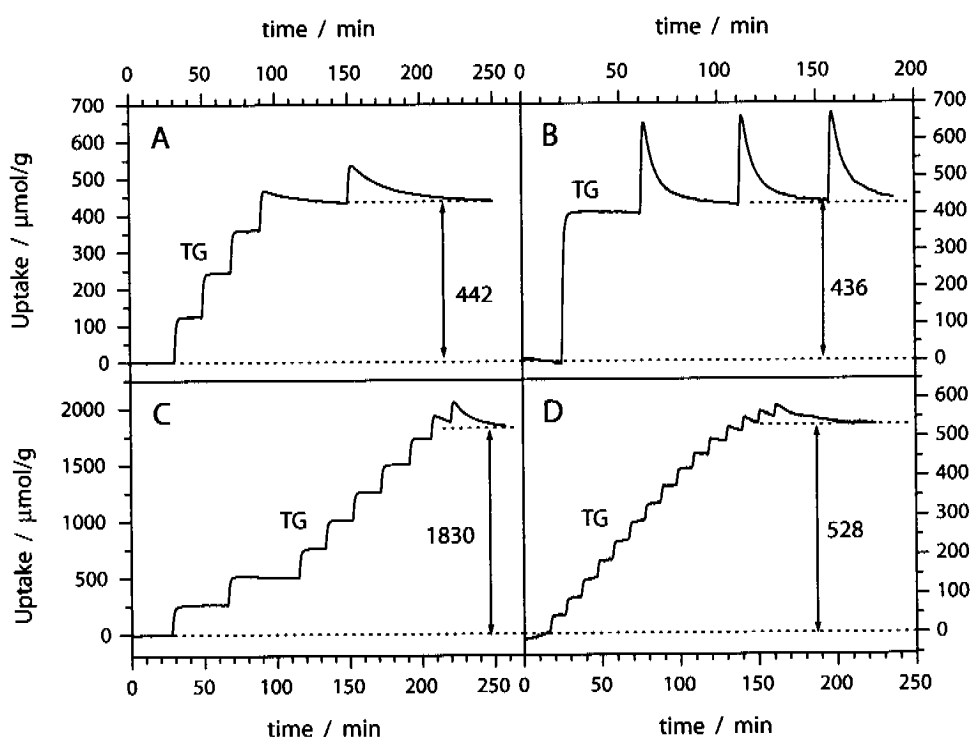


**Fig. 5-9:** Influence of experimental parameters (temperature, kind of carrier gas and its flow, amount of injected adsorptive, mass of adsorbent) on the shape of thermogravimetric curves resulting from chemisorption of ammonia on various catalyst materials.

A: H-ZSM-5, 200 °C, He, 50 ml min<sup>-1</sup>, 1 ml, 219.9 mg

B: H-ZSM-5, 200 °C, He, 50 ml min<sup>-1</sup>, 1 ml, 56.3 mg

C: H-mordenite, 200 °C, He, 50 ml min<sup>-1</sup>, 1 ml, 109.6 mg

D: Ni-5256 E3/64, 50 °C, Ar, 100 ml min<sup>-1</sup>, 0.5 ml, 135.1 mg.

Comparison of A and B illustrates the effect of the sample mass. C and D show that proper adjustment of the ratio of pulse volume to the total uptake (coverage) allows more detailed recording of the adsorption process.

adsorbed species and the heat of adsorption result from different contributions of chemi- and physisorption which becomes apparent with the last few pulses before saturation. The opportunity to distinguish between physisorption and chemisorption makes it possible to individually assign mass and thermal effects to these phenomena, thus avoiding misinterpretations.

The total characterization of the interaction between adsorptive and adsorbent requires the pretreatment of the solid at an optimal temperature, proper

selection of the temperature of adsorption, and the determination of the strength of the adsorbed species by temperature programmed desorption. The PulseTA<sup>®</sup> technique makes it possible to carry out all these procedures in the same experimental set-up, a commercial thermoanalyzer.

Finally is worthy to mention that the described method has been successfully applied in our laboratory for the study of ammonia adsorption on various catalyst materials, including mesoporous titania-silica aerogels [14], cobalt [27] and nickel [28] catalysts, and for the study of CO, CO<sub>2</sub> and O<sub>2</sub> adsorption on Au/TiO<sub>2</sub> and Au/ZrO<sub>2</sub> [29].

## 5.5 Conclusions

The PulseTA<sup>®</sup> technique provides the opportunity to study several phenomena occurring during adsorption in a conventional thermoanalyzer. Processes which can be monitored include pre-treatment of the adsorbent, adsorption and desorption. Characteristic features of PulseTA<sup>®</sup> for gas adsorption measurements are:

- Monitoring of the mass change and the kind and amount of evolved species during pre-treatment allows the determination of the optimal temperature needed to remove all pre-adsorbed species.
- Monitoring of the concentration of the adsorptive in the system and the mass changes, during and after injection of the probe molecules, provides the opportunity to study both chemi- and physisorption.
- The relationship between the measured heats of adsorption and changes in mass enables the correct interpretation of thermal effects involved in the adsorption process.
- The possibility of carrying out temperature programmed desorption just after completion of the adsorption process prevents the introduction of

artefacts caused by the contact of the sample with the surrounding atmosphere.

The reliability of the method has been demonstrated by studying adsorption of ammonia on zeolites, H-ZSM-5 and H-mordenite. Measured coverages and heats of adsorption agree well with corresponding data reported in the literature.

## 5.6 References

- [1] J.L. Lemaitre, P.G. Menon and F. Delannay in "Characterization of Heterogeneous Catalysts", Ed. F. Delannay, Dekker, New York, 1984, Vol. 15, p.299
- [2] N. Cardona-Martinez and J.A. Dumesic, *Adv. Catal.* 38 (1992) 149.
- [3] A. Auroux in *Catalyst Characterization: Physical Techniques for Solid Materials*, Eds. B. Imelik and J. Viedrine, Plenum Press, New York, 1994, p.611.
- [4] A. Auroux, *Top. Catal.* 4 (1997) 71.
- [5] H. Patashnick, G. Rupprecht, and J.C.F. Wang, *Prepr. ACS Div. Petr. Chem.* 25 (1980) 188.
- [6] F. Hershkowitz and P. D. Madiara, *Ind. Eng. Chem. Res.* 32 (1993) 2969.
- [7] H.P. Rebo, De Chen, M.S.A. Brownrigg, K. Moljord, and A. Holmen, *Collect. Czech. Chem. Commun.* 62 (1997) 1832.
- [8] D.R. Brown, and C.N. Rhodes, *Thermochim. Acta* 294 (1997) 33.
- [9] D.J. Parillo, R.J. Gorte, and W.E. Farneth, *J. Am. Chem. Soc.* 115 (1993) 12441.

- [10] J.J.F. Scholten, A.P. Pijpers, and A.M.L. Hustings, *Catal. Rev.- Sci. Eng.* 27 (1985) 151.
- [11] M. Maciejewski, C.A. Müller, R. Tschan, W.-D. Emmerich, and A. Baiker. *Thermochim. Acta* 295 (1997) 167.
- [12] A. Baiker and M. Kohler in "Handbook of Heat and Mass Transfer", Vol. 3: Catalysis, Kinetics and Reaction Engineering, P.N. Cheremisinoff (Ed.), Gulf Publishing, Houston, 1989, Chapter 1, p.34.
- [13] D.W. Breck, "Zeolite Molecular Sieves: Structure, Chemistry and Use", Wiley, New York, 1974.
- [14] C.A. Müller, M. Maciejewski, T. Mallat and A. Baiker, *J.Catal.* 184 (1999) 280.
- [15] A. Auroux, V. Bolis, P. Wierzchowski, P.C. Gravelle, and J.C. Vedrine, *J.Chem. Soc. Farad. Trans. I* 75 (1979) 2544.
- [16] A. Auroux, J.C. Vedrine in "Catalysis by Acids and Bases" (B. Imielik, C. Naccache, G. Coudurier, Y. Ben Taarit and J.C. Vedrine, Eds.) p.311, Elsevier, Amsterdam, 1985.
- [17] A. Auroux, P.C. Gravelle, J.C. Vedrine and M. Rehas in "Proceedings of the Fifth International Conference on Zeolites" (L.V. Reeds, Ed.) p. 433, Heyden, London, 1980.
- [18] J.C. Vedrine, A. Auroux, and G. Coudurier, *ACS. Symp. Ser.* 248 (1984) 253.
- [19] B.Roduit, J. Baldyga, M. Maciejewski and A. Baiker, *Thermochim. Acta* 245 (1997) 59.
- [20] D.J. Parillo and R.J. Gorte, *J. Phys. Chem.* 97 (1993) 8786.
- [21] H. Bremer and K.-H. Steinberg, *Z.Chem.* 7 (1967) 203.
- [22] A.K. Ghosh and G. Curthoys, *J.Phys.Chem.* 88 (1984) 1130.

- [23] A.K. Aboul-Gheit, M.A. Al-Hajjaji and A.M. Summan, *Thermochim. Acta* 118 (1987) 9.
- [24] Zhang Di-Chang, Da Zhi-Jian, *Thermochim. Acta* 233 (1994) 87.
- [25] S.B.S. Sharma, B.L. Mayers, D.T. Chen, J. Miller and J.A. Dumesic, *Appl. Catal. A:General* 102 (1993) 253.
- [26] D.J. Parillo, C. Lee and R.J. Gorte, *Appl. Catal. A:General* 110 (1994) 67.
- [27] A.Fischer, M. Maciejewski, T. Bürgi, T. Mallat and A. Baiker, *J. Catal.* 183 (1999) 373.
- [28] A.Fischer A, T. Mallat, and A. Baiker, *J. Mol. Catal.-A Chem.* 149 (1999) 197.
- [29] J.-D. Grunwaldt, M. Maciejewski, O.S. Becker, P. Fabrizioli, and A. Baiker, *J. Catal.* 186 (1999) 458.

Seite Leer /  
Blank leaf



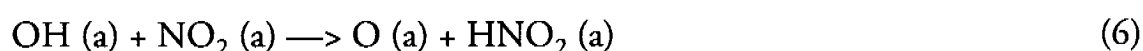
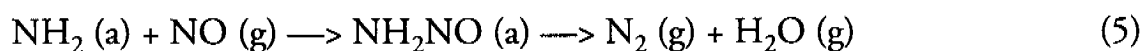
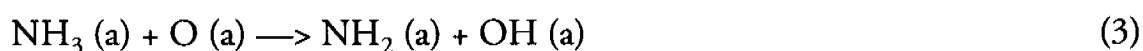
## Selective Catalytic Reduction of NO by NH<sub>3</sub> over Manganese-Cerium Mixed Oxides

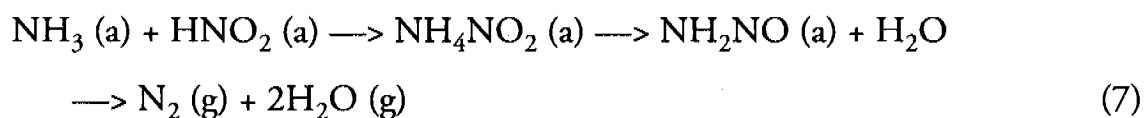
### 6.1 Introduction

The potential of TA-MS can be further extended using FTIR in addition, as demonstrated in this chapter using the example of the selective catalytic reduction of NO by NH<sub>3</sub> over manganese-cerium mixed oxides.

Exhaust gases from stationary and mobile combustion sources contain nitrogen oxides that cause a variety of environmentally harmful effects such as urban smog acid rain, ozone depletion and contribute to the greenhouse effect. Removal of these contaminants to comply with the environmental emission standard is necessary and various wet and dry processes have been put forward. Among these processes the selective catalytic reduction (SCR) of nitrogen oxides by ammonia has gained eminent importance [1,2]. A great variety of different catalyst have been reported to be active in SCR of NO<sub>x</sub> (NO, NO<sub>2</sub>), but only a few of them are applied in practice, the most prominent being V<sub>2</sub>O<sub>5</sub>/TiO<sub>2</sub> promoted by WO<sub>3</sub> and/or MoO<sub>3</sub>. The main reaction occurring on these catalysts has been formulated to be:  $4 \text{NO} + 4 \text{NH}_3 + \text{O}_2 \longrightarrow 4 \text{N}_2 + 6 \text{H}_2\text{O}$ , implying a 1:1 stoichiometry of ammonia and NO, and the consumption of some oxygen. The vanadia/titania based catalysts are suitable for application in a relatively narrow temperature window 300–400 °C. At higher

temperatures ( $> 400\text{ }^{\circ}\text{C}$ ) nitrous oxide is formed [3]. One of the possible reactions leading to nitrous oxide is:  $4\text{ NO} + 4\text{ NH}_3 + 3\text{ O}_2 \longrightarrow 4\text{ N}_2\text{O} + 6\text{ H}_2\text{O}$ . Catalysts working at low temperature have found significant interest due to their possible application downstream the de-sulfurizer and electrostatic precipitator, where the temperature is  $< 200\text{ }^{\circ}\text{C}$  [4]. Various transition metal oxide based catalysts have been shown to possess some potential for low temperature application, including manganese-ceria mixed oxides recently reported by Yang and coworkers [5]. These authors investigated the potential of manganese-ceria catalysts prepared by co-precipitation for SCR of  $\text{NO}_x$  by ammonia at low temperatures. They investigated the structural properties and catalytic properties of these catalysts and showed that both the manganese/cerium ratio as well as the calcination temperature affects the nitrogen yield. Best catalytic performance was found for mixed oxides containing 40% manganese and calcined at  $500\text{ }^{\circ}\text{C}$ .  $\text{N}_2\text{O}$  formation increased with reaction temperature and manganese content. They found that three kinds of Mn species existed in the  $\text{MnO}_x(0.3)\text{-CeO}_2$  catalyst calcined at  $650\text{ }^{\circ}\text{C}$ : aggregated  $\text{Mn}_2\text{O}_3$  on the  $\text{CeO}_2$  support, highly dispersed  $\text{Mn}_2\text{O}_3$  with strong interaction with  $\text{CeO}_2$ , and  $\text{Mn}^{3+}$  ions incorporated into the  $\text{CeO}_2$  lattice [6]. Based on FTIR studies and the knowledge gathered in the literature concerning SCR of NO on transition metal oxides they proposed an amide-nitrosoamide type mechanism for SCR of NO over manganese-cerium oxides [5]:





They concluded that the initial step of the SCR process is the adsorption of ammonia on the catalyst [7–9]. Machida et al. [10–14] studied the interactions of nitrogen oxides with manganese-cerium oxides to use them for sorptive NO<sub>x</sub> removal at low temperatures (< 150 °C). The combination of nitrogen oxide sorption and catalysis can be broadly applied to the development of low temperature NO<sub>x</sub> reduction in an oxidizing atmosphere. Best properties for sorption of NO<sub>x</sub> were found for a catalyst with a manganese content of 25%.

Although, considerable knowledge has been gained about manganese-cerium mixed oxides and their favorable properties in SCR, there is still relatively little known concerning the relationship between adsorption behavior of reactants, redox behavior of the mixed oxide and catalytic behavior in SCR. Here we have applied pulse thermal analysis combined with mass spectroscopy and FTIR spectroscopy to further this knowledge. In order to gain some insight how the composition of the manganese-cerium mixed oxides affect these properties, the manganese content was varied from 0 to 100 at.%.

## 6.2 Experimental

The MnO<sub>x</sub>-CeO<sub>2</sub> catalysts were prepared by a standard citric acid method from aqueous solutions [6,7]. Manganese nitrate, cerium nitrate and citric acid were dissolved in water and mixed in the desired proportions and the molar ratio of citric acid to metal components (manganese and cerium) was 1.0. The mixture was stirred at room temperature for 1 hour. The solution was dried at 110 °C for 12 hours, resulting in a porous, foam-like solid. The foam-like pre-

cursor was calcined in air at 500 °C for 2 hours. The pure manganese and ceria oxides were prepared using the same procedure. The catalysts are denoted as Mn(x), where x represents the molar ratio of Mn/(Mn+Ce), e.g. Mn(0.25) represents the catalyst with the composition  $(\text{MnO}_n)_{0.25}(\text{CeO}_2)_{0.75}$ . The BET surface area was determined by N<sub>2</sub> adsorption using a Micromeritics ASAP 2010 instrument. Before measurement the samples were degassed in vacuum at 150 °C. The BET surface area of the mixed oxide was found to be in the range of 20–30 m<sup>2</sup> g<sup>-1</sup>, while that of the pure MnO<sub>x</sub> and CeO<sub>2</sub> were 3 and 15 m<sup>2</sup> g<sup>-1</sup>, respectively.

Adsorption, reduction-oxidation behavior and SCR activity measurements were carried out on a Netzsch STA 449 thermoanalyzer equipped with a pulse device enabling injection of a certain amount of one or two different gases or gaseous mixtures into the carrier gas stream flowing through the system. The amount of injected gas was 1.0 ml, if not otherwise specified. The flow rate was controlled by mass flow controllers, Brook's model 5850E, based on a thermal mass flow sensing technique. The thermoanalyzer was connected by a heated (ca. 200 °C) capillary to a Bruker Vector 22 FTIR spectrometer. Gases leaving the FTIR spectrometer were passed through a heated (ca. 200 °C) capillary to a Pfeiffer Omni Star GSD 301 O mass spectrometer. The amount of the catalyst was generally 50 or 100 mg.

XRD analysis was carried out on a Siemens D5000 powder X-ray diffractometer using the Cu-K<sub>α</sub> radiation in step mode between 10 and 80° 2θ with a step of 0.01° and 0.3 s step<sup>-1</sup>.

Before the adsorption experiments the catalyst samples were heated in the thermoanalyzer to 500 °C to remove the gases adsorbed during handling, then they were cooled down to the measuring temperature and equilibrated until no mass change was detectable (cf. chapter 5). Ammonia (purity 99.98%, PanGas)

nitric oxide (purity 99.98%, Messer) and helium or 5% oxygen in helium (purity 99.999%, PanGas) were used as adsorptive and carrier gases, respectively.

Redox-experiments were performed under helium with a heating rate of 3 K min<sup>-1</sup> and each 50 °C one pulse of 1.0 ml hydrogen (99.999%, PanGas) was injected followed by a reoxidation pulse of 1.0 ml oxygen (99.999%, PanGas).

SCR activity measurements were carried out at a total gas flow rate of 50 ml min<sup>-1</sup> using the pulse method according to the following procedure: After the preparation period (calcination at 500 °C and cooling down to the desired reaction temperature) the carrier gas flow (He) was changed to 5% NO, 5% O<sub>2</sub>, balance helium, and the system was equilibrated until no mass uptake due to adsorption was recorded. Then ammonia pulses (1 ml) were injected into the carrier gas stream and the formed N<sub>2</sub>, N<sub>2</sub>O and H<sub>2</sub>O were monitored by MS, while the evolution of NO<sub>2</sub>, NO and NH<sub>3</sub> was monitored by FTIR. The pulses of nitrogen, injected at the end of each experiment, allowed quantifying the nitrogen evolution during reaction [15,16]. The reliability of the pulse method applied was tested by repetitive runs on each sample. Furthermore, the suitability of the pulse method for discriminating the samples concerning their activity was confirmed by corresponding tests using a continuous microreactor.

### 6.3 Results and Discussion

Analysis of the structural and textural properties of the manganese-cerium mixed oxides by X-ray diffraction and nitrogen adsorption corroborated that

the structural and textural properties of the samples used in this studies were similar to those reported by Machida et al. in their original work [10,11].

### 6.3.1 Adsorption Behavior

In a first step we have investigated the adsorption of the reactant gases NO/O<sub>2</sub> and NH<sub>3</sub> on selected samples. As an example, Figure 6-1 shows the mass

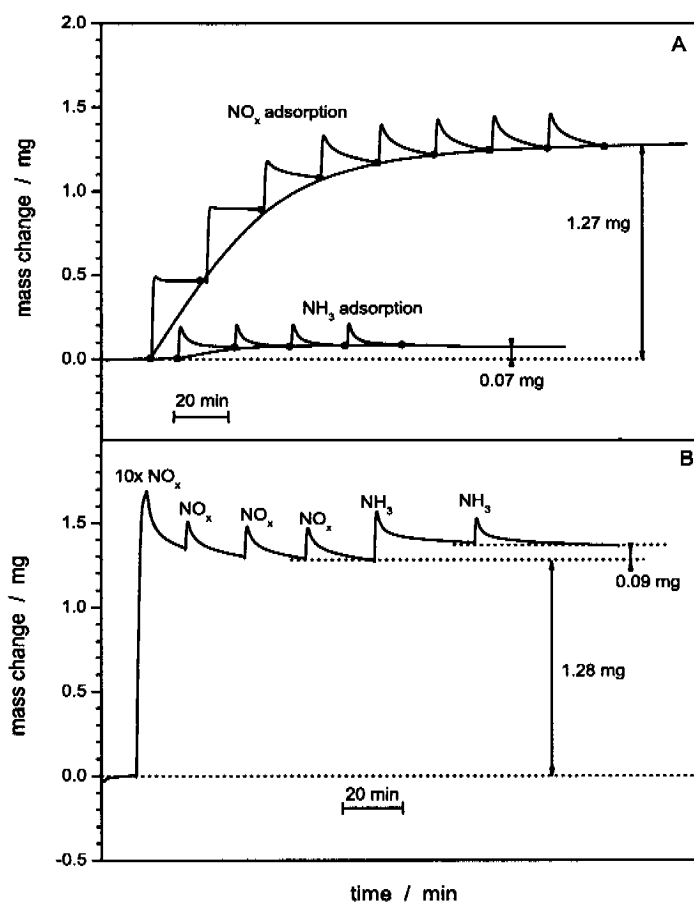


**Fig. 6-1:** Change of the mass due to adsorption of NO<sub>x</sub> and NH<sub>3</sub> on Mn(0.75) at 100 °C, catalyst mass: 100 mg, flow rate: 50 ml min<sup>-1</sup>, volume of the pulses: 1.0 ml, carrier gas: 5% O<sub>2</sub>/He. A: separate adsorption of one gas. B: consecutive adsorption - first NO<sub>x</sub>, then NH<sub>3</sub>.

changes of the sample containing 75% Mn (Mn(0.75)) at 100 °C resulting

from injection of a series of ammonia and nitric oxide pulses, respectively, into 5% O<sub>2</sub>/He carrier gas. It illustrates the typical features of the pulse technique. Strong, virtually irreversible adsorption (chemisorption) of the injected gas occurred during the first two pulses, subsequent pulses 3 and 4 resulted in both strong and weak (reversible) adsorption, whereas during further pulses only weak adsorption (physisorption) occurred. The mass gain at steady state, i.e. when no further mass changes were detectable, represents the amount of irreversibly adsorbed (chemisorbed) species (1.27 mg of NO<sub>x</sub> and 0.07 mg of NH<sub>3</sub>, Figure 6-1A). The corresponding results for all samples with different Mn content are listed in Table 6-1. Samples with a Mn content of 25–75 at.%

**Table 6-1:** NO, NO<sub>2</sub> and NH<sub>3</sub> adsorption on various manganese-ceria mixed oxides. Uptakes (coverages) determined by pulse thermogravimetry; NO pulses in helium ( $\theta_{\text{NO}}$ ), NO pulses in 5% O<sub>2</sub>, balance helium ( $\theta_{\text{NO}_2}$ ), and ammonia pulses in helium, chemisorbed ( $\theta_{\text{NH}_3 \text{ c}}$ ) and physisorbed ( $\theta_{\text{NH}_3 \text{ c+p}}$ ).

Sample	$\theta_{\text{NO}} / \mu\text{mol g}^{-1}$	$\theta_{\text{NO}_2} / \mu\text{mol g}^{-1}$	$\theta_{\text{NH}_3 \text{ c}} / \mu\text{mol g}^{-1}$	$\theta_{\text{NH}_3 \text{ c+p}} / \mu\text{mol g}^{-1}$
Mn(0.00)	77	196	0	6
Mn(0.10)	160	422	6	55
Mn(0.25)	197	559	41	135
Mn(0.50)	167	483	41	118
Mn(0.75)	70	276	41	106
Mn(1.00)	7	22	0	21

showed highest uptakes for chemisorbed ammonia, whereas uptakes due to physisorbed ammonia, NO, and NO/O<sub>2</sub> were highest for the sample containing 25 at.% Mn. Generally on the mixed oxides considerably more NO/O<sub>2</sub> was adsorbed compared to NH<sub>3</sub>. Lowest adsorption uptakes were measured for the pure oxides Mn<sub>2</sub>O<sub>3</sub> (Mn(1.00)) and CeO<sub>2</sub> (Mn(0)). The total ammonia uptake

(physisorbed and chemisorbed, cf. Figure 6-12A) of the samples with different Mn content seemed to correlate to their BET-surface areas:  $\text{m}^2\text{g}^{-1}$  (sample): 14 (0); 23 (0.10); 27 (0.25); 24 (0.50); 20 (0.75); 3 (1.00).

Particularly interesting are the results of subsequent adsorption measurements of the reactant gases presented in Figure 6-1B. These measurements clearly indicate that  $\text{NO}/\text{O}_2$  and  $\text{NH}_3$  are adsorbed at different surface sites and that coadsorption has virtually no influence on the uptakes of the reactant gases. The curve in Figure 6-1B depicts the adsorption of  $\text{NO}_x$  followed by adsorption of ammonia. The mass gains that resulted from subsequent adsorption of both gases are the same as in the case when the gases were adsorbed separately. Note the values of 1.27 and 1.28 mg for  $\text{NO}_x$  and 0.07 and 0.09 mg for ammonia for separate and consecutive adsorption, respectively (Figure 6-1A and B). Figure 6-2 depicts the TG curves of ammonia adsorption over the different catalysts at 100 °C. The amount of irreversibly adsorbed ammonia, determined after 20 min desorption into the carrier gas stream, is relatively small on all catalysts. On the other hand, the amount of weakly, reversibly adsorbed ammonia on the manganese-ceria catalysts depends on the Mn content of the investigated samples.

Subsequent to the adsorption uptake measurements the samples were subjected to *in situ* temperature programmed desorption measurements (TPD). A representative example is shown in Figure 6-3A. The desorption profiles monitored by FTIR after  $\text{NO}_x$  adsorption indicate that the mass loss between 100–400 °C is due to the evolution of nitrogen dioxide. The desorption of ammonia occurs in the range 100–250 °C, as confirmed by monitoring FTIR traces (Figure 6-3B). Note that the major part of adsorbed ammonia is oxidized to  $\text{N}_2\text{O}$  during desorption.



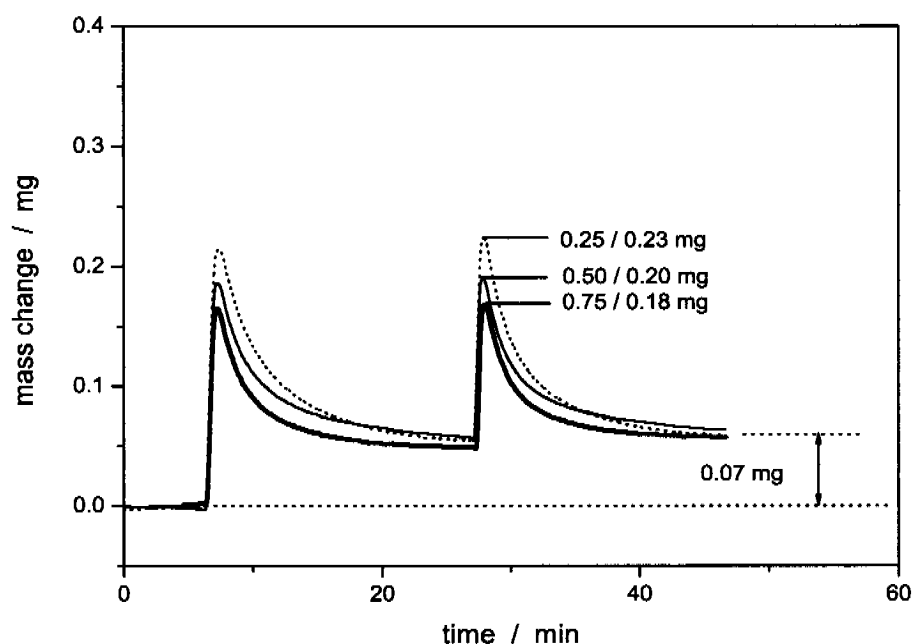


**Fig. 6-2:** Change of the mass due to adsorption of NH<sub>3</sub> on Mn(0.25), Mn(0.50), Mn(0.75) at 100 °C, catalyst mass: 100 mg, flow rate: 50 ml min<sup>-1</sup>, volume of the pulses: 1.0 ml, carrier gas: He. Manganese content, maximal mass uptake due to irreversibly and reversibly adsorbed ammonia and the mass change due to irreversibly adsorbed ammonia only are indicated on the curves.

The dependence of NO<sub>x</sub> (NO/O<sub>2</sub>) adsorption on the catalyst composition determined by the pulse technique is very similar to that found by Machida et al. [13] who measured breakthrough curves for determining the NO<sub>x</sub> uptake. Machida et al. [12] showed by DRIFT studies, that the NO<sub>x</sub> uptake increased at lower temperature and when the oxygen concentration in the gas feed was increased, suggesting chemisorption via oxidation of NO. The fact that we observed in the desorbed gas only the presence of NO<sub>2</sub> confirms the conclusion of Machida et al. [11].

Based on FTIR studies Yang and coworkers [5,6] proposed that ammonia is adsorbed on manganese-cerium mixed oxides on Lewis acid sites subse-

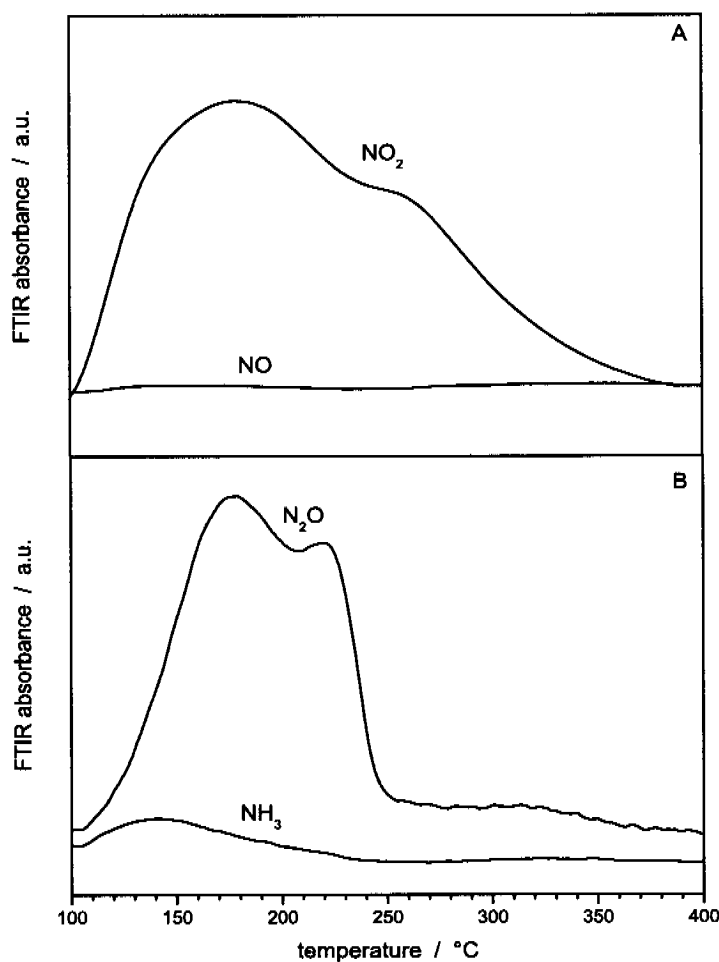


**Fig. 6-3:** A: FTIR  $\text{NO}_2$  and  $\text{NO}$  traces recorded during TPD after  $\text{NO}_x$  adsorption on  $\text{Mn}(0.50)$  at  $10\text{ }^\circ\text{C}$ , carrier gas:  $5\% \text{O}_2/\text{He}$ , heating-rate:  $10\text{ K min}^{-1}$ . B: FTIR  $\text{N}_2\text{O}$  and  $\text{NH}_3$  traces recorded during TPD after  $\text{NH}_3$  adsorption on  $\text{Mn}(0.50)$  at  $100\text{ }^\circ\text{C}$ , carrier gas:  $\text{He}$ , heating-rate:  $10\text{ K min}^{-1}$ .

quently transforming into  $\text{NH}_2$  according to step 3 of the proposed mechanism (cf. Introduction). i.e.  $\text{NO}/\text{O}_2$  exposure leads to adsorbed nitrite species ( $\text{NO}_2$ ) which is corroborated by the desorption profiles shown in Fig. 3A. Our adsorption measurements clearly indicate that  $\text{NO}/\text{O}_2$  and  $\text{NH}_3$  adsorption do not interfere, supporting that these species are adsorbed at different surface sites.

### 6.3.2 Redox Behavior

In order to check the possible dependence between redox properties of the catalysts and their reactivity in SCR their redox behavior was investigated by both, temperature programmed reduction (TPR) and differential reduction followed by reoxidation. As reducing agents ammonia and hydrogen were applied.

The behavior of Mn(1.00) and Mn(0.50) during interaction with ammonia pulses at 100 °C and 300 °C is shown in Figure 6-4. At 100 °C no significant reduction occurs due to ammonia pulses, only a small adsorption uptake

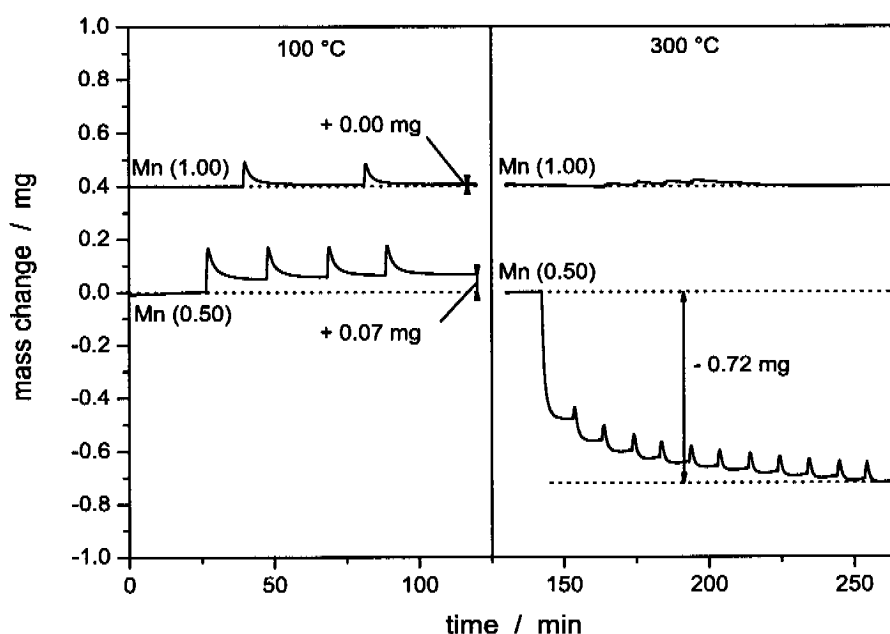


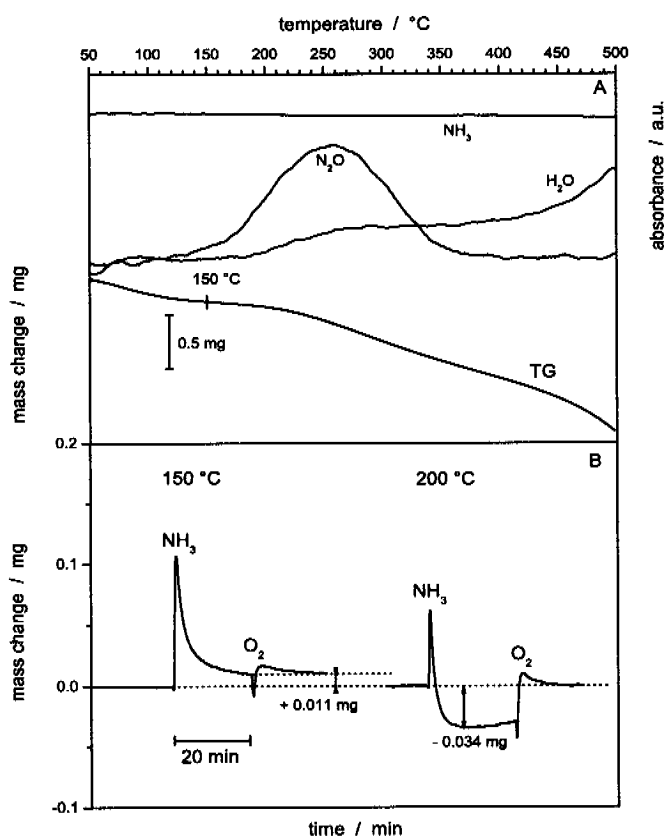
**Fig. 6-4:** Mass changes resulting from 1 ml NH<sub>3</sub> pulses over Mn(1.00) and Mn(0.50) at 100 °C and 300 °C, sample mass: 100 mg.

is observed. However, at 300 °C Mn(0.50) shows a weight loss of 0.72 mg (0.72%) which corresponds to an extent of reduction of ca. 68%, assuming

that  $\text{Mn}_2\text{O}_3$  is reduced to  $\text{Mn}_3\text{O}_4$ . Thus the interaction of  $\text{NH}_3$  with  $\text{Mn}(0.50)$  at  $300\text{ }^\circ\text{C}$  leads to strong reduction of the catalyst and oxidation of ammonia by the lattice oxygen. After injecting oxygen pulses into the carrier gas stream the initial mass (before the reduction step) could be regained after a few pulses, indicating the reversibility of the process.

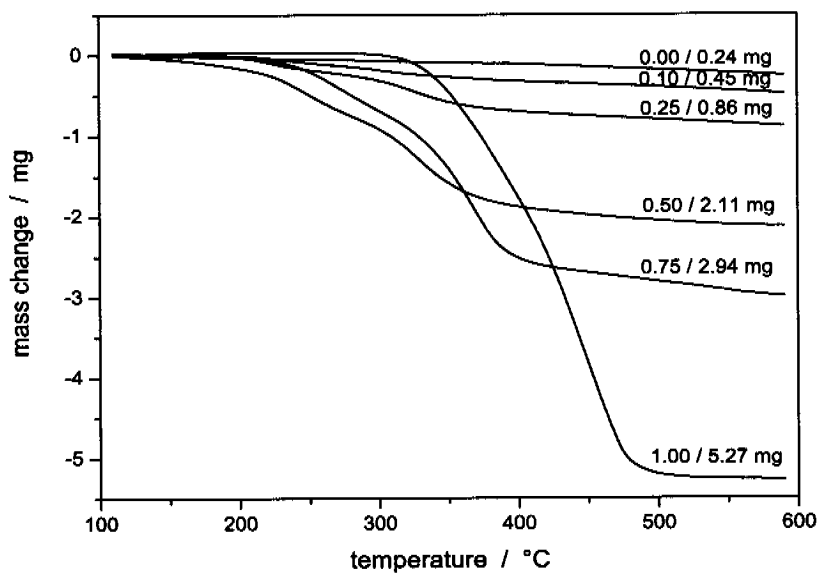
Figure 6-5A shows the TPR profile of  $\text{Mn}(0.50)$  in 5%  $\text{NH}_3/\text{He}$ . Beyond ca.  $150\text{ }^\circ\text{C}$ , reduction of the catalyst by ammonia started and evolution of  $\text{N}_2\text{O}$  was monitored, with a maximum at ca.  $250\text{ }^\circ\text{C}$ . Further mass loss observed was due to the oxidation of ammonia by the lattice oxygen resulting in formation of water and nitrogen (observed by MS, not shown). Figure 6-5B shows the change of the mass due to a  $\text{NH}_3$  pulse for  $\text{Mn}(0.50)$  followed by an oxygen pulse at  $150\text{ }^\circ\text{C}$ , which resulted in adsorption (chemi- and physisorption) and desorption of physisorbed ammonia species. Further oxygen pulses at this temperature did not lead to any change in the catalyst mass corroborating that at this temperature no reduction occurred due to ammonia exposure. At  $200\text{ }^\circ\text{C}$ , however, weak adsorption was followed by desorption and reduction, both occurring simultaneously. The observed mass loss indicated the reduction of the catalyst by ammonia and the initial mass was regained after an oxygen pulse that reoxidized the reduced sample.

Figure 6-6 shows the TPR-profiles in hydrogen of the manganese-cerium mixed oxides, as monitored by TG. Mn content in the catalysts and corresponding mass losses recorded up to  $575\text{ }^\circ\text{C}$  are indicated on the curves. The observed mass loss during reduction increased with the manganese content, for pure ceria only a negligible mass change was observed. In order to check the differential reducibility of the catalyst, the experimental strategy was changed and 1 ml hydrogen pulses were injected each  $50\text{ }^\circ\text{C}$  followed by 1 ml oxygen pulses which reoxidized the catalyst (Figure 6-7). Below  $200\text{ }^\circ\text{C}$  no reduction



**Fig. 6-5:** A: FTIR traces of N<sub>2</sub>O, H<sub>2</sub>O and NH<sub>3</sub> recorded during heating of 50 mg Mn(0.50), carrier gas: 5% NH<sub>3</sub>/He, 10 K min<sup>-1</sup>; 50–150 °C desorption of NH<sub>3</sub>(a), above 150 °C: reduction by NH<sub>3</sub>. B: Change of the mass due to NH<sub>3</sub> pulse on 100 mg Mn(0.50) followed by O<sub>2</sub> pulse at 150 °C (only NH<sub>3</sub> adsorption and desorption of physisorbed species) and 200 °C (NH<sub>3</sub> adsorption, desorption and catalyst reduction followed by reoxidation by oxygen).

was observed but with increasing temperature mass loss due to hydrogen pulses increased significantly. In contrast to the total reduction shown in Figure 6-6, the Mn(1.00) did not show the largest mass loss at temperatures below 400 °C. Thus different reduction behaviors emerge when total and differential reduction are considered, which is important when relating the redox behavior to the catalytic activity of the samples, as will be done in the next chapter.



**Fig. 6-6:** TPR of Mn(x) catalysts in 5% H<sub>2</sub> in He, heating rate: 5 K min<sup>-1</sup>, Mn content in the catalyst and mass loss from 50 mg sample is indicated on the curves.

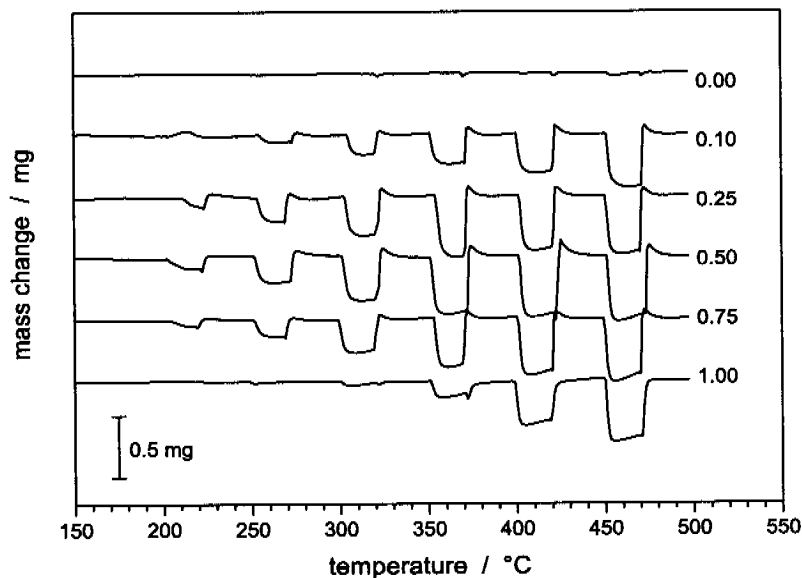


**Fig. 6-7:** Redox-behavior of Mn(x) catalysts as a function of the temperature and catalyst composition. 1 ml H<sub>2</sub> pulses followed by 1 ml O<sub>2</sub> pulses each 50 °C. heating rate: 3 K min<sup>-1</sup>, sample mass: 100 mg. Mn content in the catalysts is indicated on the curves.

### 6.3.3 Catalytic Activity in SCR

In order to investigate the SCR activity of the various manganese-cerium mixed oxides by means of the pulse technique, NH<sub>3</sub> pulses were injected into a carrier gas stream containing 5% NO/5% O<sub>2</sub>, balance helium. Activity tests using a continuous system corroborated that the pulse method was suitable for discriminating the SCR activities of the different manganese-cerium mixed oxide catalysts.

The influence of the temperature on the composition of the gaseous products of the SCR reaction and the change of the mass of catalyst Mn(0.25) due to ammonia pulses are shown in Figure 6-8. The two N<sub>2</sub>-pulses at the end of the experiment were used for the quantitative calibration of the FTIR signal. Above 100 °C only negligible mass change during the reactions was observed, but at 50 °C there was a distinct mass gain due to formation of NH<sub>4</sub>NO<sub>3</sub>.

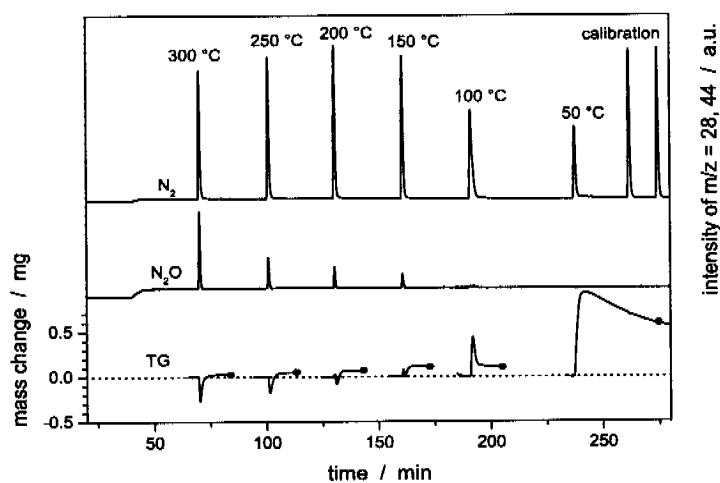


**Fig. 6-8:** Change of the mass (TG) of Mn(0.25) and spectroscopic signals of N<sub>2</sub> and N<sub>2</sub>O recorded during pulses of NH<sub>3</sub> at different temperatures. Catalyst mass: 100 mg, flow rate 50 ml min<sup>-1</sup>, carrier gas: 5% NO, 5% O<sub>2</sub> balance He.

Ammonium nitrate formation showed also a clear dependence on the Mn-Ce mixed oxide composition, showing a maximum for Mn(0.75). The amounts of deposited  $\text{NH}_4\text{NO}_3$  on 100 mg samples due to injections of 1 ml reactive gas were: mg (sample): 0.15 (0); 0.45 (0.10); 0.34 (0.25); 0.96 (0.50); 1.62 (0.75); 0.19 (1.00). The formation of  $\text{NH}_4\text{NO}_3$  was confirmed by comparing the results of the thermal analysis of the catalyst after reaction at 50 °C with TA results of the fresh catalyst impregnated by aqueous solution of  $\text{NH}_4\text{NO}_3$ . Results of this analysis are depicted in Figure 6-9. Decomposition of  $\text{NH}_4\text{NO}_3$

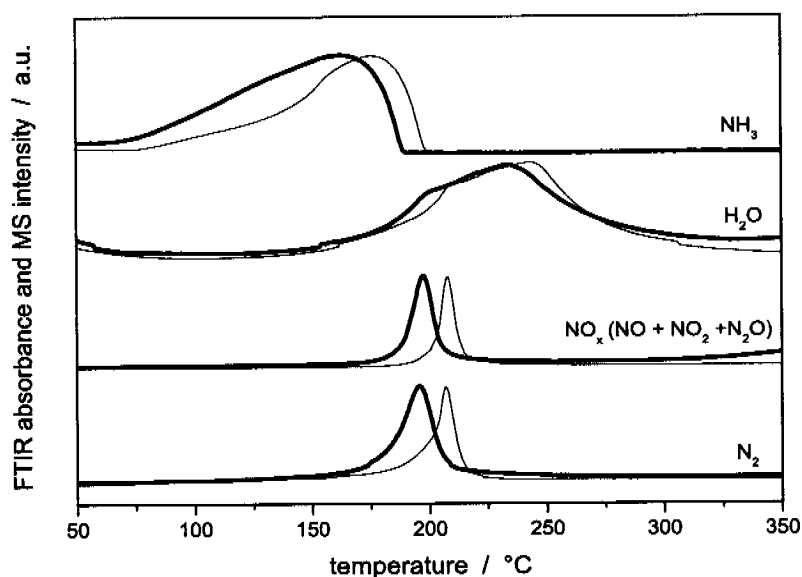


**Fig. 6-9:** Comparison of the  $\text{NH}_3$ ,  $\text{H}_2\text{O}$ ,  $\text{NO}_x$  and  $\text{N}_2$  traces recorded during decomposition of the deposited material on the catalyst (Mn(0.50)) after  $\text{NH}_3$  and  $\text{NO}_x$  co-adsorption at 50 °C (thick lines) and during decomposition of the  $\text{NH}_4\text{NO}_3$  impregnated catalyst (Mn(0.50)).

shows that this salt is stable up to 150–200 °C. For the catalyst impregnated with the aqueous solution of  $\text{NH}_4\text{NO}_3$  the evolution profiles of  $\text{NO}_x$ ,  $\text{N}_2$  and  $\text{H}_2\text{O}$  are similar as those observed during decomposition of the solid deposit



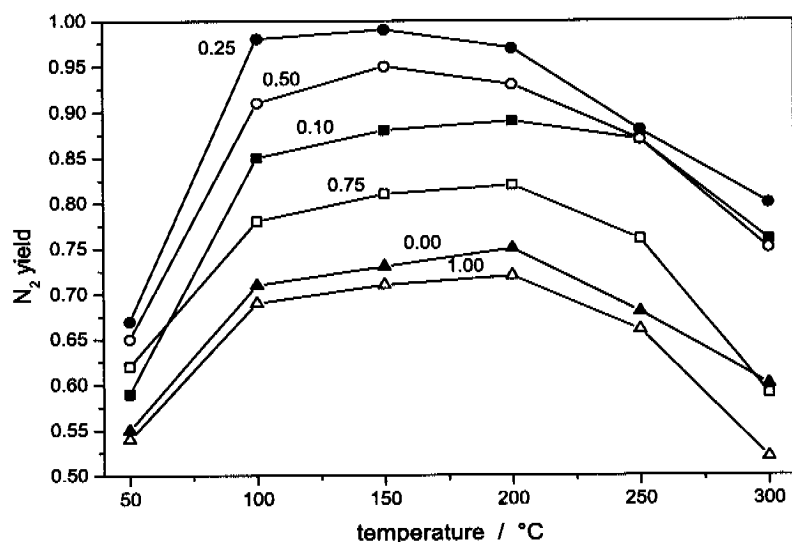
formed on the catalyst at lower temperatures. The small shift in the N<sub>2</sub> and NO<sub>x</sub> profiles could be explained by the different amount of deposited NH<sub>4</sub>NO<sub>3</sub> in the probe and reference sample. According to a quantitative model for temperature programmed reactions peaks are shifted to higher temperature with increasing sample mass [17].

Table 6-2 lists the results of the comparative activity tests of the catalysts

**Table 6-2:** Catalytic Performance of Mn-Ce mixed oxides: N<sub>2</sub> / N<sub>2</sub>O yield (%) at different temperatures. Catalyst mass: 100 mg, flow rate: 50 ml min<sup>-1</sup>, atmosphere: 5% NO, 5% O<sub>2</sub> balance He.

Sample	50 °C	100 °C	150 °C	200 °C	250 °C	300 °C
Mn(0.00)	55/-	71/-	73/-	75/-	68/-	60/1
Mn(0.10)	59/-	85/-	88/-	89/-	87/1	76/7
Mn(0.25)	67/-	98/1	99/1	97/3	88/5	80/11
Mn(0.50)	65/-	91/2	95/5	93/7	87/13	75/23
Mn(0.75)	62/-	78/2	81/6	82/8	76/15	59/32
Mn(1.00)	54/1	69/1	81/4	72/6	66/14	52/28

with different manganese content. N<sub>2</sub> and N<sub>2</sub>O yields (%) are given at different temperatures. The activity is very low for pure ceria, and increases significantly with manganese addition. Selectivity to nitrogen decreases with increasing reaction temperature and manganese content, whereas the formation of N<sub>2</sub>O increases. At temperatures below 150 °C, beside N<sub>2</sub>, only very small amounts of nitrous oxide were observed. The temperature dependence of the catalytic performance (N<sub>2</sub>-yield) of the various Mn-Ce mixed oxides is shown in Figure 6-10. At all temperatures the best catalyst concerning conversion and selectivity to nitrogen was Mn(0.25) and the highest N<sub>2</sub>-yield (99%) was



**Fig. 6-10:**  $N_2$  yield as a function of the temperature and catalyst composition (marked on curves) obtained during pulsing of  $NH_3$ , carrier gas: 5%  $NO$ , 5%  $O_2$  balance  $He$ .

found with this catalyst at 150 °C. The SCR-performance decreased in the following sequence:  $Mn(0.25) > Mn(0.50) > Mn(0.10) > Mn(0.75) > Mn(0.00) > Mn(1.00)$ .

In order to gain some insight into the mechanism of low-temperature SCR over these catalysts a series of experiments were performed in which the sequence of reactant pulses was changed. Representative examples are shown for catalyst  $Mn(0.50)$  in Figure 6-11A. First the catalyst was exposed to  $NO$  pulses in oxygen containing carrier gas (5%  $O_2/He$ ) till saturation by  $NO_x$  was achieved, then  $NH_3$  pulses were injected, but they resulted only in  $NH_3$  adsorption, no nitrogen production was observed. However, upon injection of further  $NO_x$  pulses, the adsorbed ammonia reacted with the  $NO_x$  in the gas phase till complete consumption of the adsorbed ammonia by the SCR reaction occurred. After four  $NO_x$  pulses no significant nitrogen formation could be detected anymore and the catalyst mass (TG) reached the same value as

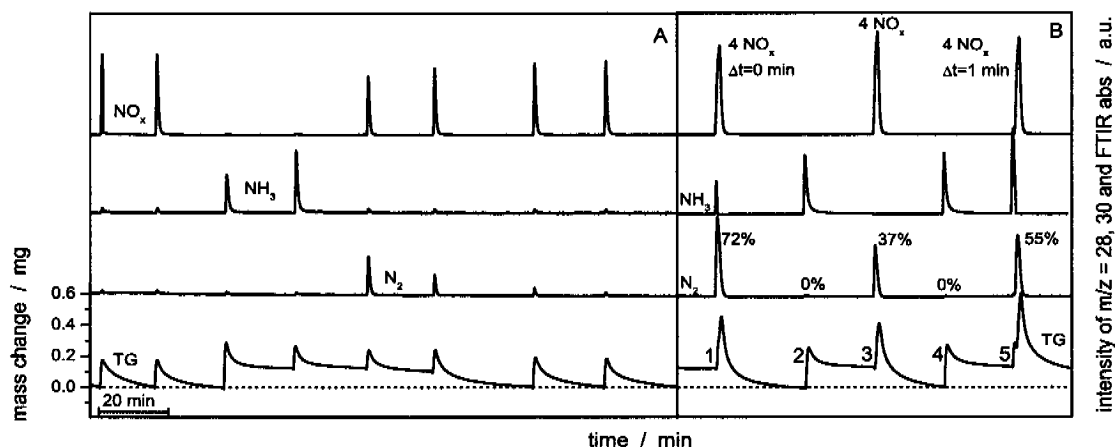
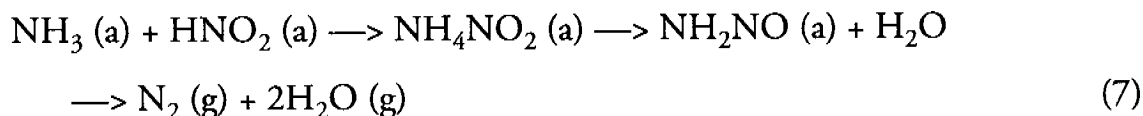
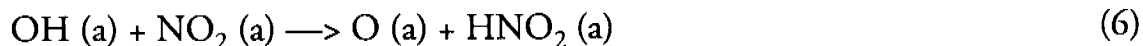


**Fig. 6-11:** N<sub>2</sub> production due to pulses of reactive gas (NO<sub>x</sub> and NH<sub>3</sub>) over Mn(0.50) at 100 °C, catalyst mass: 100 mg, flow rate: 50 ml min<sup>-1</sup>, carrier gas: 5% O<sub>2</sub> balance He. **A:** catalyst was saturated first by NO<sub>x</sub>, then further NH<sub>3</sub> pulses were injected and they resulted only in adsorption, no N<sub>2</sub> production was observed, further NO<sub>x</sub>(g) pulses reacted with NH<sub>3</sub>(a) forming nitrogen (ER-mechanism) until NH<sub>3</sub>(a) is completely consumed. **B:** After saturation by NO<sub>x</sub> following pulses were injected: 1: 1 ml NH<sub>3</sub> and 4 ml NO<sub>x</sub> simultaneously, N<sub>2</sub> yield: 72% 2: 1 ml NH<sub>3</sub>, 3: 4 ml NO<sub>x</sub>, N<sub>2</sub> yield: 37%, 4: 1 ml NH<sub>3</sub>, 5: 1 ml NH<sub>3</sub> followed by 4 ml NO<sub>x</sub> with a delay of 1 min, N<sub>2</sub> yield: 55%

before ammonia injection, corroborating that all adsorbed ammonia reacted with NO<sub>x</sub>.

To further elucidate the role of adsorbed ammonia in the SCR reaction, several NH<sub>3</sub> pulses were injected in the presence of an excess of NO<sub>x</sub> under an oxidative atmosphere (5% O<sub>2</sub>/He), after complete adsorption of both, NO<sub>x</sub> and ammonia as presented in Figure 6-11B. First, one pulse of ammonia and four pulses of NO<sub>x</sub> were simultaneously injected resulting in a nitrogen yield of 72%. The TG curve shows first a distinct mass gain due to mainly physisorption of both gases followed by mass loss due to the consumption of adsorbed ammonia which reacts with the gaseous NO<sub>x</sub> species. Then one pulse of ammonia was introduced (pulse No. 2) in order to re-adsorb the ammonia removed in the preceding SCR reaction. As a consequence the mass of the cata-

lyst reached the same value as before the SCR reaction. During the ammonia pulse no nitrogen production was observed, indicating that  $\text{NH}_3$  either adsorbed or in gas phase does not react with adsorbed  $\text{NO}_x$  species. In the third pulse (No. 3 in Figure 6-11B) 4 ml  $\text{NO}_x$  was injected leading to significant nitrogen production, but the yield was half of that observed when the gaseous  $\text{NO}_x$  reacted with chemi- and physisorbed ammonia (pulse No. 1). Then the ammonia pulse was repeated (pulse No.4) in order to reach equilibrium of ammonia adsorption. During the fifth pulse (No. 5 in Figure 6-11B) injection of an ammonia pulse was followed by the injection of four ml  $\text{NO}_x$  delayed by one minute. This delay resulted in a decrease of the amount of physisorbed ammonia by ca. 20% (cf. Figure 6-2) due to desorption and lead to ca. 24% lower nitrogen yield than obtained during simultaneous introduction of both gases. However, the yield was still higher compared to that originating from pulse No. 3, where only irreversibly adsorbed ammonia reacted with  $\text{NO}_x$  (g). This experiment and a series of analogous investigations carried out in the temperature range 100–150 °C indicated that in the absence of  $\text{NO}_x$  in the gas phase no significant nitrogen formation occurred. Based on these observations we can conclude that at 100–150 °C the dominant mechanism of SCR on the manganese-cerium mixed oxides is an Eley-Rideal type mechanism, where adsorbed ammonia reacts with  $\text{NO}_x$  from the gas phase. This implies that step 5 of the mechanism proposed by Yang and coworkers is mainly contributing to  $\text{N}_2$  formation, whereas the Langmuir-Hinshelwood type step 7 seems to be of minor importance under the conditions applied. Whether this behavior has to be attributed to too slow  $\text{HNO}_2$  (a) formation (step 6) or reaction of  $\text{NH}_3$  (a) with  $\text{HNO}_2$  (a) (step 7) can not be discriminated based on the pulse experiments presented in this study and needs further investigations.



It is interesting to note that our proposal that the dominant mechanism of SCR is an Eley-Rideal type mechanism is in line with the kinetic study of Qi and Yang [7] who found at 120 °C a reaction order of one with respect to NO and zero with respect to NH<sub>3</sub>, respectively. This would imply that the surface coverage of ammonia was virtually constant in the investigated partial pressure range. Kijlstra et al. [18] proposed for SCR over MnO<sub>x</sub>/Al<sub>2</sub>O<sub>3</sub> that adsorbed NH<sub>3</sub> species can react with both, gas phase NO (Eley-Rideal mechanism) and reactive nitrite intermediates (Langmuir-Hinshelwood mechanism). Most of the mechanistic studies reported in the literature deal with SCR on V<sub>2</sub>O<sub>5</sub> based catalysts. An Eley-Rideal (ER) mechanism was proposed by Inomata et al. [19]. Takagi et al. [20] proposed a Langmuir-Hinshelwood mechanism, where NO<sub>2</sub> (ad) and NH<sub>3</sub> (ad) react on the catalyst surface in the presence of oxygen to form nitrogen and water, whereas Ozkan et al. [21] reported a different mechanism of this reaction. By means of isotopic tracer studies they found that it is possible that NO does not reside on the surface to react with ammonia and that the SCR proceeds via adsorbed ammonia species reacting with gaseous NO through an Eley-Rideal mechanism. Marban et al. [22] suggested also an ER mechanism, in which NO<sub>2</sub> (or the less reactive NO) reacts from the gas phase with the surface active ammonia species. They proposed two different SCR mechanisms, in which ammonium ions or aminooxy groups are involved.

Finally we come back to the main objective of our study, namely the investigation of the relationship between adsorption behavior, redox properties and catalytic behavior. The results in Figure 6-12A, B and C clearly indicate that

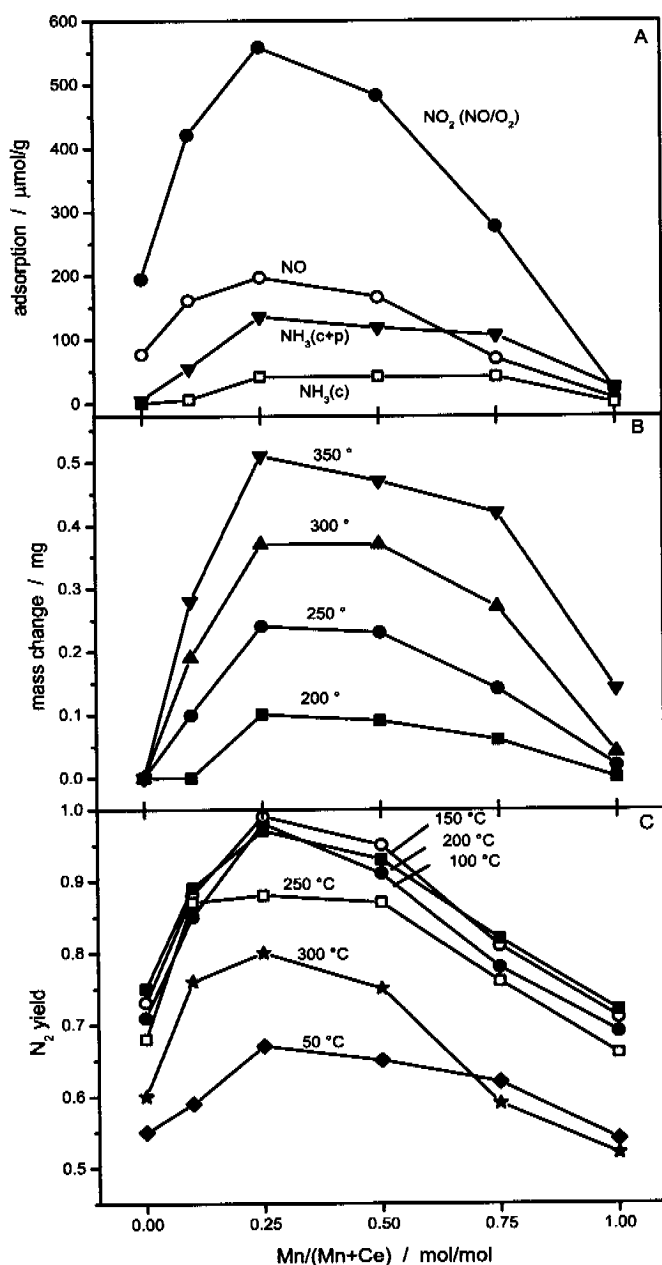


**Fig. 6-12:** A: Adsorption behavior: Dependence of the amount of adsorbed  $\text{NO}_2$  ( $\text{NO}$  pulses in 5%  $\text{O}_2/\text{He}$ ),  $\text{NO}$  ( $\text{NO}$  pulses in  $\text{He}$ ) and  $\text{NH}_3$  ( $\text{NH}_3$  pulses in  $\text{He}$ ), chemi- and physisorbed or only chemisorbed, at 100 °C on the catalyst composition, catalyst mass: 100 mg, flow rate: 50 ml  $\text{min}^{-1}$ . B: Redox properties: Mass loss due to 1 ml  $\text{H}_2$  pulsed over 50 mg of catalyst as a function of temperature and catalyst composition. C:  $\text{N}_2$  yield as a function of the catalyst composition and temperature obtained during pulsing of  $\text{NH}_3$ , carrier gas: 5%  $\text{NO}$ , 5%  $\text{O}_2$  balance  $\text{He}$ .

these properties change strongly with the composition of the manganese-cerium oxides and that there is a striking correlation between adsorption behavior, redox behavior and catalytic properties in SCR. Pulse thermal analysis combined with mass spectroscopy and FTIR proved to be a very suitable tool for elucidating such a correlation because it provides quantitative measures for all these properties.

## 6.4 Conclusions

The selective reduction of NO<sub>x</sub> by NH<sub>3</sub> over manganese-cerium mixed oxides catalysts of different composition has been studied using pulse thermal analysis combined with mass spectroscopy and FTIR. The SCR activity of the mixed oxides depended on their composition, showing a maximum for samples with a Mn content of about 25 at.% Mn. All mixed oxides showed improved catalytic activity compared to the pure constituents oxides. Studies of the adsorption of both reactants, NH<sub>3</sub> and NO, and of the redox behavior revealed a similar dependence on the composition of the mixed oxides, indicating a striking correlation between these properties and the catalytic behavior in SCR. The pulse technique applied allowed to discriminate whether the SCR reaction on Mn-Ce mixed oxide proceeds via an Eley-Rideal mechanism or a Langmuir-Hinshelwood mechanism. The studies indicate that at 100–150 °C nitrogen was produced via an Eley-Rideal mechanism, where the adsorbed NH<sub>3</sub> species reacts with gaseous NO<sub>x</sub> to form nitrogen and water.

## 6.5 References

- [1] H. Bosch, F. Janssen, *Catal. Today* 2 (1988) 369.
- [2] V. I. Parvulescu, P. Grange, B. Delmon, *Catal. Today* 46 (1998) 233.
- [3] M. Koebel, M. Elsener, M. Kleemann, *Catal. Today* 59 (2000) 335.
- [4] K. Kawamura, A. Hirasawa, S. Aoki, H. Kimura, T. Fujii, S. Mizutani, T. Higo, R. Ishikawa, K. Adachi, S. Hosoki, *Rad. Phys. Chem.* 13 (1979) 5.
- [5] G. Qi, R. T. Yang, R. Chang, *Appl. Catal. B* 51 (2004) 93.
- [6] G. S. Qi, R. T. Yang, *J. Phys. Chem. B* 108 (2004) 15738.
- [7] G. Qi, R. T. Yang, *J. Catal.* 217 (2003) 434.
- [8] G. S. Qi, R. T. Yang, R. Chang, *Catal. Lett.* 87 (2003) 67.
- [9] G. Qi, R. T. Yang, *Appl. Catal. B* 44 (2003) 217.
- [10] M. Machida, *Catal. Lett.* 5 (2002) 91.
- [11] M. Machida, M. Uto, D. Kurogi, T. Kijima, *J. Mater. Chem.* 11 (2001) 900.
- [12] M. Machida, M. Uto, D. Kurogi, T. Kijima, *Chem. Mater.* 12 (2000) 3158.
- [13] M. Machida, D. Kurogi, T. Kijima, *Chem. Mater.* 12 (2000) 3165.
- [14] M. Machida, A. Yoshii, T. Kijima, *Int. J. Inorg. Mater.* 2 (2000) 413.
- [15] M. Maciejewski, A. Baiker, *Thermochim. Acta* 295 (1997) 95.
- [16] M. Maciejewski, C. A. Muller, R. Tschan, W. D. Emmerich, A. Baiker, *Thermochim. Acta* 295 (1997) 167.
- [17] D. A. M. Monti, A. Baiker, *J. Catal.* 83 (1983) 323.
- [18] W. S. Kijlstra, D. S. Brands, H. I. Smit, E. K. Poels, A. Bliet, *J. Catal.* 171 (1997) 219.
- [19] M. Inomata, A. Miyamoto, Y. Murakami, *J. Catal.* 62 (1980) 140.



- [20] M. Takagi, T. Kawai, M. Soma, T. Onishi, K. Tamaru, *J. Catal.* 50 (1977) 441.
- [21] U. S. Ozkan, Y. P. Cai, M. W. Kumthekar, *J. Catal.* 149 (1994) 390.
- [22] G. Marban, T. Valdes-Solis, A. B. Fuertes, *J. Catal.* 226 (2004) 138.

Seite Leer /  
Blank leaf

## Final Remarks

The present study showed that the quantification of evolved gases during thermal analysis by the pulse technique using MS or FTIR spectroscopy requires careful optimization of the experimental settings. Quantification based on FTIR is strongly affected by the chosen experimental parameters, whereas MS analysis is only little affected. The most important factors to be considered in gas quantification by means of TA-FTIR are: the choice of the spectral resolution and carrier gas flow rate. High spectral resolution leads to poor time resolution, which is crucial for accurate quantification.

Among the various possibilities of combining TA with evolved gas analysis (EGA), another promising method would be gas chromatography (GC). The great advantage of this method is that one can separate and identify the gases evolved during multistage or parallel reactions, which is difficult when using MS or FTIR. Gases and vapors, simultaneously released during TA, may possess similar fragmentation ions or overlapping vibrational spectra which can severely affect the use of MS or FTIR for quantification. Preliminary results showed that a Micro GC using short and extremely narrow capillaries and micro packed columns, increases the efficiency of the separation process. This strategy may be suitable to run analysis every two minutes with two or optional four columns in parallel, which provides the opportunity for separation and identification of the evolved species. However, a limitation compared to FTIR

or MS systems is that: the quantification of the evolved gases with the pulse method is less accurate because of the relatively poor time resolution in GC systems, which is discussed for FTIR and MS methods in chapter 4.

The extension of the present system to a TA-MS-FTIR-GC system would provide further analytical possibilities particular for gas-solid reactions and adsorption phenomena, where neither MS nor FTIR is the appropriate analytical tool.

Seite Leer /  
Blank leaf

Seite Leer /  
Blank leaf

## List of Publications

### List of publications related to the thesis

The following list summarizes chronologically the publications which are based on this thesis. The pertinent chapters of the thesis are given in brackets.

“Quantitative Calibration of Spectroscopic Signals in Combined TG-FTIR System“

F. Eigenmann, M. Maciejewski, A. Baiker, *Thermochim. Acta* (in press)

(Chapter 3)

“Influence of Measuring Conditions on the Quantification of Spectroscopic Signals in TA-FTIR-MS System“

F. Eigenmann, M. Maciejewski, A. Baiker, *J. Therm. Anal. Cal.* (in press)

(Chapter 4)

“Gas Adsorption Studied by Pulse Thermal Analysis“

F. Eigenmann, M. Maciejewski, A. Baiker, *Thermochim. Acta* 359 (2000) 131.

(Chapter 5)

“Selective Reduction of NO by NH<sub>3</sub> over Manganese-Cerium Mixed Oxides: Relation between adsorption, redox and catalytic behavior“

F. Eigenmann, M. Maciejewski, A. Baiker, Appl. Catal. B 62 (2005) 311.

(Chapter 6)

### **List of other publications**

Following publication was published during the thesis but covers another research topic.

“Continuous Epoxidation of Propylene with Oxygen and Hydrogen on a Pd-Pt/TS-1 Catalyst“

G. Jenzer, T. Mallat, M. Maciejewski, F. Eigenmann, A. Baiker, Appl. Catal. A-Gen. 5304 (2000) 1.

### **Patents**

“Process for the Production of Molybdenum Oxide, Molybdenum Oxide produced from this Process and Use thereof”

R. Nesper, F. Krumeich, M. Niederberger, A. Baiker, F. Eigenmann

Eur. Patent Appl. No. 01810072.7, 2001 Applicant: Swiss Federal Institute of Technology (ETH), Zürich (Switzerland)



### List of Conference Contributions

“Pulsthermoanalyse: Neue Möglichkeiten für STA-FTIR”, 2nd Selber Coupling Days (2nd SKT 1999) from 18–22 April 1999 in Selb (Germany),  
F. Eigenmann, M. Maciejewski, A. Baiker,  
proceedings, oral presentation and leading a workshop.

“Quantitative Kalibrierung von FTIR Signalen”, Analytica, 13 April 2000 in München (Germany),  
F. Eigenmann, M. Maciejewski, A. Baiker,  
poster and oral presentation.

“Quantitative Calibration of Spectroscopic FTIR Signals”, 3rd Selber Coupling Days (3rd SKT 2000) from 28–31 May 2000 in Bad Orb (Germany),  
F. Eigenmann, M. Maciejewski, A. Baiker,  
proceedings, oral presentation and leading a workshop.

“Gas Adsorption Studied by Pulse Thermal Analysis”, Fall Meeting of the Swiss Chemical Society 2000, Lausanne (Switzerland),  
F. Eigenmann, M. Maciejewski, A. Baiker,  
poster.

“Methanol Oxidation Studied by Pulse Thermal Analysis”, Fall Meeting of the Swiss Chemical Society 2001, Zürich (Switzerland),  
F. Eigenmann, M. Maciejewski, A. Baiker,  
poster.

# Curriculum Vitae

Name	Florian Eigenmann
Date of Birth	5 July 1973
City of Birth	Zürich
Citizen of	Waldkirch (SG)
Nationality	Swiss

## Education

1986–1992	Kantonsschule Zürich-Wiedikon Graduation with Matura Type B
1993–1998	ETH Zürich, Chemistry Department Chemical Engineering Studies Graduation as Dipl. Chem. Ing. ETH
1999–2005	ETH Zürich, Institute for Chemical and Bioengineering Doctoral Thesis under the Supervision of Prof. Dr. A. Baiker